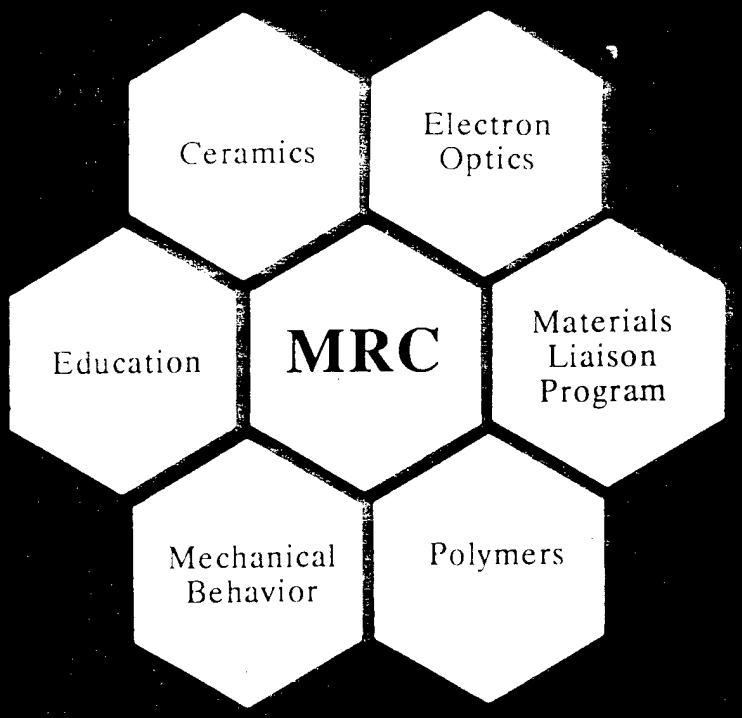

Final Report

(Also see the reports covering the periods: 6/1/94-5/31/95; 6/1/95-5/31/96)

TAILORING OF GRAIN BOUNDARY CHEMISTRY FOR THE DEVELOPMENT OF HIGHLY CREEP RESISTANT ALUMINA

Professors M. P. Harmer (P.I.), H. M. Chan (Co-P.I.), J. Rickman (Co-P.I.) and Research Assistants/Associates J. Bruley, J. Cho, A. Khan, Y.Z. Li, and C.M. Wang

Sponsored by

U.S. Air Force - Office of Scientific Research

Contract No. F49620-94-1-0284

Report Period: 1 June 1996 - 31 May 1997

Materials Research Center, MRC
Lehigh University

REPORT DOCUMENTATION PAGE

Form Approved
OMB No. 0704-0188

1. AGENCY USE ONLY *(Leave blank)*	2. REPORT DATE	3. REPORT TYPE AND DATES COVERED
	29 August 1997	Final Technical Report 1 Jun 94 to 31 May 97

4. TITLE AND SUBTITLE
Tailoring of Grain Boundary Chemistry for the Development of Highly Creep Resistant Alumina

5. FUNDING NUMBERS
F49620-94-1-0284

6. AUTHOR(S)
Prof. M. P. Harmer, H. M. Chan, J. Rickman, and
Research Assistants/Associates J. Bruley, J. Cho, A. Khan, Y.Z. Li, C. M. Wang

7. PERFORMING ORGANIZATION NAME(S) AND ADDRESS(ES)
Lehigh University
Materials Research Center
Whitaker Laboratory
5 E. Packer Avenue
Bethlehem, PA 18015-3194

8. PERFORMING ORGANIZATION REPORT NUMBER

9. SPONSORING/MONITORING AGENCY NAME(S) AND ADDRESS(ES)
AFOSR/NA
110 Duncan Avenue, Suite B115
Bolling AFB, DC 20332-8050

10. SPONSORING/MONITORING AGENCY REPORT NUMBER

11. SUPPLEMENTARY NOTES

12a. DISTRIBUTION AVAILABILITY STATEMENT
Approved for public release; distribution unlimited.

12b. DISTRIBUTION CODE

13. ABSTRACT *(Maximum 200 words)*

Research has demonstrated that the controlled doping of ultra-high purity alumina with small amounts (<1OOOppm) of rare earth elements, such as La and Y, dramatically lowers the sintering and creep rate. Due to the large ionic radius of the rare earth elements, rare earth elements have a low solubility in alumina and segregate strongly to the grain boundaries. Chemical composition (STEM) profiles indicate that segregation of Y and La is localized to within about 2nm of the grain boundary i.e. about a single unit cells width. The concentration is about 9 atom % within 1 nm of the boundary. It is hypothesized that grain boundary segregation plays a key role in slowing down grain boundary diffusion and creep. Atomistic computer simulation has been utilized to predict the distribution of point defects and dopants near grain boundaries and free surfaces and will eventually permit a determination of the boundary diffusivity along segregated boundaries. Selective co-doping with lOOppm Zr and lOOppm Nd has been found to produce the largest reduction in creep rate, of about a factor 500. The creep kinetics suggest that, in the Nd/Zr co-doped alumina, grain boundary diffusion has been suppressed to such a degree that lattice diffusion is rate controlling.

14. SUBJECT TERMS

15. NUMBER OF PAGES

16. PRICE CODE

17. SECURITY CLASSIFICATION OF REPORT	18. SECURITY CLASSIFICATION OF THIS PAGE	19. SECURITY CLASSIFICATION OF ABSTRACT	20. LIMITATION OF ABSTRACT
UNCLASSIFIED	UNCLASSIFIED	UNCLASSIFIED	UL

Standard Form 298 (Rev. 2-89) (EG)
Prescribed by ANSI Std. 239.18
Designed using Perform Pro, WHS/DIOR, Oct 94

ABSTRACT

Research has demonstrated that the controlled doping of ultra-high purity alumina with small amounts (<1000ppm) of rare earth elements, such as La and Y, dramatically lowers the sintering and creep rate. Due to the large ionic radius of the rare earth elements, rare earth elements have a low solubility in alumina and segregate strongly to the grain boundaries. Chemical composition (STEM) profiles indicate that segregation of Y and La is localized to within about 2nm of the grain boundary i.e. about a single unit cells width. The concentration is about 9 atom % within 1 nm of the boundary. It is hypothesized that grain boundary segregation plays a key role in slowing down grain boundary diffusion and creep. Atomistic computer simulation has been utilized to predict the distribution of point defects and dopants near grain boundaries and free surfaces and will eventually permit a determination of the boundary diffusivity along segregated boundaries. Selective co-doping with 100ppm Zr and 100ppm Nd has been found to produce the largest reduction in creep rate, of about a factor 500. The creep kinetics suggest that, in the Nd/Zr co-doped alumina, grain boundary diffusion has been suppressed to such a degree that lattice diffusion is rate controlling.

TABLE OF CONTENTS

1. Technical Reports

Section 1.1

SIMS Micrograph Showing the Segregation of La/Y Dopants in the Grain Boundaries of Alumina

by

A. M. Thompson, K. K. Soni, H. M. Chan, M. P. Harmer, D. B. Williams, J. M. Chabala, and R. Levi-Setti

A picture selected by the American Ceramic Society as A Cover Page of The Journal of The American Ceramic Society

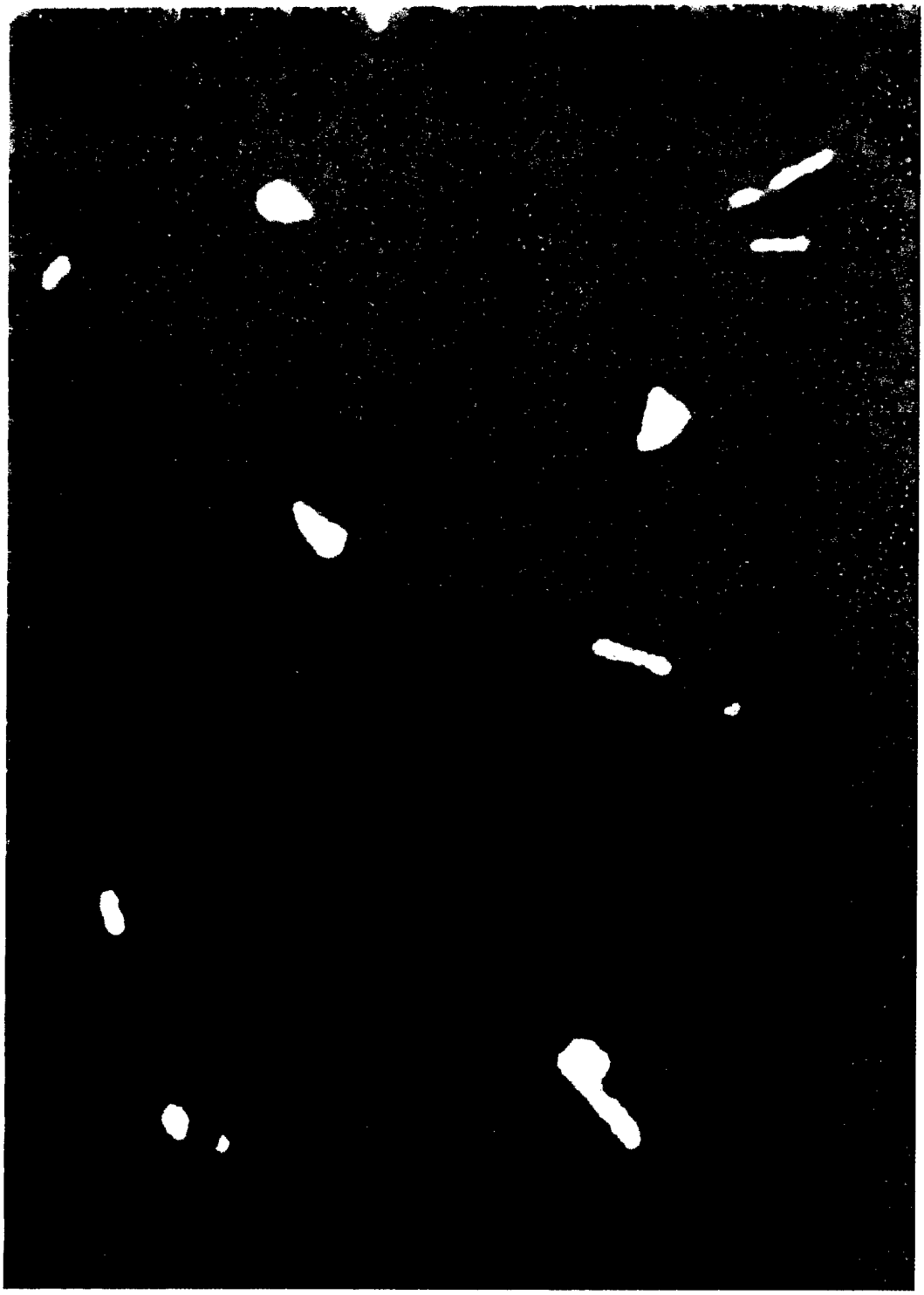

Journal

of the American Ceramic Society
Incorporating Advanced Ceramic Materials and Communications
Volume 80 Number 2 February 1997

Section 1.2

Dopant Distributions in Rare-Earth-Doped Alumina

by

A. M. Thompson, K. K. Soni, H. M. Chan, M. P. Harmer, D. B. Williams, J. M. Chabala, and R. Levi-Setti

Published in Journal of the American Ceramic Society, Volume 80, Pages 373-76(1997)

Dopant Distributions in Rare Earth-Doped Al_2O_3

A. Mark Thompson[1,*, †], Kamal K. Soni[2,*, ‡] Helen M. Chan[1,*], Martin P. Harmer[1,*], David B. Williams[1], Jan M. Chabala[2], and Riccardo Levi-Setti[2].

1. *Dept. of Materials Science and Materials Research Center,*
   Lehigh University
   Bethlehem, PA 18015

2. *Enrico Fermi Institute and Dept. of Physics*
   University of Chicago
   Chicago, IL 60637

The distribution of yttrium and lanthanum dopants was mapped in Y-doped and La-doped polycrystalline aluminas using imaging secondary ion mass spectrometry (imaging-SIMS). Both dopants are found to segregate to grain boundaries and pore surfaces. It was determined that on average, Y occupies 7.1-9.0 % of the available grain boundary cation sites, whereas La occupies only 2.0-5.2 %. In 1000 ppm Y-doped Al_2O_3, an abundance of YAG precipitates is also observed. Implications of these observations to the creep behavior of Al_2O_3 are discussed. The similarity in the segregation behavior of Y and La highlights the potential of La-doped Al_2O_3 for improved creep properties.

Key words (alumina, yttrium, lanthanum, segregation, secondary ion mass spectrometry).

* Member ACerS

† Now at GE Corporate Research & Development, Schenectady, NY 12301

‡ Now at Corning Incorporated, Corning, NY 14831.

I. Introduction

Recently it has been shown that yttrium additions dramatically improve the creep resistance of polycrystalline Al_2O_3[1-4]. At an yttrium doping level of 1000 ppm, the tensile creep rate of Al_2O_3 is reduced by 2 orders of magnitude[1]. Explanations of this beneficial effect focus on the ability of yttrium to inhibit grain boundary diffusion, the primary mechanism for creep in Al_2O_3. It is also known that, as a reactive element additive, yttrium improves the oxidation resistance of FeCrTiAl and NiAl alloys[5,6], presumably by reducing the rate of grain boundary diffusion in the Al_2O_3 surface layer. In both the creep and the oxidation work, it has been proposed that yttrium segregates to the Al_2O_3 grain boundaries, where it either (i) reduces the rate of ion transport along the grain boundaries[5-7] (possibly through the formation of a continuous two-dimensional second phase[7]), or (ii) inhibits the interface reaction believed to be controlling the rate of ion transport along the grain boundaries.[1]

As a consequence, numerous investigators have examined the distribution of yttrium in polycrystalline Al_2O_3, employing a variety of techniques including X-ray energy dispersive spectroscopy (EDS)[5,7-12], extended x-ray absorption fine structure (EXAFS),[10] x-ray photoelectron spectroscopy (XPS)[13,14] Auger electron spectroscopy (AES),[15,16] and secondary ion mass spectrometry (SIMS).[6,13] All studies found yttrium segregating as an Y-rich, grain-boundary monolayer. A few studies have also detected fine precipitates of YAG ($3Y_2O_3.5Al_2O_3$) scattered throughout the microstructure.[5,7,10,15] The degree of grain boundary enrichment depended on the dopant level, the Al_2O_3 grain size, and the impurity content of Al_2O_3.

The objective of this work was to map the Y-distribution in a 1000 ppm Y-doped polycrystalline Al_2O_3 sample which has exhibited favorable creep properties.[1] In addition, a 1000 ppm La-doped sample was examined, primarily to compare the segregation behavior of the two isovalent rare earth elements, and partly to assess the potential of La-doped Al_2O_3 for improved creep properties.

Mapping of the dopant distributions was performed using a high-resolution scanning ion microprobe developed at the University of Chicago.[17] This unique instrument uses a finely-focused gallium beam to sputter secondary ions from the uppermost layers of the specimen surface. For many elements, this imaging SIMS system offers excellent analytical sensitivity, approaching ppm levels. Depending on the secondary ion signal intensity, the spatial resolution in maps can approach the probe diameter (~35 nm). Thus, this technique provides both the high spatial resolution and the analytical sensitivity necessary to characterize the spatial distribution of trace dopants in ceramics,[18] as demonstrated by the recent mapping of Mg segregation in single-phase, polycrystalline Al_2O_3.[19]

II. Experimental Procedure

Samples were prepared using an ultra-high purity, monosized α-alumina powder (Sumitomo AKP-53) for which the maufacturer claims >99.995% purity and a mean particle size of 0.45 μm The powder was mixed with a suitable aliquot of either yttrium or lanthanum nitrate solution to yield a doping level of 1000 ppm (yttrium/aluminum ion) and 500 ppm (lanthanum/aluminum ion). After drying, the powders were crushed and calcined in air at 600°C for 10 h to remove carbon and sulfur contaminants. In order to minimize powder contamination, all powder processing was carried out using precleaned Teflon® ware under clean-room conditions.

Samples were fabricated by hot-pressing calcined powder in a graphite die under vacuum for 30 mins at 50 MPa. The hot pressing temperature was 1475°C for the 1000 ppm Y-doped alumina, and 1450°C for the 1000 ppm La-doped alumina. After hot-pressing, the materials were >99% theoretical density as measured by the Archimedes method, with deionized water as the immersion medium. A piece of each doped Al_2O_3 was polished to a 1 μm diamond finish, sputter-coated with Au, and analyzed in the as-polished condition with the imaging-SIMS instrument. Subsequently, the Au coating was removed (in aqua regia) and the samples were thermally etched

in air at 1400_C for 1 hour in order to reveal the grain structure. The samples were then lightly coated with Au/Pd (approximately 20 nm thick) and imaged using a field emission gun (FEG) scanning electron microscope (SEM). By careful mapping of the specimen surfaces, the areas scanned in the SIMS were relocated in the SEM. Grain sizes were determined from SEM micrographs using the linear intercept method (assuming grain size = 1.5x mean intercept) with at least 450 grains counted per sample.

In the scanning ion microprobe, the primary ion beam is extracted from a liquid Ga source, accelerated to 40 keV and focused to a spot approximately 35 nm in diameter. The probe is scanned over the surface using a 512x512 raster, spanning areas ranging from 10x10 to 80x80 μm^2. Secondary ions are collected normal to the specimen surface (to minimize edge effects) and are mass-analyzed with a magnetic sector mass spectrometer. It is also possible to obtain topographic images of the scanned area by collecting the total ion-induced secondary ion (ISI) signal via a channel multiplier detector overlooking the target at a glancing angle. The ISI images are useful in locating areas of interest and for identifying microstructural features such as pores. The SIMS map were acquired in 1-9 minutes, depending on the signal statistics.

III. Results

The microstructure of the 1000 ppm Y-doped Al_2O_3 is shown in Fig. 1. Only a few isolated pores are observed, confirming that the sample was close to theoretical density. Grains appear to be relatively equiaxed with an average size of 2.5 ± 0.3 μm. The SIMS maps shown in Fig. 1(A) and 1(B) were recorded from the same area of the polished specimen surface: (A) represents the ISI image displaying topographic contrast, and (B) the mass-resolved Y^+ map. The polishing procedure left little surface topography and thus the only features visible in the ISI image (Fig. 1(A)) are residual pores and polishing scratches. In the accompanying Y^+ map, a bright network of Y^+ is observed. This network corresponds directly to the grain structure revealed by thermal etching (See Fig. 1(C)) indicating that almost all of the alumina grain

boundaries were enriched with yttrium. (The few boundaries not evident in the SIMS map either were obscured by limitations in counting statistics, or were deficient in Y.) In addition, segregation of yttrium to the surfaces of the isolated pores is also observed, as indicated in Figs. 1(B) and (C).

From the series of images shown in Fig. 1, it could be concluded that yttrium was accommodated only as a grain-boundary and surface segregant. However, an Y^+ map taken from another area of the polished section (see Fig. 2 (B)) reveals an abundance of discrete Y-rich regions located predominantly at the grain boundaries. The corresponding SEM micrograph shown in Fig. 2(C) confirms that these regions represent Y-rich precipitates (presumably YAG[5,7,10,15]) rather than grain boundary porosity. It should be noted that the contrast in this Y^+ map has been enhanced to reveal the (low intensity) grain-boundary segregation of yttrium. At this contrast level, the image displays not only the precipitates themselves, but also yttrium enrichment surrounding the precipitates, at the same brightness. Thus, the precipitates appear to be larger in the Y^+ map than in the accompanying SEM image of the same area (Fig. 2(C)).

The extent of Y segregation to the grain boundaries was quantified by determining the fraction of grain boundary cation sites occupied by the rare earth dopant. First, intensity profiles along operator-defined vectors were measured retrospectively with the *Image* (v. 1.55) program.[20] Each profile was oriented normal to a grain boundary and averaged over a width of 20 pixels (~0.8 μm) in order to reduce the statistical noise. The maximum signal intensity along this scan represented the solute signal arising from the grain boundary region. Because the primary beam diameter was significantly larger than the effective grain boundary width, this signal included significant contribution from the matrix surrounding the boundary. Corrected values of solute signal emitted per unit boundary area were calculated assuming a boundary width of 2 monolayers (1 nm) and a probe size equal to the pixel size (39 nm at this magnification). At least 20 boundaries were analyzed for each sample. These corrected grain boundary signal intensities were then converted to solute concentrations via an internal calibration procedure. Sensitivity factors for Y (signal intensity/concentration) were determined by using both the average

maximum signal intensity arising from YAG precipitates (corresponds to Y/(Al+Y) = 0.375) and the average intensity of the complete Y^+ map (corresponds to the bulk concentration, Y/(Al+Y) = 1000 ppm) as standards.[21] With this approach, it was calculated that the percentage of grain boundary cation sites occupied by Y solute ions was in the range of 7.1 ± 2.4 % (from bulk concentration as standard) and 9.0 ± 0.2% (from YAG standard).

In addition, the grain boundary enrichment of solute can be expressed in terms of enrichment factor, the ratio of solute concentration at the grain boundary to that within the grains. Assuming matrix effects to be uniform across the grain and grain boundary regions, the enrichment factor is given by the ratio of corresponding signal intensities per unit area. Solute concentrations within the grain interiors were determined by averaging the signal intensity within each grain, with at least 20 grains being sampled. For the Y-doped sample, the grain boundary enrichment factor was 900 ± 80.

The 500 ppm La-doped Al_2O_3 sample was nearly fully-dense with a finer grain structure (2.1 ± 0.3 μm) that was more elongated than that of the Y-doped sample (see Fig. 3(C)). The La^+ map in Fig 3(B) reveals segregation of La to the Al_2O_3 grain boundaries. Similar to the Y-doped Al_2O_3, the dopant appears to be distributed along almost all the grain boundaries. In addition, pore surfaces are enriched with the La, and La-rich precipitates are observed. By calibration with the average intensity of the complete La^+ map, it was determined that approximately 2.0 ± 0.8% of the grain boundary cation sites were occupied by La. When the La average intensity was calibrated using second phase particles as a standard (assumed to be $La_2O_3Al{:}11Al_2O_3$), the grain boundary cation coverage was determined to be 5.2 ± 0.2%. The grain boundary enrichment factor was calculated to be 250 ± 10 ppm.

IV. Discussion

In this study, Y and La dopants were found to segregate to grain boundaries and pore surfaces of alumina, consistent with previous microanalytical studies.[5-10,15,16] Excess dopant that

is not accommodated within the Al_2O_3 grains or at the grain boundaries is concentrated in discrete second phases. The ability to distinguish between dopant segregation to grain boundaries, pore surfaces, and precipitates within a single map underscores the microanalytical capabilities of the imaging-SIMS technique. Compositional imaging samples every point in a large area without bias, in contrast to traditional point analyses. In combination with high-resolution FEG-SEM, this technique enables correlation of microstructural features with corresponding microchemistry.

Quantitative information extracted from these SIMS maps compares favorably with values determined via other microanalytical techniques. In the Y-doped Al_2O_3, the average grain boundary cation coverage was in the range of 7.1 - 9.0%, which is in good agreement with previous results[7,9,14,15], in particular those of Gruffel and Carry[7] who also determined a cation coverage of 7-9% (20-25 wt% Y/(Al+Y)) for Y-doped alumina. The corresponding enrichment factor (900 ± 80) is within an order of magnitude of grain-boundary and surface enrichment factors determined in other studies (100-570) using similar yttrium dopant levels.[8,9,15] This represents good agreement, especially considering the inherent difficulty in the measurement of low solute concentrations within the grains, at the detectability limits of these microanalytical techniques.

In contrast to other studies,[7,12] no significant variation in Y coverage between grain boundaries was detected and Y-depleted special grain boundaries were not observed. The error in the calculated Y enrichment factor represents the statistical variation in the measured secondary ion signal. For example, individual measurements taken from several locations along a boundary yielded a statistical variation in the Y coverage. If anisotropic segregation was present, the degree of anisotropy was insufficient to be distinguished from this statistical variation. Alternatively, the absence of anisotropic segregation may be consequence of the high powder purity. Materials used in other studies[7,12] contained additional dopants and impurities (such and Mg and Si) which may have affected the segregation behavior of Y.

Lanthanum occupied 2.0-5.2% of the grain-boundary cation sites in the La-doped Al_2O_3, a lower coverage than that determined for Y in the Y-doped Al_2O_3. The presence of dopant-rich

second phases indicates that, in both cases, the grain boundaries are saturated with solute. If it is assumed that the grain boundary region is a more open structure than the grain interior and has an enhanced solubility for large substitutional cations, then it is reasonable to expect from volume strain considerations that the grain boundary would be able to accommodate more Y than La ions at saturation.

The corresponding grain-boundary enrichment factor for La is 500 ± 20, which is in good agreement with that obtained by Li and Kingery[8] (400). Assuming that the driving force for segregation arises from the strain misfit between the dopant and matrix cation,[8,22] it is rather surprising that the enrichment factor for La is lower than that determined for Y-doped Al_2O_3. Lanthanum, the larger ion, would be expected to segregate more strongly than Y. This discrepancy is believed to be a consequence of the inherent difficulty of measuring solute concentrations within the grains under high-resolution imaging-SIMS conditions. For example, combining the grain boundary coverage and the enrichment factor, the bulk solubility limit of both Y and La in Al_2O_3 is calculated to be approximately 80 ppm. This contrasts with previous work[23] in which the solubility limit of Y is presumed to be less than 10 ppm. Thus it is believed that the cation fraction coverage is the more accurate of the two segregation measurements.

In the light of these observations, it is appropriate to reconsider the role of yttrium in lowering the tensile creep rate of alumina. In a previous creep study, it was proposed that the principal effect of yttrium was to reduce the interface reaction believed to be governing the rate of grain boundary transport.[1] This hypothesis was based on microstructural observations which indicated an absence of second phases. Certainly, there exist regions of the Y-doped Al_2O_3 in which the YAG precipitates are sparse. However, the present analysis has also revealed areas of the material that contain an abundance of YAG precipitates. It is possible that these precipitates play a role in reducing the creep rate. For example, grain-boundary precipitates could inhibit the boundary sliding that must accompany diffusional creep. Alternatively, diffusion along the grain boundaries may be limited by the creation of defects at, or the rate of diffusion along, the particle-matrix interface.

The non-uniform distribution of YAG precipitates across the sample section is attributed to incomplete mixing of the Y-doped powder. It is interesting to note, however, that this artifact did not appear to diminish either the beneficial effect of yttrium doping on the tensile creep behavior, or the reproducibility of creep results[1]. Two possible explanations for this favorable result are: (i) the creep behavior was dominated by the Y-rich grain boundary layer, and was insensitive to the YAG precipitates, or (ii) the scale of the non-uniform distribution of precipitates was sufficiently fine to yield an average and reproducible creep behavior across the sample section. These observations have some interesting implications. If the precipitates play no role in the creep behavior, then a similar creep behavior should be achieved at lower doping levels. Conversely, if the precipitates play a significant role, then by increasing the volume fraction of precipitates the tensile creep properties should be improved further. Additional creep studies in this area should therefore prove fruitful.

The similarity in the segregation behavior of Y and La highlights the potential of La-doping for reducing the creep rate of Al_2O_3. If the creep behavior arises from an inherent property of the dopant-rich boundaries or the grain-boundary precipitates, then La-doped Al_2O_3 could also exhibit improved creep properties. Indeed, preliminary work has shown that lanthanum also reduces the creep rate of alumina.[24]

V. Conclusions

(1) Yttrium and lanthanum segregate to the grain boundaries and pore surfaces of polycrystalline alumina. Excess dopant is incorporated as discrete dopant-rich precipitates located predominantly at the grain boundaries.

(2) By internal calibration of SIMS signal intensities, the cation coverages in the grain boundary region are calculated to lie in the range of 7.1-9.0% Y/(Al+Y) and 2.0-5.2% La/(Al+Y) for Y-doped Al_2O_3 and La-doped Al_2O_3, respectively.

(3) The imaging-SIMS technique is a powerful tool for the microanalysis of ceramics. When combined with high resolution SEM, microstructural features and microchemistry can be correlated.

Acknowledgments

The authors gratefully acknowledge the assistance of Dr. L. M. Braun and Dr. J. D. French in preparation of the samples. They would also like to thank Dr. D. A. Smith and Dr. J. Bruley for their helpful discussions. This work was supported in part by AFOSR under grant # F49620-94-1-0284 (Lehigh University) and in part by the MRSEC Program of the National Science Foundation under Award Number DMR-9400379 (University of Chicago).

References

(1) J. D. French, "High Temperature Deformation and Fracture Toughness of Duplex Ceramic Microstructures," Ph.D. Thesis, Lehigh University, (1993).

(2) S. Lartigue, C. Carry, and L. Priester, "Grain Boundaries in High Temperature Deformation of Yttria and Magnesia Co-Doped Alumina," *Coll. Phys. C1*, **51** [1] 985-90 (1990).

(3) P. Gruffel, and C. Carry, "Strain Rate Plateau in Creep of Yttria Doped Fine Grained Alumina," pp305-311 in Proc. of the 11th RISO International Symposium on Metallurgy and Materials Science: *Structural Ceramics - Microstructure and Properties*. Ed. by J. J. Bentzen, J. B. Bilde-Sorensen, N. Christiansen, A. Horsewell, and B. Ralph, Riso National Lab. Roskilde, Denmark, 1990.

(4) A. G. Robertson, D. S. Wilkinson, and C. H. Caceres, "Creep and Creep Fracture in Hot-Pressed Alumina," *J. Am. Ceram. Soc.*, **74** [5] 915-21 (1991).

(5) K. Przybylski, A. J. Garratt-Reed, B. A. Pint, E. P. Katz, and G. J. Yurek, "Segregation of Y to Grain Boundaries in the Al_2O_3 Scale Formed on an ODS Alloy," *J. Electrochem. Soc.*, 134 3207-3208 (1987).

(6) B. A. Pint, J. R. Martin and L. W. Hobbs, "^{18}O/SIMS Characterization of the Growth Mechanism of Doped and Undoped-Al_2O_3," *Oxidation of Metals*, **39** [3-4] 167-195 (1993).

(7) P. Gruffel, and C. Carry, "Effect of Grain Size on Yttrium Grain Boundary Segregation in Fine Grained Alumina, " *J. Eur. Ceram. Soc.*, **11** 189-99 (1993).

(8) C-W. Li, and W. D. Kingery, "Solute Segregation at Grain Boundaries in Polycrystalline Al_2O_3," pp 368-378 in Advances in Ceramics Vol. 10, *Structure and Properties of MgO and Al_2O_3 Ceramics*. Ed. W. D. Kingery, American Ceramic Society, Columbus, OH (1984).

(9) B. Bender, D. B. Williams, and M. R. Notis, "Investigation of Grain-Boundary Segregation in Ceramic Oxides by Analytical Scanning Transmission Electron Microscopy," *J. Amer. Ceram. Soc.*, **63** [9-10] 542-546 (1980).

(10) M. K. Loudjani, J. Roy, and A. M. Huntz, "Study by Extended X-Ray Absorption Fine-Structure Technique and Microscopy of the Chemical State of Yttrium in _-Polycrystalline Alumina, " *J. Amer. Ceram. Soc.*, **68** [11] 559-562 (1985).

(11) H. M. Tawancy and N. M. Abbas, "An Analytical Electron Microscopy Study of the Role of La and Y During High-Temperature Oxidation of Selected Ni-Base Alloys," *Scripta Metall et Mater.*, **29** 689-94 (1993).

(12) F. Dupau, D. Bouchet, and S. Lartigue-Korinek, "Intergranular Segregation Studied by EDXS Analysis and HREM in Yttria Doped Aluminas," ICEM 885-886 (1994).

(13) G. Petot-Ervas, C. Monty, D. Prot, C. Severac, and C. Petot, "Yttrium, Calcium and Silicon Segregation in Alumina During Cooling," pp 465-70 in Proc. of the 11th RISO International Symposium on Metallurgy and Materials Science: *Structural Ceramics - Microstructure and Properties*. Ed. by J. J. Bentzen, J. B. Bilde-Sorensen, N. Christiansen, A. Horsewell, and B. Ralph, Riso National Lab. Roskilde, Denmark, 1990.

(14) G. Petot-Ervas, S. Lartigue, C. Severac, M. Barj, and C. Petot, "Surface Impurity Segregation in Submicron Alumina Powders," pp 465-70 in Proc. of the 11th RISO International Symposium on Metallurgy and Materials Science: *Structural Ceramics - Microstructure and Properties*. Ed. by J. J. Bentzen, J. B. Bilde-Sorensen, N. Christiansen, A. Horsewell, and B. Ralph, Riso National Lab. Roskilde, Denmark, 1990.

(15) R. C. McCune, W. T. Donlon, and R. C. Ku, "Yttrium Segregation and YAG Precipitation at Surfaces of Yttrium-Doped -Al_2O_3," *J. Amer. Ceram. Soc.*, **69** [8] C196-C199, (1986).

(16) P. Nanni, C. T. H. Stoddart, and A. D. Hondros, "Grain Boundary Segregation and Sintering in Alumina," *Materials Chemistry*, **1** 297-320 (1976).

(17) R. Levi-Setti, J. M. Chabala, J. Li, K. L. Gavrilov, R. Mogilevsky, and K. K. Soni, "Imaging-SIMS (Secondary Ion Mass Spectroscopy) Studies of Advanced Materials," Scanning Microscopy, **7** [4] 1161-1172 (1994).

(18) K. K. Soni, J. M. Chabala, R. Mogilevsky, R. Levi-Setti, W. S. Wolbach, S. R. Bryan, "Imaging Microanalysis of Ceramic Materials with Scanning Ion Microprobe," *Surface and Interface Analysis*, **21** 117-122 (1994).

(19) K. K. Soni, A. M. Thompson, M. P. Harmer, D. B. Williams, J. M. Chabala, and R. Levi-Setti, "Solute Segregation to the Grain Boundaries of MgO-doped Alumina," *Appl. Phys. Lett.*, **66** (21) 1-3 1995.

(20) W. Rasband, Image (v. 1.43), National Institutes of Health, Bethesda, Maryland (1992).

(21) D. E. Newbury, "Methods for Quantitative Analysis in Secondary Ion Mass Spectrometry," *Scanning*, **3** 110-118 (1980).

(22) D. McLean, "Grain Boundaries in Metals." Oxford University Press, London (1957).

(23) J. D. Cawley and J. W. Halloran, "Dopant Distribution in Nominally Yttrium-Doped Sapphire," *J. Am. Ceram. Soc.*, **69** [8] C195-C196 (1986).

(24) A. M. Thompson, unpublished work.

Figure Captions

Figure 1: 1000 ppm Y-doped Al_2O_3; (A) ISI topographic image of an unetched polished section, (B) Y^+ SIMS map of same area clearly showing segregation of Y to grain boundaries and pore surfaces, (C) SEM micrograph of the same area after thermal etching.

Figure 2: 1000 ppm Y-doped Al_2O_3; (A) ISI topographic image of an unetched polished section, (B) Y^+ SIMS map of same area showing additional Y-rich regions, which are identified as precipitates in the accompanying SEM micrograph (C).

Figure 3: 500 ppm La-doped Al_2O_3; (A) ISI topographic image of an unetched polished section, (B) La^+ SIMS map of same area clearly showing segregation of La to grain boundaries, pore surfaces and precipitates, (C) SEM micrograph of the same area after thermal etching.

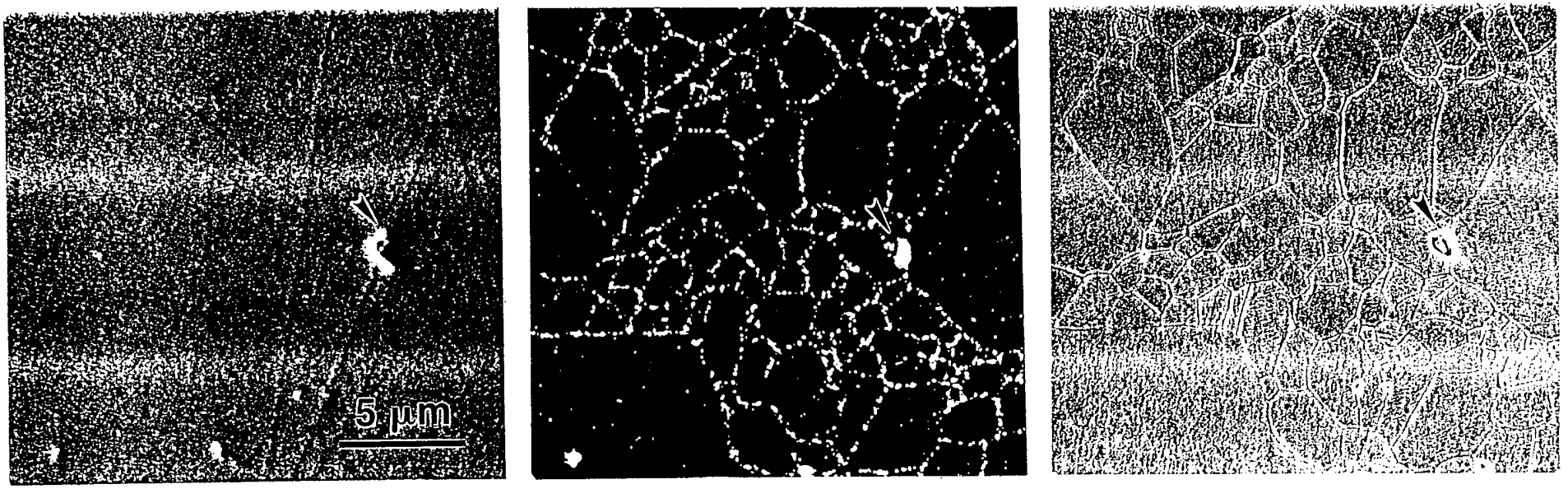

FIGURE 1 (Thompson et al.)

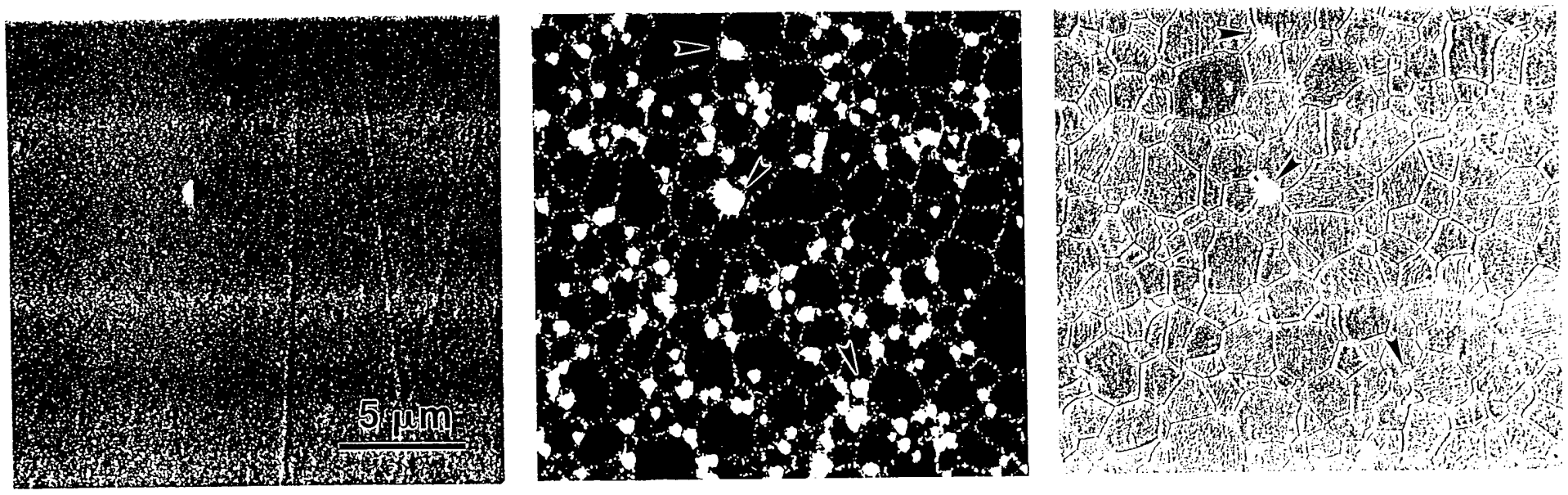

FIGURE 2 (Thompson et al.)

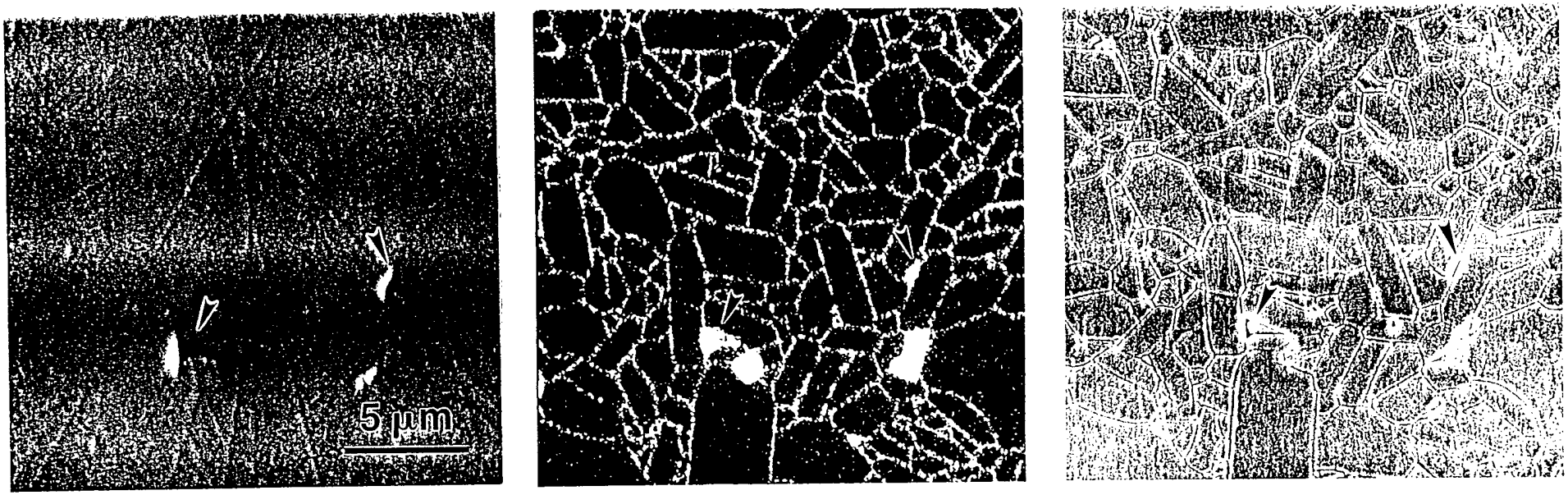

FIGURE 3 (Thompson et al.)

Section 1.3

Effect of Yttrium and Lanthanum on the Tensile Creep Behavior of Aluminum Oxide

by

J. Cho, M. P. Harmer, H. M. Chan, J. M. Rickman and A. M. Thompson

Published in Journal of the American Ceramic Society, Volume 80, Pages 1013-17(1997)

Effect of Y and La on the Tensile Creep Behavior of Aluminum Oxide

Junghyun Cho*, Martin P. Harmer*, Helen. M. Chan*, Jeffrey. M. Rickman*, and

A. Mark Thompson*†

Lehigh University

Dept. of Materials Science and Engineering

Whitaker Laboratory

Bethlehem, PA 18015, USA

ABSTRACT

The tensile creep behavior of two rare-earth dopant systems, lanthanum and yttrium-doped alumina, are compared and contrasted in order to better understand the role of oversized, isovalent cation dopants in determining creep behavior. It was found that, despite some microstructural differences, these systems displayed qualitatively a similar improvement in creep resistance, supporting the hypothesis that creep is strongly influenced by segregation. Differences in primary creep behavior and activation energy for steady-state creep were, however, observed for these systems. Given these results, it is expected that creep behavior can be further optimized by adjusting the dopant level and by controlling the microstructure.

Supported by the United States Air Force Office for Scientific Research under Contract No. F49620-94-1-0284

*Member, American Ceramic Society

†Present address: GE Corporate Research and Development, Bldg. K1, Rm. 4B4, P.O.Box 8, Schenectady, NY 12301

1. INTRODUCTION

Mechanical properties of structural ceramics in a high temperature environment have been the subject of numerous investigations over the years. For this reason, creep properties have been studied and modeled extensively and creep mechanisms are well-established.[1-4] In particular, much recent work has involved the addition of impurities and the tailoring of microstructures with the goal of obtaining desirable properties over a range of temperatures. The creep rate in doped alumina depends strongly on the type of dopant, and most single dopants have been found either to increase the creep rate of alumina or to have little to no effect.[5,6] It should be noted here, however, that the role of (oversized) dopants, such as Y (co-doped with Mg), in the superplastic deformation in alumina has been discussed in several studies.[7,8] In addition, it has been previously reported that the tensile creep rate of α-Al_2O_3 can be dramatically reduced (by several orders of magnitude) by adding 1,000 ppm Y_2O_3.[9]

In order to understand the basic mechanism responsible for this behavior, it is advantageous to consider here the impact of other dopants on creep behavior. With this in mind and in order to focus on the role of dopant size, we introduce another dopant system, namely La, into alumina and examine the creep behavior in some detail. This investigation will involve not only mechanical testing but also a quantitative characterization of the microstructure of the doped system so that the role of interfacial processes in creep may be examined. While it has already been found that creep behavior is strongly influenced by interfaces present in a polycrystalline sample,[10] a detailed understanding of creep behavior is lacking owing to the structural complexity of doped oxide systems.

A number of preliminary observations have guided this study. For example, it is known that the bulk solubility of Y^{3+} and La^{3+} in alumina is very small[11,12] and the size mismatch between Al^{3+} and the aforementioned dopant cations is quite large. Thus, it might be expected that Y and La

ions will segregate preferentially to extended defects, such as free surfaces and grain boundaries. This expectation was validated in a previous SIMS (Secondary Ion Mass Spectroscopy) mapping study[13] and STEM (Scanning Transmission Electron Microscopy) work[14,15] in which both Y and La dopant segregation was observed. Indeed, sintering studies show that Y and La retard grain growth and greatly reduce the densification rate in these systems.[16] Further, it has been reported that Y can reduce the growth of polycrystalline alumina scales.[17]

As mentioned above, the present work consists of tensile creep testing and microstructural characterization of both Y and La-doped alumina. Microstructural analyses center on quantifying differences in average grain size and shape between these two systems as well as grain evolution during the test. The goal of this effort is to relate microstructural features of the oxide to the (macroscopic) steady-state creep rate, as determined by a tensile creep test. As will be seen below, such complementary testing is helpful in formulating structure-property relations.

2. EXPERIMENTAL PROCEDURE

Samples used in this study were prepared by using the same commercial powders of α-Al_2O_3 (AKP-53, Sumitomo Chemical America, New York, NY) utilized in previous studies.[9,13] The powder was mixed with a suitable proportion of either yttrium or lanthanum nitrate solution to achieve dopant levels of 1,000 ppm (Y/Al ion) and 500 ppm (La/Al ion). Such dopant levels are both well above the respective bulk solubility limits of these materials in alumina. Fully dense materials were hot-pressed at 1475°C for Y-doped alumina, and 1450°C for La-doped alumina in vacuum for 30 minutes at 50 MPa. Pure alumina samples were calcined at 850°C for 10 hours and pressureless sintered at 1400°C for 1 hour and subsequently at 1650°C for 4 hours.[18]

Dog-bone-shaped tensile specimens were tested under constant load conditions according to the procedure outlined by Caroll et al..[19] In some cases, the La-doped alumina was pre-annealed by heating for approximately 6 days under a 7.1 MPa applied tensile stress in the creep machine

(Applied Test Systems, Inc., Butler, PA). A laser extensometer (LaserMike Inc., Dayton, OH) was used to measure the gauge length, established by SiC flags, as a function of time under load. The stress used in various tests was 50 MPa in a temperature range from 1200°C to 1350°C. Given that the objective of this procedure was to obtain the steady-state creep rate as a function of temperature, it was important to establish that the tested sample was in the secondary creep regime. This was accomplished *a posteriori* by examining the temporal dependence of the strain rate. Further, to confirm the consistency of our results, the creep rates under the same conditions were measured at least twice on a given specimen. In addition, a stress-rupture test was performed at 1250°C and 50 MPa.

Microstructural analysis was used to correlate mechanical behavior with grain size distribution. Grain sizes were measured from the resulting scanning electron micrographs and subsequently analyzed by the LECO 2001 image analysis system (Leco Instruments Ltd., Longueuil, Quebec). This procedure enabled us to carry out a stereological analysis of the microstructures of interest, including a determination of the volume fraction of each grain sections. In addition, bulk density was measured by the classical Archimedes method.

3. RESULTS

Figure 1 (a) shows the temporal evolution of the strain, ε, in the form of a stress-rupture curve at 1250°C and 50 MPa for both Y and La-doped alumina. As is evident from the figure, the Y-doped material was in the steady-state creep regime ($d\varepsilon/dt \sim$ constant) essentially throughout the test. By contrast, the La-Al_2O_3 system exhibited a long primary creep regime followed by a short steady-state regime prior to rupture. This difference in approach to the steady-state is apparent in Fig. 1 (b) in which the strain rate, $\dot{\varepsilon}$, observed during the test is plotted as a function of strain, ε. The contrasting creep behavior of these two materials is quite striking given the observation that both Y and La segregate to grain boundaries.[13-15] In an effort to reduce the primary creep regime,

the La-doped alumina was also pre-annealed at 1250°C under a small load (7.1 MPa) for several days prior to conducting the test. The resulting stress-rupture curve is presented in Fig. 2 and compared to that for the case of no pre-annealing. Clearly, the pre-anneal led to a substantially longer steady-state regime and a negligible primary regime. Furthermore, the steady-state strain rate decreased slightly from 3.2×10^{-8} sec^{-1} to 2.4×10^{-8} sec^{-1} as a result of pre-annealing.

The microstructures of these materials are shown in Fig.3 (a), (b), and (c). The grain structure of the La-doped alumina is seen to be somewhat more elongated compared with that for Y-doped alumina, the former having an (average) aspect ratio of 1.9 ± 0.6, and the latter having an aspect ratio of 1.6 ± 0.5. Further, a number of precipitates, believed to be $Y_3Al_5O_{12}$ (YAG),[20] formed in the Y-doped system in contrast with the La-doped system which was found to have relatively few precipitates ($LaAl_{11}O_{18}$). The average grain size before (after) testing was 2.2 ± 1.0 (2.5 ± 1.1) μm and 1.7 ± 0.8 (1.7 ± 0.8) μm for Y and La-doped alumina, respectively. From these data, it can be seen that, in general, some grain growth occurred in the Y-doped material during the test, whereas the grain sizes in the La-doped material showed little change. Also, from the SEM micrographs, it can be seen that bimodal grain growth occurred in both materials, presumably due to a non-uniform spatial distribution of dopant ions, although the volume fraction of large grains (≥ 6.0 μm diameter) was less than 2.0 % for Y-doped alumina and 1.0 % for La-doped alumina. Thus, we infer that creep properties in these systems are controlled, to a great extent, by the large fraction of small grains present. In addition, an increase in porosity was evident along grain boundaries and at triple junctions for La-doped alumina after creep testing, consistent with the measured density decrease. Specifically, the final porosities of La and Y-doped alumina were approximately 2.6% and 1.5%, respectively, each having an initial porosity of less than 1%.

It remains to compare the creep behavior in these two doped systems. Although the initial microstructures of these materials are somewhat different (Fig.3 (a) and (b)), it was found that the creep strain rate associated with each system was similar, provided that a proper account of differences in grain size is made. In order to compare creep in these materials which have different

average grain size, it was assumed that creep is grain boundary diffusion controlled, consistent with the Coble creep mechanism.[21] Indeed, sintering studies of Y and La doped alumina for the same powders have shown that densification rates are governed by grain boundary diffusion.[16] In doped systems, Y was reported to decrease the oxygen diffusivity at grain boundaries because of precipitation or segregation, with little effect on bulk diffusion.[22] From these considerations, then, we define a normalized strain rate, $[\dot{\varepsilon}]$, which accounts for differences in grain size by

$$[\dot{\varepsilon}] = \left(\frac{1}{d_0/d}\right)^3 \dot{\varepsilon} \quad , \qquad (1)$$

where $\dot{\varepsilon}$ is the measured strain rate, d is the grain size and d_0 is the grain size of a reference material. The normalized strain rates as a function of the (inverse) temperature, T, are shown in Fig.4, for both doped aluminas and pure alumina (initial density > 99 % and grain size $\approx 8.9 \pm 3.0$ μm). The normalized creep rate of pure alumina in this study was very close to values obtained in a previous study on hot-pressed pure alumina from the same starting powder.[9] As seen from the figure, the creep rate was reduced by approximately two orders of magnitude at 1250°C for both materials. From this data the activation energy was found to be 800 kJ/mole for La-doped alumina and 685 kJ/mole for Y-doped alumina, respectively. Thus, one might infer that as the ionic radius of a dopant element increases, the associated activation energy increases.

4. DISCUSSION AND CONCLUSIONS

The stress-rupture tests for the two materials revealed qualitatively different creep behavior. It should be emphasized here that the relatively long primary creep regime in the La-doped material was problematic for the required steady-state analysis, although pre-annealing the sample did

increase the duration of the steady-state (secondary) regime. We have found that a pre-annealing treatment can substantially alter the duration of the primary creep regime. There is, however, to date no comprehensive understanding of the operative primary creep mechanisms in doped alumina. One possibility is a diffusional creep mechanism wherein grain boundary sliding in response to an applied stress generates an internal stress distribution which decays with time, ultimately reaching a steady state.[23] Clearly, the duration of this transient would depend, in detail, on the degree of microstructural heterogeneity.

The length of this regime may, for example, be associated with the redistribution of solute in the system via diffusion. In this case, it is expected that a long pre-annealing treatment can change dopant concentration at some grain boundaries and thereby the primary creep rate. Some other reasons for the success of the pre-annealing treatment may be the promotion of grain growth[24] and/or the modification of glassy layers on grain boundaries. Such layers are thought to be responsible for primary creep in silicon nitride.[25-28] In our study, however, no significant grain growth was detected during the test and no evidence of glassy layers was observed in the TEM. Thus, further work is needed in order to better understand primary creep behavior in these systems.

Density measurements performed before and after the creep tests add still more information to this study. Both the La and Y-doped materials were dense initially. However, as seen in Fig.3 (c), there are several pores around the elongated grain structures in La-doped alumina after the test. This suggests that La-doped alumina is more prone to cavitation than Y-doped alumina. Now, due to relatively low dopant levels and the precipitate composition ($La_2O_3 \cdot 11Al_2O_3$), the La-doped material contained few precipitates. As the Y-doped sample contained many precipitates, as seen in the microstructure in Fig.3 (a), clearly it would be useful to vary the precipitate content of the La-doped material and assess the impact of these precipitates on creep behavior.

Several conclusions can be drawn from this study. The addition of oversized, isovalent cation dopants to alumina results in a dramatic reduction in the creep rate. For the two dopant systems

considered here, Y and La, the creep rates were quite similar despite differing ionic radii ($r_{Y^{3+}}$ = 0.89 Å, $r_{La^{3+}}$ = 1.03 Å) as well as some microstructural differences. It is possible that observed decreases in the creep rate might "saturate" for sufficiently large ions as their mobilities become quite small. Clearly, it would be advantageous to consider other dopants with a range of ionic radii to better correlate ionic size with creep rate. In this regard, future experiments with other trivalent dopants are ongoing and, in addition, a computer simulation study of transport in doped ceramic oxides is currently underway.[29] Such studies will be augmented with other experiments which focus on the control of grain size (by controlling the spatial distribution of dopants) in order to achieve a more uniform microstructure.

ACKNOWLEDGMENT : The authors would like to thank United States Air Force Office for Scientific Research for financial support for this project under contract # F49620-94-1-0284 (monitored by Dr. A. Pechenik). We also thank Dr. J. D. French for his initial efforts for providing the motivation for this work. The efforts of Dr. J. Zhao are gratefully acknowledged for generating pure alumina specimens. Helpful discussions with Drs. J. Bruley and Y. Li are also gratefully acknowledged.

REFERENCES

[1]A. H. Heuer, R. M. Cannon, and N. J. Tighe, "Plastic deformation in Fine-Grain Ceramics"; pp.339-65 in *Ultrafine-Grain Ceramics*, Proceedings of the 15th Sagamore Army Materials Research Conference (Raquette Lake, NY, August, 1968). Edited by J. J. Burke, N. L. Reed, and V. Weiss. Syracuse University Press, Syracuse, NY, 1970.

[2]R. M. Cannon and R. L. Coble, "Review of Diffusional Creep of Al_2O_3"; pp.61-100 in *Deformation of Ceramic Materials*, Proceedings of a Symposium on Plastic Deformation of Ceramic Materials (Pennsylvania State University, July, 1974). Edited by R. C. Bradt and R. E. Tressler. Plenum Press, New York, NY, 1975.

[3]W. R. Cannon and T. G. Langdon, "Review Creep of Ceramics : Part 2. An Examination of Flow Mechanisms," *J. Mater. Sci.*, **23**, 1-20 (1988).

[4]A. H. Chokshi and T. G. Langdon, "Diffusion Creep in Ceramics : A Comparison with Metals"; pp.1205-26 in Defect and Diffusion Forum, Vol.66-9, *Diffusion in Metals and Alloys DIMETA 88.* Edited by F. J. Kedves and D. L. Beke. Sci-Tech Publications, Brookfield, VT, 1990.

[5]P. A. Lessing and R. S. Gordon, "Creep of Polycrystalline Alumina, Pure and Doped with Transition Metal Impurities," *J. Mater. Sci.*, **12**, 2291-302 (1977).

[6]G. W. Hollenberg and R. S. Gordon, "Effect of Oxygen Partial Pressure on the Creep of Polycrystalline Al_2O_3 Doped with Cr, Fe, or Ti," *J. Am. Ceram. Soc.*, **56** [3] 140-7 (1973).

[7]C. Carry and A. Mocellin, "Structural Superplasticity in Single Phase Crystalline Ceramics," *Ceram. Int.*, **13**, 89-98 (1987).

[8]S. L. Korinek and F. Dupau, "Grain Boundary Behavior in Superplastic Mg-doped Alumina with Yttria Codoping," *Acta. metall. mater.*, **42** [1] 293-302 (1994).

[9]J. D. French, J. Zhao, M. P. Harmer, H. M. Chan, and G. A. Miller, "Creep of Duplex Microstructures," *J. Am. Ceram. Soc.*, **77** [11] 2857-65 (1994).

[10]R. S. Gordon, "Understanding Defect Structure and Mass Transport in Polycrystalline Al_2O_3 and MgO via the Study of Diffusional Creep"; pp.418-37 in Advances in Ceramics, Vol. 10, *Structure and Properties of MgO and Al_2O_3 Ceramics*. Edited by W. D. Kingery. American Ceramic Society, Columbus, OH, 1984.

[11]J. D. Cawley and J. W. Halloran, "Dopant Distribution in Nominally Yttrium-Doped Sapphire," *J. Am. Ceram. Soc.*, **69** [8] C195-6 (1986).

[12]E. M. Levin, C. R. Robbins and H. F. McMurdie, *Phase Diagram for Ceramists 1969 Supplement*, The American Ceramic Society, Columbus, OH, 1969.

[13]A. M. Thompson, K. K. Soni, H. M. Chan, M. P. Harmer, D. B. Williams, J. M. Chabala,

and R. Levi-Setti, "Rare Earth Dopant Distributions in Creep-Resistant Al_2O_3," accepted in *J. Am. Ceram. Soc.*

[14]J. Bruley, J. Cho, J. C. Fang, A. M. Thompson, Y. Z. Li, H. M. Chan, M. P. Harmer, "STEM Analysis of Grain Boundaries of Creep Resistant Y and La Doped Alumina," in preparation, *J. Am. Ceram. Soc.*

[15]C.-W. Li and W. D. Kingery, "Solute Segregation at Grain Boundaries in Polycrystalline Al_2O_3"; pp.368-78 in Advances in Ceramics, Vol. 10, *Structure and Properties of MgO and Al_2O_3 Ceramics*. Edited by W. D. Kingery. American Ceramic Society, Columbus, OH, 1984.

[16]J. Fang, A. M. Thompson, M. P. Harmer and H. M. Chan, "Effect of Y and La on the Sintering Behavior of Ultrahigh-purity Al_2O_3," accepted in *J. Am. Ceram. Soc.*

[17]K. Przybylski and G. J. Yurek, "Segregation of Y to Grain Boundaries in Cr_2O_3 and Al_2O_3 Scales," *J. Electrochem. Soc.*, **134** [8B] C469 (1987).

[18]J. Zhao, unpublished work.

[19]D. F. Caroll, S. M. Wiederhorn, and D. E. Roberts, "Technique for Tensile Testing of Ceramics," *J. Am. Ceram. Soc.*, **72** [9] 1610-4 (1989).

[20]M. K. Loudjani, A. M. Huntz and R. Cortes, "Influence of Yttrium on Microstructure and Point Defects in α-Al_2O_3 in Relation to Oxidation," *J. Mater. Sci.*, **28**, 6466-73 (1993).

[21]R. L. Coble, "A Model for Boundary Diffusion Controlled Creep in Polycrystalline Materials," *J. Appl. Phys.*, **34**, 1679-82 (1963).

[22]M. Le Gall, A. M. Huntz, B. Lesage, C. Monty, and J. Bernardini, "Self-diffusion in α-Al_2O_3 and Growth Rate of Alumina Scales formed by Oxidation : Effect of Y_2O_3 Doping," *J. Mater. Sci.*, **30**, 201-11 (1995).

[23]H. J. Frost and M. F. Ashby, *Deformation-Mechanism Maps*; pp.117-20. Pergamon Press, Oxford, England, 1982.

[24]A. H. Chokshi and J. R. Porter, "Analysis of Concurrent Grain Growth During Creep of Polycrystalline Alumina," *J. Am. Ceram. Soc.*, **69** [2] C37-9 (1986).

[25]C. J. Gasdaska, "Tensile Creep in an *in Situ* Reinforced Silicon Nitride," *J. Am. Ceram. Soc.* **77** [9] 2408-18 (1994).

[26]T. Ohji and Y. Yamauchi, "Tensile Creep and Creep Rupture Behavior of Monolithic and SiC-Whisker-Reinforced Silicon Nitride Ceramics," *J. Am. Ceram. Soc.*, **76** [12] 3105-12 (1993).

[27]S. M. Wiederhorn, B. J. Hockey, D. C. Cranmer and R. Yeckley, "Transient Creep Behavior of Hot Isostatically Pressed Silicon Nitride," *J. Mater. Sci.*, **28**, 445-53 (1993).

[28]M. N. Menon, H. T. Fang, D. C. Wu, M. G. Jenkins, and M. K. Ferber, "Creep and Stress Rupture Behavior of an Advanced Silicon Nitride : Part II, Creep rate Behavior," *J. Am. Ceram. Soc.*, **77** [5] 1228-34 (1994).

[29]J. Cho, J. M. Rickman, M. P. Harmer, H. M . Chan and J. Bruley, "Creep Behavior of Doped Aluminum Oxide : Experimental Results and Computer Simulation"; pp.1839-51, Proceedings of 1996 World Federation Meeting of Korean Scientists and Engineers (Seoul, Korea, June, 1996), Korean Federation of Science and Technology Societies, Seoul, 1996.

FIGURE CAPTIONS

Fig.1 (a) Stress-rupture behavior of La and Y-doped alumina at 1250 °C and 50 MPa. (b) The corresponding plot of strain rate vs. strain, which reveals the steady-state (minimum) creep regime.

Fig.2 The effect of a pre-anneal (with stress of 7.1 MPa) on stress-rupture curve of La-doped alumina. For reference, the stress rupture behavior without pre-annealing is also shown. The stress was 50 MPa and the test temperature was 1250 °C.

Fig.3 Microstructures of Y and La-doped alumina. (a) Al_2O_3 + 1000 ppm Y, secondary electron image (before testing) (b) Al_2O_3 + 500 ppm La, secondary electron image (before testing) (c) Al_2O_3 + 500 ppm La, backscattered electron image with higher magnification than (a) and (b) (after testing).

Fig.4 Arrhenius plot of normalized creep rates for Y and (annealed) La-doped alumina and pure alumina at 50 MPa. The plots were normalized to the same grain size. Q is the activation energy (kJ/mole).

(a)

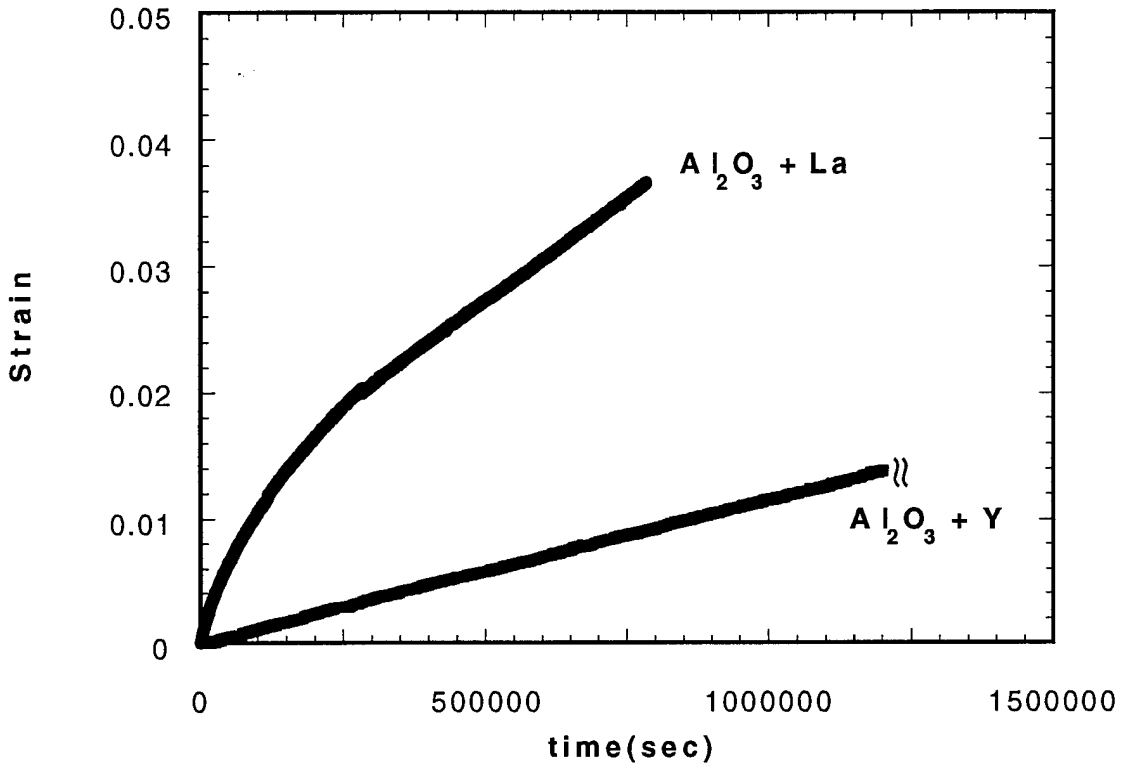

(b)

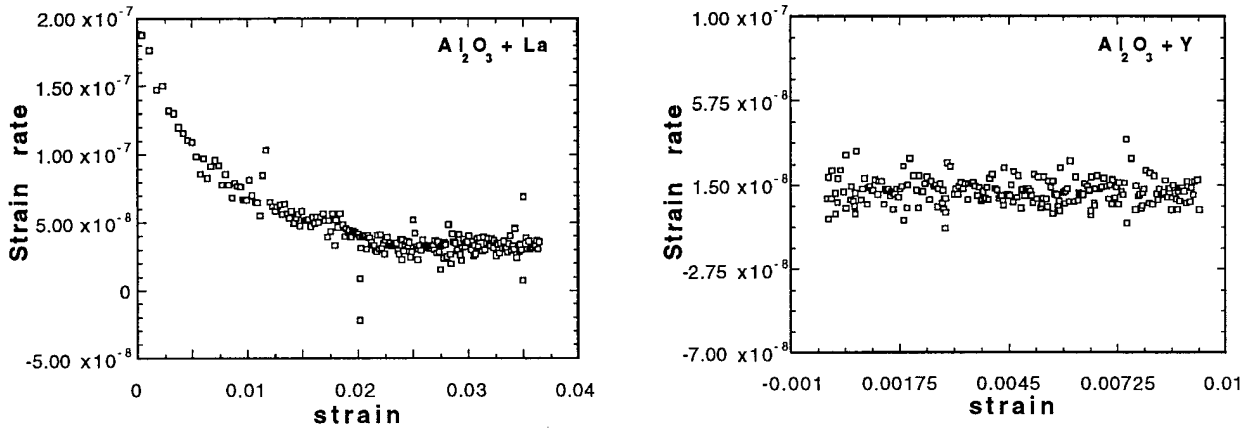

Fig. 1. (a) Stress-rupture behavior of La and Y-doped alumina at 1250 °C and 50 MPa. (b) The corresponding plot of strain rate vs. strain, which reveals the steady-state (minimum) creep regime.

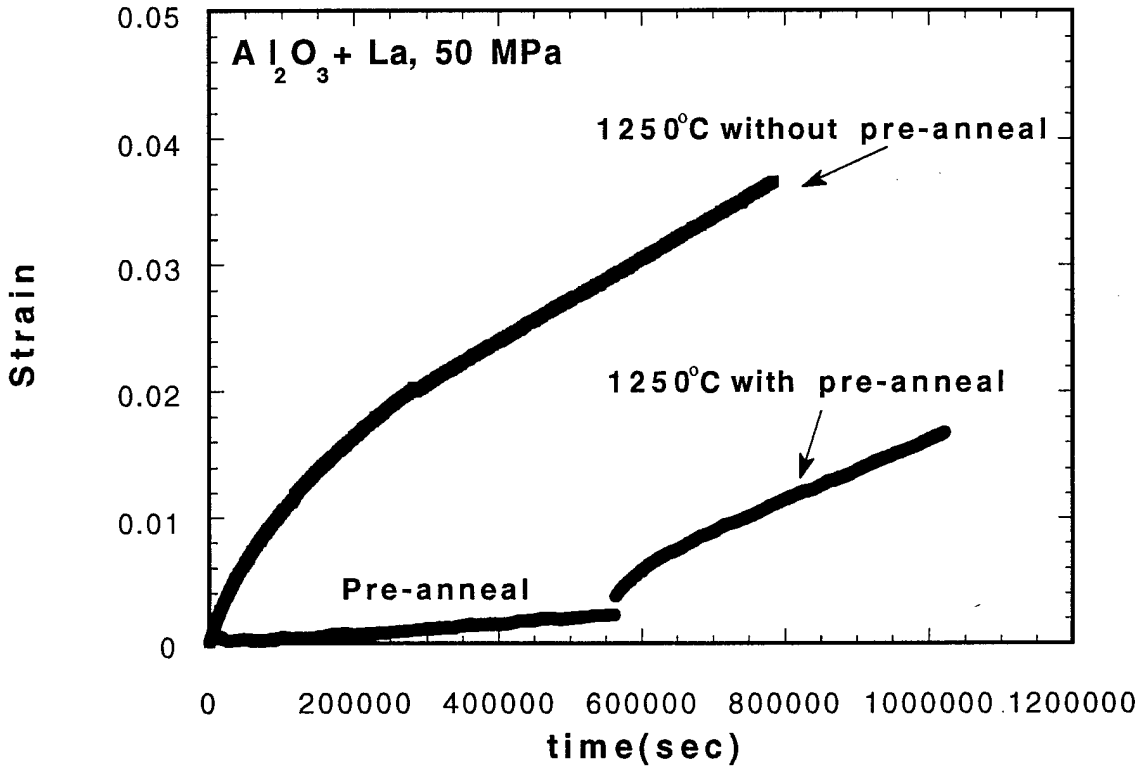

Fig.2. The effect of a pre-anneal (with stress of 7.1 MPa) on stress-rupture curve of La-doped alumina. For reference, the stress-rupture behavior without pre-annealing is also shown. The stress was 50 MPa and the test temperature was 1250 °C.

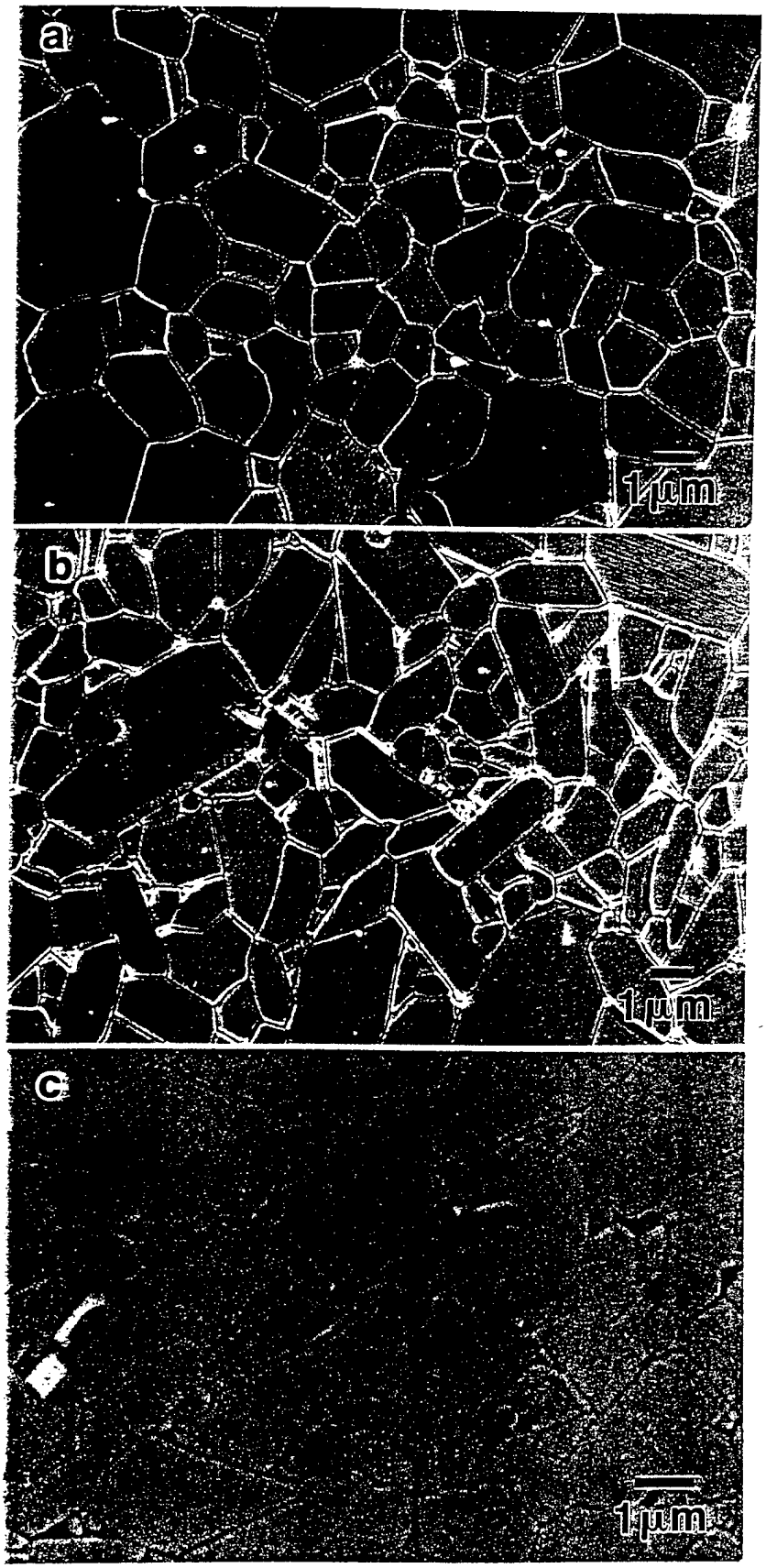

Fig.3. Microstructures of Y and La-doped alumina. (a) Al_2O_3 + 1000 ppm Y, secondary electron image (before testing) (b) Al_2O_3 + 500 ppm La, secondary electron image (before testing) (c) Al_2O_3 + 500 ppm La, backscattered electron image with higher magnification than (a) and (b) (after testing).

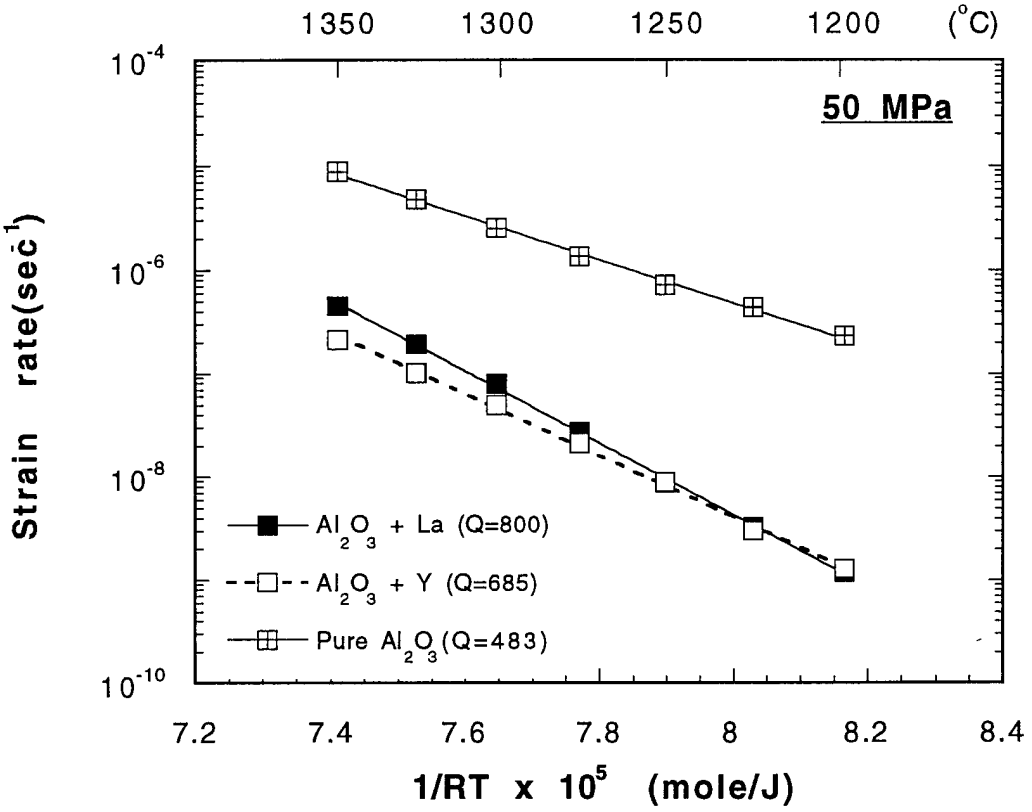

Fig.4. Arrhenius plot of normalized creep rates for Y and (annealed) La-doped alumina and pure alumina at 50 MPa. The plots were normalized to the same grain size. Q is the activation energy (kJ/mole).

Section 1.4

STEM Analysis of Grain Boundaries of Creep Resistant Y and La Doped Alumina

by

J. Bruley, J. Cho, J. Fang, A. M. Thompson, H. M. Chan. M. P. Harmer,

To be Published in Journal of the American Ceramic Society

STEM Analysis of Grain Boundaries of Creep Resistant Y and La Doped Alumina

J. Bruley, J. Cho, J.C. Fang, A.M. Thompson, Y.Z. Li, H.M. Chan, M.P. Harmer

Department of Materials Science and Engineering,
Whitaker Laboratory,
Lehigh University,
Bethlehem, Pa 18015, USA

To be submitted to: J. of Materials Research

Abstract

High spatial resolution analytical electron microscopy using energy dispersive x-ray (EDX) and electron energy loss spectrometry (EELS) of Y and L doped alumina material has been carried out to ascertain the level of segregation of these impurities to grain boundaries. Line profile analyses indicate that the segregation is confined to a layer narrower than 3 nm. Similar amounts of excess solute are observed in both cases, 4.5 at/nm^2. Assuming all the segregant is uniformly distributed within $\pm$ 0.5 nm of the boundary, this excess corresponds to 9 $\pm$ 3 at. %. Examination of the spatially resolved electron energy-loss near-edge structures (ELNES) on the Al L_{23} edge in both systems point to a loss in octahedral symmetry and slight Al-O bond-length expansion. No significant change is noted in the O K edge.

September 6, 1996

Introduction

The controlled doping of ultra-high purity alumina with small amounts (< 1000 ppm) of rare earth elements, such as La and Y, dramatically alters properties such as sintering and creep rates [1-4]. It is also noted that similar dopants in many metal alloy systems also influence the high temperature oxidation properties of those alloys [5]. Because of the low solubility of these elements in Al_2O_3, most studies have pointed to grain-boundary segregation as critical which suggests that diffusion along the boundaries plays a key role in controlling the properties. The effect of lattice strain energy through solute ion misfit and the presence and role of a space-charge layer due to the accumulation of charged point defects in the vicinity of boundaries are factors that influence transport properties [6-11].

By measuring grain boundary segregation of variously doped (including La and Y) alumina samples using EDX in the scanning transmission electron microscope (STEM), Li and Kingery [12] concluded that the chief driving force for segregation of isovalent ions was due to atomic misfit strain. Recent calculations are in accord with this picture [4, 13]. Recently it was demonstrated that Y doping enhances the population of special "near coincidence" boundaries in hot-pressed alumina [1, 14]. Y was found segregated to all grain boundaries, being a maximum on dense $(01\bar{1}2)$ planes. Even in apparently clean boundaries, they reported significant segregation to grain-boundary dislocation cores. On basal (0001) planes there is found a reduced level of Y but a significant amount of Si.

Thompson et al. [3] made use of a scanning ion microscope (SIMS) to vividly demonstrate the widespread uniformity of grain-boundary segregation of La and Y doped alumina. Qualitatively, the images indicate that segregation is isotropic with very few boundaries denuded of segregant. Although providing such elemental maps with parts per million sensitivity, the technique is unfortunately not yet reliable for quantification and offers inadequate lateral spatial resolution (of the order of 0.1 μm) to enable modeling of grain boundary structures. Strain tests made on the same material showed a 2 order of magnitude reduction in creep-rate.

The goal of the present work is to use EDX and electron energy loss spectroscopy (EELS) in the dedicated STEM, to quantitatively analyze the segregation profile in a number of grain boundaries in the same

doped high purity alumina examined earlier [2-4]. A second aim is to investigate the coordination environment of the aluminum and oxygen ions in the vicinity of the boundary using spectrum-line profiling. This is accomplished by examining the characteristic near edge structures of the elemental ionization edges.

Method

The two samples selected for this AEM analysis were produced for and described in earlier studies [2-4]. In brief, the first was high purity commercial alumina powder (Sumitomo AKP-53), doped with 1000 atomic ppm, and hot pressed at 1475°C in vacuum to full density (>99% theoretical density). The microstructure of this sample indicated the presence of YAG precipitates and an average alumina grain size of 2 ± 1 μm. The second sample was doped with 500 ppm La, pressed at 1450°C and also observed to contain second phase particles. The average grain size of the La-doped sample is 1.7 ± 0.8 μm. There is evidence for some elongated grains. The presence of second phase in both systems indicates that in both cases the solubility limit of both the bulk and grain boundaries had been reached. The samples were prepared for the AEM by conventional polishing, dimpling followed by ion-milling. Examination of the material in the TEM failed to reveal the presence of an amorphous or other grain boundary phases.

The analytical microscopy was carried out in the VG microscopes' HB603 and the HB501 dedicated STEMs operating at 300 keV and 100 keV, respectively. The 300 keV microscope is fitted with a Link systems' windowless Si(Li) detector and enables the highest spatial resolution and best detection sensitivity for EDX analysis, and the 100 keV instrument, fitted with a Gatan parallel EELS detector, was used predominantly for the EELS analysis. In both cases the machines were operated to provide a beam current of the order of 0.5 nA with a probe diameter of about 1.0 nm, though these values were not explicitly determined for this study. For typical foil thicknesses of about 50 nm the electron beam broadening for 300 keV electrons is expected to be about 2 nm. To accomplish the analysis only those boundaries that appeared flat and edge-on to the beam were examined. Two analytical procedures were followed. The first involved acquiring spectral data whilst simultaneously scanning the probe over a small square area of sample (typically 64 nm^2). The second involved data acquisition at each point along a line across the boundary using Gatan's Digiscan to control the beam

position. EELS "spectrum-lines" were acquired using a custom function running within Gatan's EL/P software, written by G. Duscher at the Max-Planck Institut, Stuttgart.

Results

Compositional Information

1) Y-doped alumina

Figure 1 shows a typical EDX spectrum recorded with the beam located over a grain boundary compared with the spectrum recorded under identical conditions from the region besides. The high-angle ADF (or "Z-contrast") image taken of the same boundary exhibits bright contrast at the boundary reflecting the segregation of high atomic number yttrium to the boundary plane, figure 2. A bright particle of 2nd phase is seen pinning the grain boundary in the image. Similar data was recorded at 7 other grain boundaries, each indicating similar levels of segregant in qualitative agreement with the SIMS data. No distinction is made here between special and general boundaries, though studies are currently in progress to ascertain if there exists in these materials a higher than expected number of special boundaries as suggested by Bouchet and co-workers [14]. Quantification of the EDX spectra is accomplished by application of the Cliff-Lorimer equation [15]. The Y-to-Al atomic sensitivity k-factor for the lines was determined using $Y_3Al_5O_{12}$ powder (Alfa Aesar) as a standard and found to be $k_{YAl} = 0.53$. The mass absorption correction factor is estimated to be greater than 0.97 for a 50 nm thick foil and is therefore ignored. A summary of the analyses is given in Table 1. To convert the measured intensity ratio, (I_i/I_{Al}), to a segregated grain boundary excess amount a simple geometric model is used. The illuminated volume of material is taken to be the thickness multiplied by the irradiated area, d^2, where d is taken to be the larger of the dimension of the beam raster or probe size. The area of grain boundary illuminated is taken to be equal d multiplied by the foil thickness. The grain boundary excess, Γ_i, of element i, is then given by

$$\Gamma_i = d \cdot \rho_{Al} \cdot k_{iAl} \cdot (I_i/I_{Al}) \qquad 1,$$

where ρ_{Al} is the atomic density of Al in α-Al_2O_3. The data in column 4 represents the amount of Y assuming that is in homogeneously

distributed within a 1 nm thick boundary layer. The average Y excess content of the boundary is found to be 4.4 ± 1.5 atoms per nm^2 which is equivalent to a cation fraction of 9 at. % for a 1 nm thick grain boundary layer. No other significant level of impurity segregant was detected (sensitivity limit ≈ 0.5 at. % in 1 nm).

Figure 3 shows a EELS spectrum revealing the onset of the weak Y $L_{2,3}$ edge at 2080 eV superimposed on an intense background. The Al- K edge onset is located at 1560 eV. Note that because of the very low signal to background ratio of the Y (S/B < 0.05) visibility of the edge is poor even though its signal to noise is similar to the EDX spectrum in figure 1 (S/N ≈ 30). A consequence of the low S/B ratio is that conventional procedures to remove the background, such as power-law fitting, is not possible. To view and determine the integrated counts in the edge the background is modeled using a standard spectrum taken under identical conditions, in this case from the neighboring alumina matrix. The residual given by the difference between the boundary and standard spectra is equivalent to forming a spatial-difference. The two dimensional raw spectrum-line data has energy-loss along one axis, and beam-coordinate along the second. The Y spatial distribution is determined from the spectrum-line by convoluting a one dimensional top-hat filter with the beam position coordinate. In the limit of a very narrow filter this process is equivalent to generating a 2nd derivative with respect to beam position and is sensitive to slope changes accompanying the weak edge. Figure 4 represents a line profile generated from the 2nd difference Y-edge intensity spectrum-line, integrated over a 20 eV window and shows the position of the grain boundary.

2) La-doped alumina

As in the case of Y, La was found to be segregated at all boundaries examined. A line profile extracted from a line series of EDX spectra taken across one such boundary shows that the La is localized to a region of full-width-half-height equal to 3 nm, figure 5. The width is probably limited by beam broadening. The quantitative analysis for the amount of La at 8 separate boundaries is summarized in table 2. The La-to-Al atomic k-factor was determined to be $k_{LaAl} = 0.51$ using as a standard $LaAlO_3$ powder (Alfa Aesar). Absorption and fluorescence effects are ignored. We find the average La excess of the boundary is 4.5 ± 0.9 atoms/nm^2, which is equivalent to 10 ± 2 percent of the cation population uniformly distributed within a 1 nm thick layer. In addition to the presence of La, a small concentration

of Si was detected segregated to the boundary, as seen in figure 5. The amount was estimated to be about 2 at. % within ± 0.5 nm of the boundary and is too small to be associated with a continuous siliceous intergranular layer. The line-profile showing La segregation determined using EELS is slightly narrower than EDX, 1.5 nm.

Near-Edge Structure Analysis

In addition to providing compositional information, EELS is able to provide the density of unoccupied electronic states lying above the Fermi energy, through the fine structures on the ionization edges. Through the dipole selection rule, the energy-loss near-edge structures (ELNES) of the Al $L_{2,3}$ and the O K edges from the same grain boundary reveals the site specific Al s and d and O p states [16-22]. These edges have been acquired for the La doped material.

Figure 6 displays a spectrum-line series, consisting of 30 spectra of the Al $L_{2,3}$ edge recorded along a line perpendicular to the grain boundary. Figure 7 shows the O-K edge series recorded across the same 30 nm long line. In both cases, the data shown has been processed to remove the smooth power-law background. The boundary plane is readily located at the region corresponding to the reduction in intensity of the Al and O edges, which is probably due to slight grain boundary grooving. Preliminary inspection of the O series does not apparently show up any grain-boundary dependent component. On the other hand the Al L_{23} edge is slightly modified by the presence of the boundary. Very similar spectral structure was reproduced at other boundaries. The initial peak intensity at 79 eV, corresponding to the 2p core state to 3s conduction band transition, appears somewhat attenuated at the boundary relative to the remaining ELNES absorption features about 5 eV above threshold at 83 eV.

To discern if such qualitative observations are significant, a principal component analysis (PCA) is performed on the O K-edge and the Al $L_{2,3}$ edge data. PCA, or factor analysis is a matrix transformation tool that results in a list, in order of significance, of a series of principal components (Eigenvectors) of the original data set [23]. An assumption is made that the data can be described by a linear combination of components. Each Eigenvector has its Eigenvalue, which is proportional to the amount of variance in the data. The Eigenvectors are not themselves physically interpretable but may be used to represent a projection of the original data onto a minimal

basis set. This "new" vector space enables one to automatically identify the presence of localized spectral changes without a priori assertion that such changes exist. To indicate the significance of the 30 resultant components the two way F-test was performed on the reduced Eigenvalues. Only those components with F value exceeding the tabulated value at 5 % significance are considered. For the Al edge data the first three Eigenvectors are significant components whereas the O edge data has only two. The PCA was carried out using MATLAB software (Mathworks Inc). Previous EELS studies using PCA of a spinel alumina grain boundary were able to expose a grain boundary sensitive component [24].

The projection of the data onto these principal axes yields the loading (or coordinates) of each spectrum in abstract factor space. The loading of the Al and O spectrum-lines on the principal axes are plotted as a function of beam position in figures 8 and 9 respectively. The first principal component of the Al data is uniformly distributed across the whole line, whilst the 2nd component shows a position dependence being most intense at the grain boundary and almost zero in the bulk on either side of the boundary. The full width of the profile is about 3 to 4 pixels wide, corresponding to an approximate width of about 3 to 4 nm which is similar to the chemical width of the boundary. The 3rd principal component is position independent and therefore not related to the grain boundary. The two oxygen principal components show no interface dependence. It is noted here that a preliminary investigation of the ELNES of the Y doped system indicates similar changes to the Al edge at those boundaries. To help interpret the observed spectral changes of the Al L_{23} ELNES at grain boundaries, the data is compared to the ELNES of two lanthanum aluminate compounds, $LaLaO_3$ and $LaAl_{11}O_{18}$. These Al $L_{2,3}$ edges are shown in figure 10.

Discussion

Comparison of average composition data measured here with those reported by SIMS shows a agreement for the Y-doped sample but is a factor of 5 higher for the La doped sample. Such a difference is higher than could be anticipated by random errors in the experiments. This discrepancy may, in part, be due to the difference in grain boundary sampling. For the SIMS technique, data is acquired over micron sized regions containing several grains whilst for these AEM measurements, only a limited subset of boundaries

are present as flat and edge-on to the electron probe. Another further contribution to the different values reported could lie in an inaccuracy of the SIMS sensitivity calibration. According to Thompson et al. [3] the amount of segregant is determined by measuring the boundary signal relative to the total signal collected over a large area of sample. This ratio must then be multiplied by the nominal concentration of dopant to give the grain boundary content. If the local dopant concentration within the sampled region were higher than the global content then the grain boundary content may be underestimated by a significant factor.

A factor of 5 difference between the SIMS and EDX data for La segregation has a consequence for modeling the grain boundary structure. A guide to the significance of the actual grain boundary excess is seen in the "effective width" of a continuous grain boundary film assuming the local structure and density of two possible stoichiometric compounds $LaAlO_3$ or $LaAl_{11}O_{18}$. The thicknesses are given in table 3. A layer thickness less than the atomic dimension merely represents the possibility of sub-monolayer coverage. Comparison of these widths to the lattice parameters for the La-Al-O compounds suggest that there is not enough segregant to form a full unit cell thickness of any known compound, but there might be enough to forma s single plane or two of characteristic structure-units. The discrepancy between the analytical techniques might be resolved by performing atomic resolution microscopy on the boundaries. An investigation to search for characteristic structure units of a lanthanum aluminate phase is in progress.

The grain boundary dependence of the 2nd principal component of the PCA of the Al L_{23} spectrum-line profile demonstrates the presence of significant bonding changes to the Al cations in the neighborhood of the boundary. The spatial extent of these changes correlates with the chemical profile. Such structure and bonding changes will clearly influence the population and mobility of defects near the boundary and are therefore important to materials properties. By comparing the ELNES fingerprints one can immediately exclude the formation of the $LaAlO_3$ phase. Covalent overlap between Al s and d states with the narrow atomic-like f states of La leads to the sharp onset of the Al $L_{2,3}$ edge in $LaAlO_3$ which is absent in the boundary spectrum. At the boundary the Al edge onset is much less peaked. This observation is reasonable since in the alumina rich phase field formation of a La-rich 2nd phase would be thermodynamically unlikely. The edge structure does bear

some resemblance to the Al in the $LaAl_{11}O_{18}$ phase. This is consistent with the formation of up to 1 nm of the Al-rich second phase, or the equivalent of about one half of a unit cell's thickness. It is tempting to speculate that grain boundary saturation of La corresponds to the formation of a monolayer of characteristic lathanate structure units.

A simpler picture is that of direct La substitution for Al at the boundary. Such substitution of the large La cation (ionic radius 1.0Å) might be expected to locally "separate" the (0001) close-packed O basal planes, thereby lowering the octahedral symmetry about the smaller neighboring Al ions (ionic radius 0.51Å). Theory predicts this would lead to mixing of the 3s and 3p final states in the conduction band, which would remove the sharp edge onset characteristic of $Al\text{-}O_6$ structural units. Such a diffuse edge is observed in gamma alumina [25], inverse spinel [18], and pure alumina grain boundary structures [19] and is a characteristic of tetrahedral units. Further evidence of such dilatation is given by the position of the shape resonance at about 100 eV. The energy of this resonance above the Fermi-energy has been shown to scale inversely with the square of the average Al-O bond length. Assuming the Fermi energy remains constant across the boundary and is fixed in the middle of the band-gap, the resonance for bulk alumina is 25.1 eV whilst that at the boundary is 23.6 eV. According to the inverse quadratic scaling this 1.5 eV reduction corresponds to a local 3 % Al-O bond-length expansion.

We note that similar changes in the oxygen data are absent. At first this is a little surprising as one might have expected to see some hybridization between the oxygen p states with the La f states. An electronic structure model will be needed to affirm that with only 10 at % of segregant the oxygen density of states is unaffected in the boundary region within the detection sensitivity of the EELS technique.

The role of the segregating ions in affecting creep may be two-fold. First the large misfitting ions alter the structure of the boundary which will modify possible diffusion paths, one view is that the diffusion paths are "blocked" by the segregation of large ions. This will result in reduced defect mobility. Secondly, the segregation appears to modify the Al ions' local bonding. Such a change in its binding energy will alter the population of point defects. Both defect

mobility and population density are factors that control grain boundary diffusivity.

Conclusions

Chemical composition profiles indicate that segregation of Y and La is localized to within about 2 nm of the grain boundary, i.e about a single unit cells width. In both cases, the amount is about 9 at % within 1 nm of the boundary which is consistent with the formation of a single layer of Al-rich 2nd phase, though none has yet been confirmed. Modification of the Al $L_{2,3}$ near-edge structure for the La-doped sample indicates a significant alteration in the cation bonding with a 3 % Al-O bond length expansion. With such changes to the grain boundary structure and cation binding energy, one would anticipate a significant alteration in the diffusional creep properties as reported in the literature.

Acknowledgments

Financial support for this project has been provided by the United States Office for Scientific Research under contract number F49620-94-1-0284 . Discussions with Drs. K. Soni, J. Rickman are gratefully acknowledged.

Tables

Table 1: Grain boundary EDX analysis of Y doped Al_2O_3

N_Y/N_{Al}	d (nm)	Γ_Y (at./nm^2)	ρ_Y/ρ_{Al} in 1 nm
0.0046	12	2.6	0.06
0.0020	43	4.1	0.08
0.0035	43	7.1	0.13
0.0027	43	5.5	0.12
0.0117	4	2.2	0.05
0.0556	2	5.2	0.11
0.0509	2	4.8	0.10
0.0420	2	4.0	0.08
		<4.4 ± 1.5>	**<0.09 ± 0.03>**

ρ_{Al}= 47.1 at/nm^3,
Γ_{Al} on (0006) in α-Al_2O_3 = 10 at./nm^2

Table 2: Grain Boundary EDX Analysis of La doped Al_2O_3

N_{La}/N_{Al}	d (nm)	Γ_{La} (at./nm^2)	ρ_{La}/ρ_{Al} in 1 nm
0.011	8	4.1	0.09
0.010	8	3.8	0.08
0.013	8	4.9	0.10
0.015	8	5.7	0.12
0.015	8	5.7	0.12
0.026	4	4.9	0.10
0.012	5	2.8	0.06
0.047	2	4.4	0.09
		<4.5 ± 0.9>	**<0.10 ± 0.02>**

Table 3: Thickness of Lanthanum Aluminate Phases for Mean Coverage Measured by SIMS and AEM techniques

	SIMS Measurement (2at%)	AEM Measurement (9 at. %)
$LaAlO_3$ (cubic: a_0 = 3.8Å)	0.04 nm	0.2 nm
$LaAl_{11}O_{18}$ (hexagonal: a_0=5.5Å c=22Å)	0.2 nm	1.0 nm

(thickness < 0.2 nm corresponds to sub-monolayer coverage)

Figure Captions

figure1: EDX of Y doped boundary
figure 2: ADF image of Y doped sample
figure 3: EELS of Y doped boundary
figure 4: Spectrum 2nd-difference profile
figure 5: EDX/EELS Profile of La-doped alumina
figure 6: Spectrum-line of Al $L_{2,3}$ edge in La-doped alumina
figure 7: Spectrum-line of Al $L_{2,3}$ edge in La-doped alumina
figure 8: Line profile of Al Principal Components (Eigenvectors)
figure 9: Line profile of O Principal Components
figure 10: Spectra of grain boundary, α-Al_2O_3 and standard La-Al-O compounds

References

[1] S. Lartigue-Korinek and F. Dupau, Acta Metall et Mater. 42 (1994) 293.

[2] J.C. Fang, A.M. Thompson, M.P. Harmer and H.M. Chan. in *SIntering 95*. 1995.

[3] A.M. Thompson, K.K. Soni, H.M. Chan, M.P. Harmer, D.B. Williams, J.M. Chabala and R. Levi-Sitti, J. Am. Cer. Soc. 1996)

[4] J. Cho, M.P. Harmer, H.M. Chan, J.M. Rickman and A.M. Thompson, J. Am. Cer. Soc. 1996 (submitted))

[5] M.L. Gall, A.M. Huntz, B. Lesage, C. Monty and J. Bernardini, J. Mater. Sci. 30 (1995) 201.

[6] K.L. Kliewer and J.S. Koehler, Phys Rev. 140 (1965) 1226.

[7] M.F. Yan, R.M. Cannon and H.K. Bowen, J. Appl. Phys. 54 (1983) 764.

[8] S.K. Tiku and F.A. Kröger, J. Amer. Cer. Soc. 63 (1980) 183.

[9] R.L. Coble, J. Appl. Phys. 34 (1963) 1679.

[10] R.M. Cannon, W.H. Rhodes and A.H. Heuer, J. Am. Cer. Soc. 63 (1980) 46.

[11] K.R. Venkatachari and R. Raj, J. Am. Ceram. Soc. 69 (1986) 135.

[12] C.W. Li and W.D. Kingery, in *Advances in Ceramics*, W.D. Kingery, Editor. 1984, American Ceramic Society: Columbus, OH. p. 368.

[13] M. Exner and M.W. Finnis, Materials Science Forum 207-209 (1996) 225.

[14] D. Bouchet, F.Dupau and S. Lartigue-Korinek, Materials Science Forum 207-209 (1996) 205.

[15] J.I. Goldstein, D.B. Williams and G. Cliff, in *Priciples of Analytical Electron Microscopy*, D.C. Joy, A.D. Romig andJ.I. Goldstein, Editor. 1986, Plenum: New York. p. 155.

[16] A. Balzarotti and A. Bianconi, Phys. Stat. Sol. (b) 76 (1976) 689.

[17] A. Balzorotti, F. Antonangeli, R. Girlanda and G. Martino, Solid State Communications 44 (1982) 275.

[18] J. Bruley, M.W. Tseng and D.B. Williams, Microsc., Microstruct. and Microanal. 6 (1995) 1.

[19] J. Bruley, Microscopy, Microanalysis, Microstructures 4 (1993) 23.

[20] R. Brydson, H. Sauer, W. Engel and E. Zeitler, Microsc. Microanal. Microstr. 2 (1991) 159.

[21] R. Brydson, H. Sauer, W. Engel, J.M. Thomas and E. Zeitler, J. Chem. Soc. Chem. Commun. 15 (1989) 1010.

[22] P.L. Hansen, D.W. McComb, R. Brydson and I. Richardson, Microsc., Microanal. & Microstruc. XX (1994) xx.

[23] E.R. Malinowski and D.G. Howery, *Factor Analysis in Chemistry*. 1989, Malabar, Fl: Robert E. Krieger.

[24] S.J. Splinter, J. Bruley and D.A. Smith. in *Microscopy and Microanalysis 1995*. 1995. Kansas City: Jones and Begell.

[25] I.A. Brytov and Y.N. Romaschenko, Sov. Phys. Solid State 20 (1978) 384.

Y segregation to Al_2O_3 grain boundary

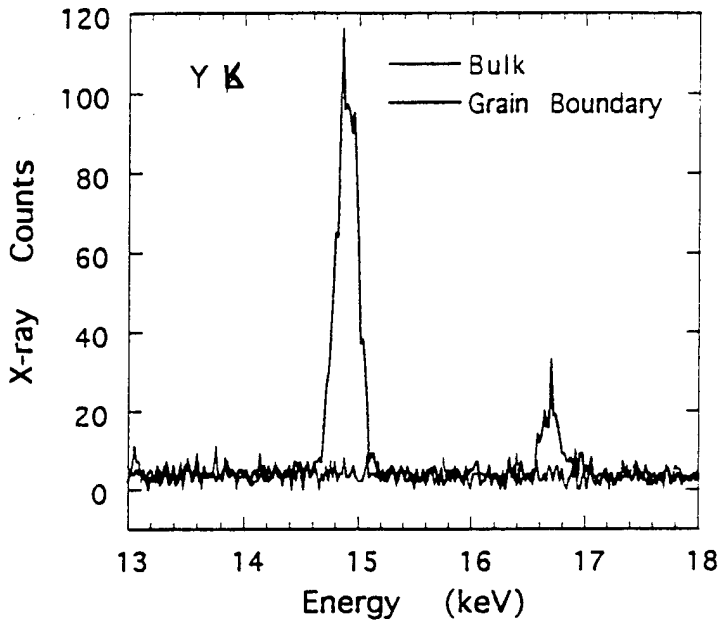

Fig 1

fig 2

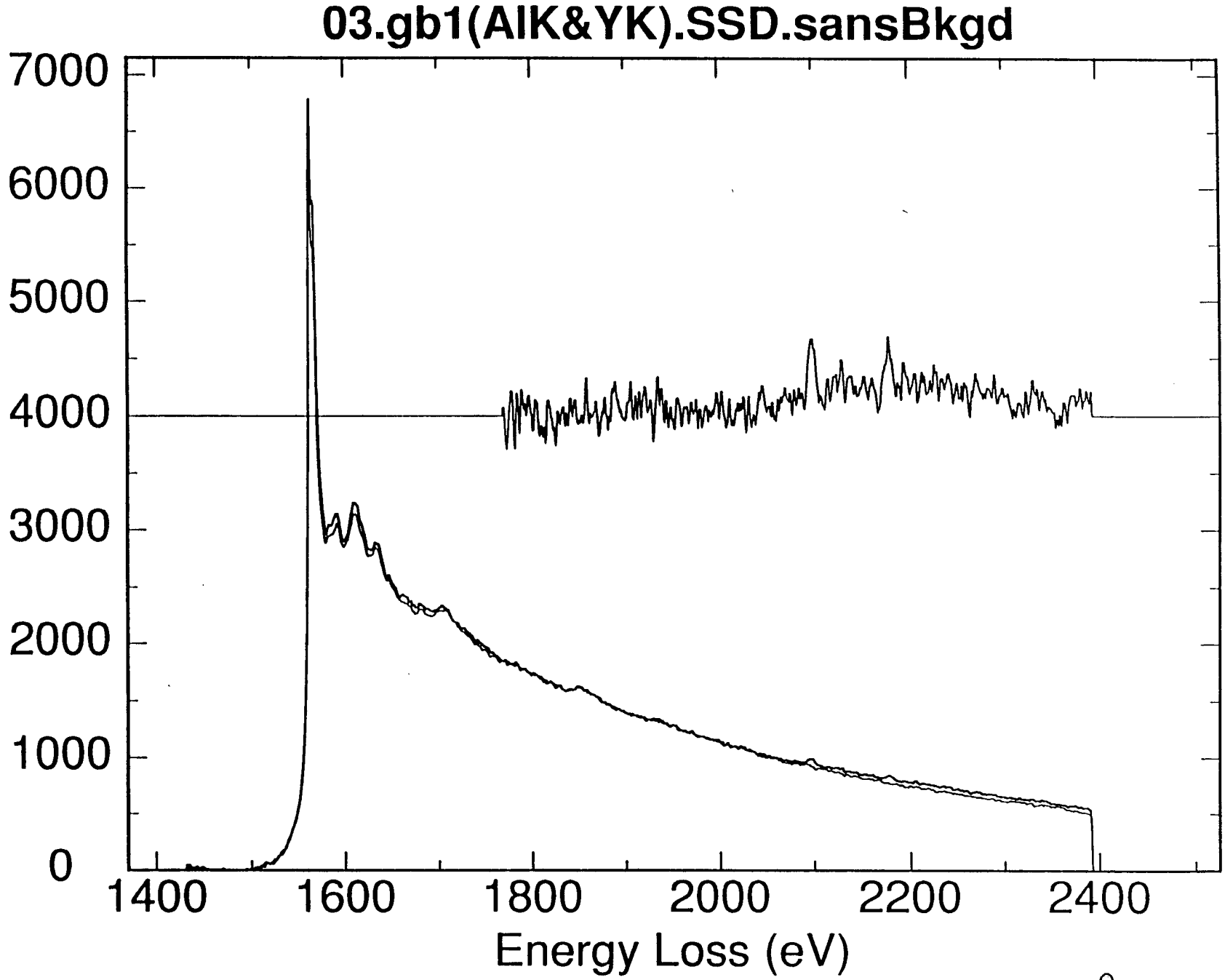
03.gb1(AlK&YK).SSD.sansBkgd
7000
6000
5000
4000
3000
2000
1000
0
1400
1600
1800
2000
2200
2400
Energy Loss (eV)

fig 3

EELS Profile

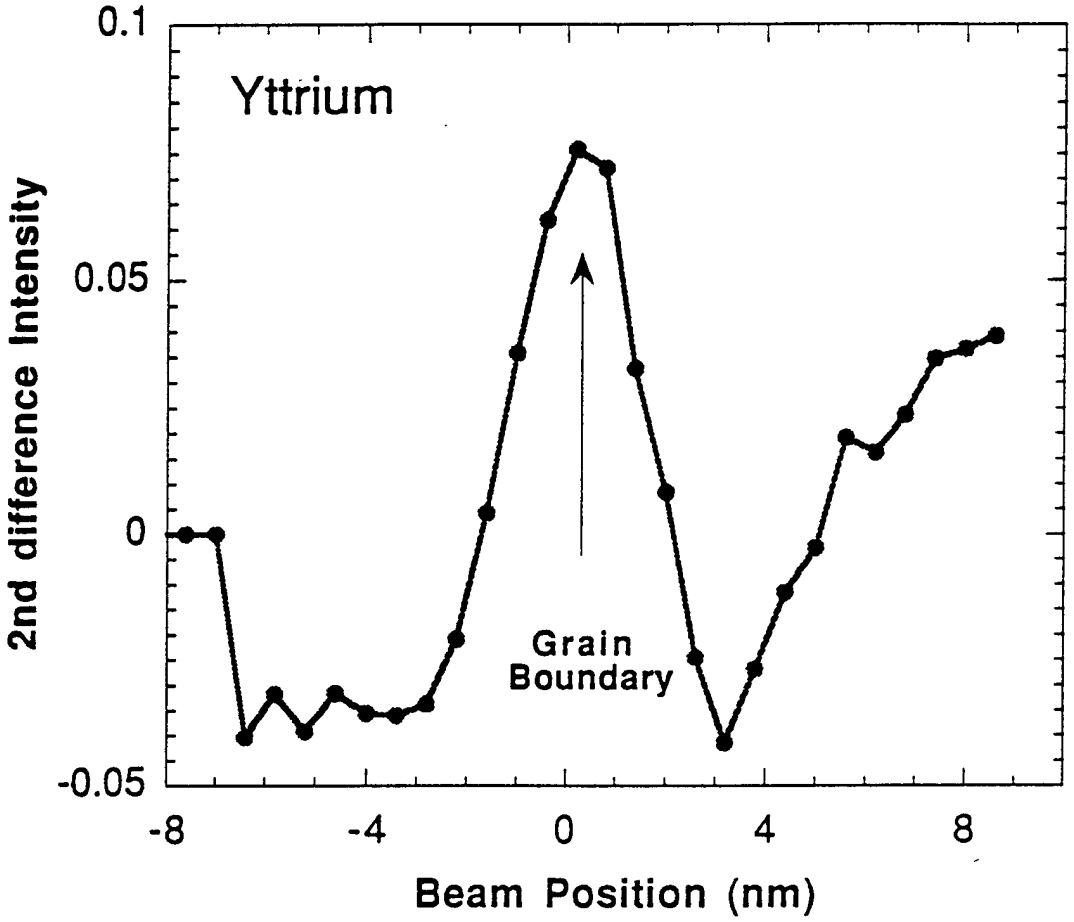

Fig 4

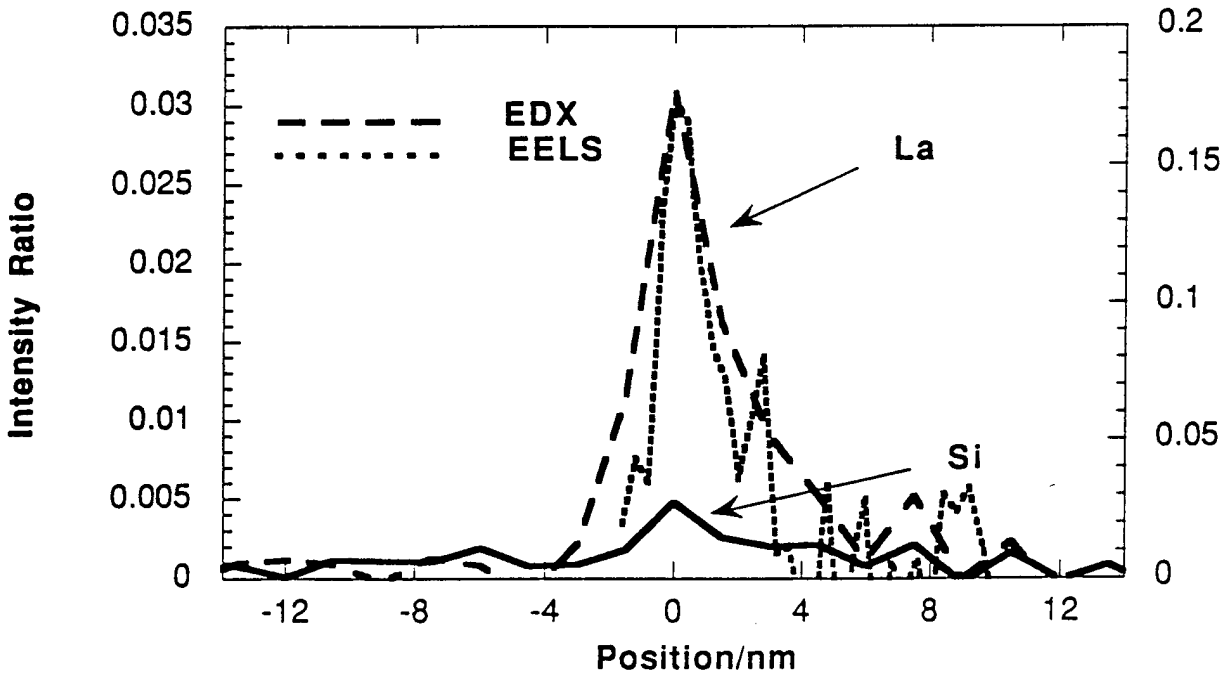
Intensity Ratio
0.035
0.03
0.025
0.02
0.015
0.01
0.005
0
0.2
0.15
0.1
0.05
0
EDX
EELS
La
Si
-12
-8
-4
0
4
8
12
Position/nm

fig 5

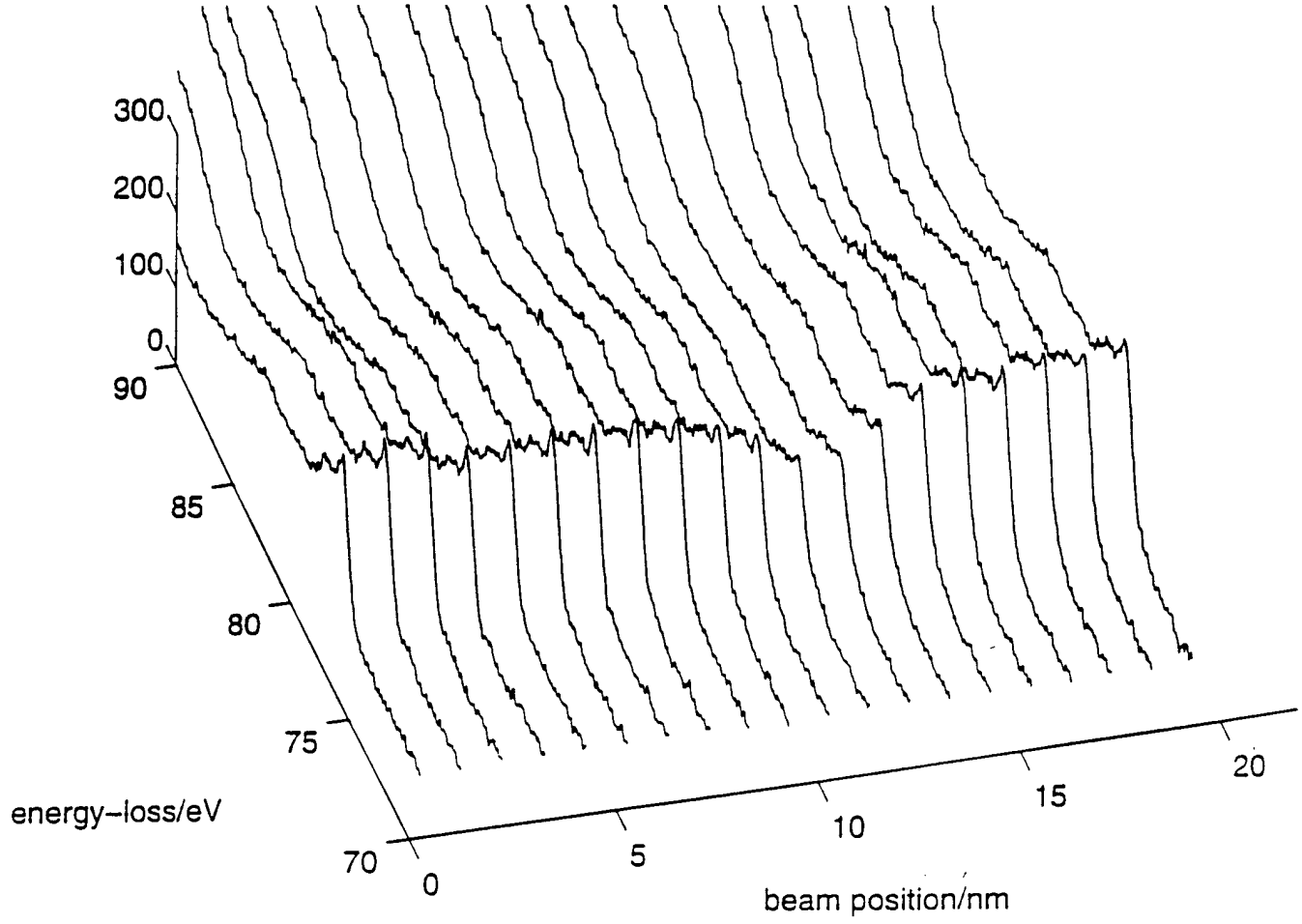
AL L23 profile across La–doped alumina
300
200
100
0
90
85
80
75
70
energy–loss/eV
0
5
10
15
20
beam position/nm

Fig 6

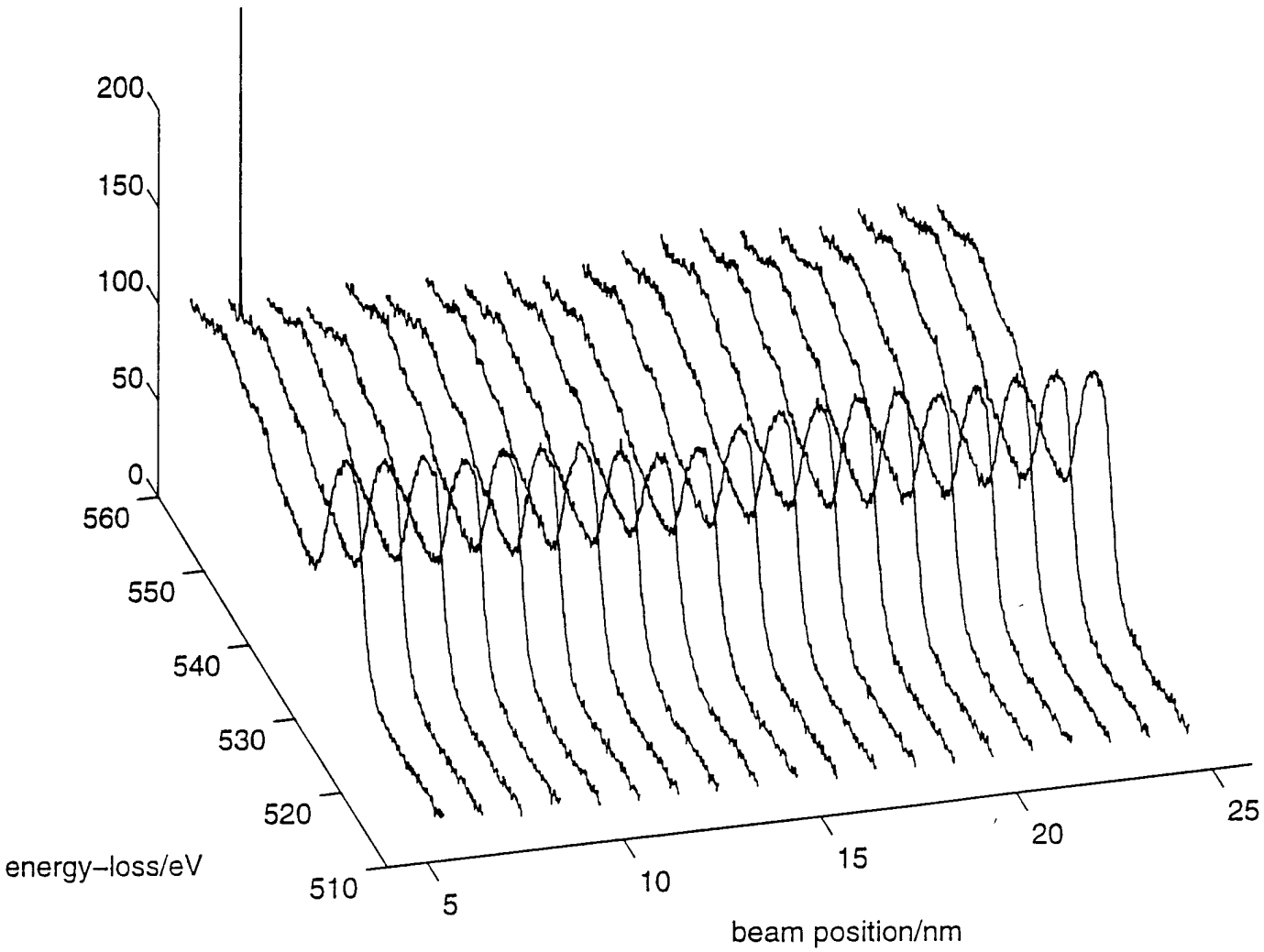
O K–edge across boundary in La doped alumina
200
150
100
50
0
560
550
540
530
520
510
energy–loss/eV
5
10
15
20
25
beam position/nm

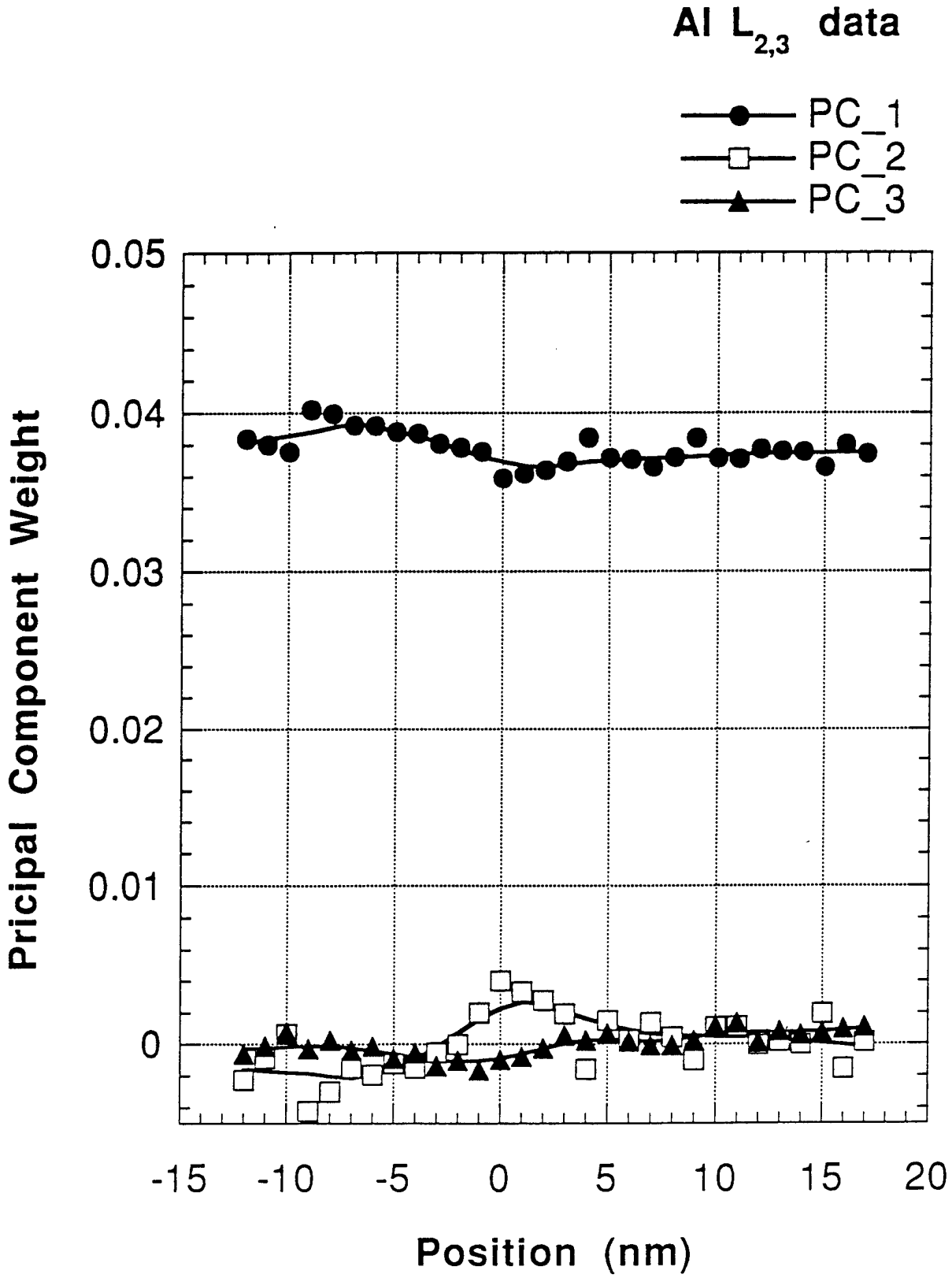
Al $L_{2,3}$ data
PC_1
PC_2
PC_3
Pricipal Component Weight
0.05
0.04
0.03
0.02
0.01
0
-15
-10
-5
0
5
10
15
20
Position (nm)

Fig 8

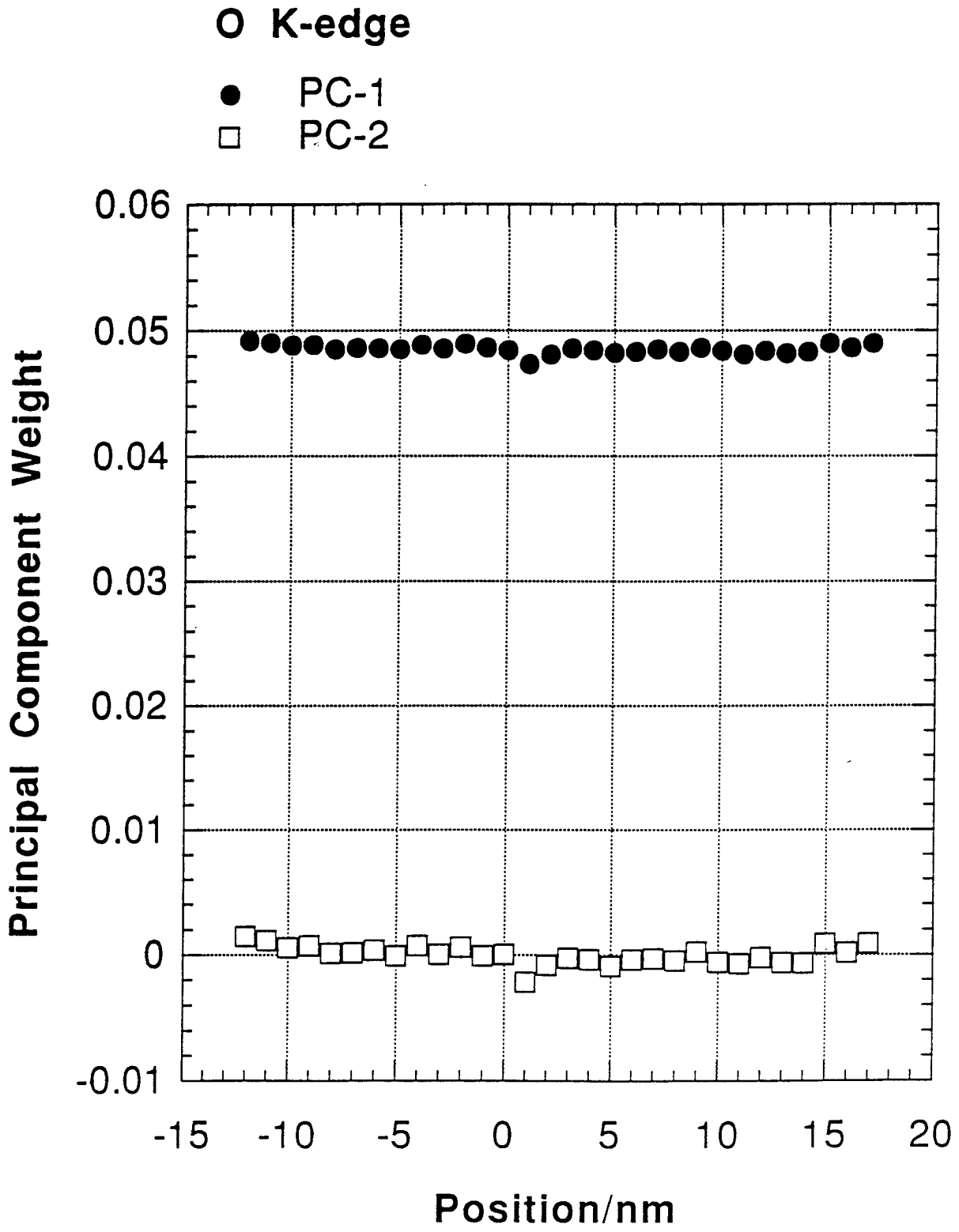
O K-edge
PC-1
PC-2
Principal Component Weight
0.06
0.05
0.04
0.03
0.02
0.01
0
-0.01
-15
-10
-5
0
5
10
15
20
Position/nm

Fig 9

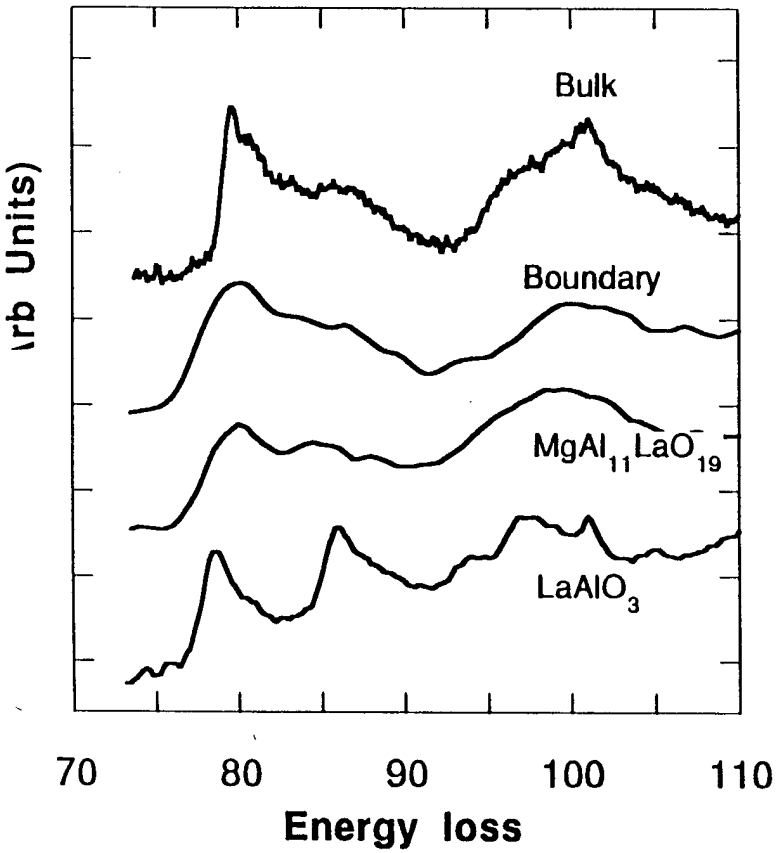
Bulk
Boundary
$MgAl_{11}LaO_{19}^-$
$LaAlO_3$
70
80
90
100
110
Energy loss

Section 1.5

Effect of Y and La on The Final-Stage Sintering Behavior of Ultra-High-Purity Al_2O_3

by

J. Fang, A. M. Thompson, M. P. Harmer, and H. M. Chan

Published in Journal of the American Ceramic Society, Volume 80, Pages 2005-12(1997)

EFFECT OF Y AND La ON THE FINAL-STAGE SINTERING BEHAVIOR OF ULTRA-HIGH-PURITY Al_2O_3

Jianxin Fang*, A. Mark Thompson*, Martin P. Harmer* and Helen M. Chan*, Department of Materials Science and Engineering and Materials Research Center, Lehigh University, Bethlehem, Pennsylvania 18015

Abstract

Final-stage sintering has been investigated in ultra-high-purity alumina, and alumina doped individually with 1000 ppm Y and 1000 ppm La. In both the undoped and doped materials, the dominant densification mechanism was found to be consistent with grain-boundary diffusion. Doping with Y and La decreased the densification rate by a factor of about 11 and 21, respectively. It is postulated that these large rare earth cations, which segregate strongly to the grain boundaries in Al_2O_3, block the diffusion of ions along grain boundaries, leading to reduced grain boundary diffusivity and decreased densification rate. In addition, Y and La doping decreased grain growth during sintering. Whereas in the undoped alumina surface-diffusion-controlled pore drag governed grain growth, in the doped materials, no grain growth mechanism could be unambiguously identified. Overall, Y and La decreased the coarsening rate relative to the densification rate and, hence, shifted the grain size/density trajectory to higher density for a given grain size. It is believed that the effect of the additives is linked strongly to their segregation to the alumina grain boundaries.

Keywords: alumina, yttrium, lanthanum, sintering, kinetics, grain boundary diffusion.

Presented at the 97th Annual Meeting of the American Ceramic Society, Cincinnati, OH, May 3, 1995 (Paper No. SXV-22-95).

* Member, the American Ceramic Society.

I. Introduction

Recent studies have shown that doping with 500~1500 ppm yttrium can improve both the tensile and compressive creep resistance of Al_2O_3[1-3]. For instance, French *et al.*[3] found that the addition of 1000 ppm Y to ultra-pure alumina significantly decreased the creep rate. Specifically, at 1250°C under applied tensile stresses ranging from 35 MPa to 75 MPa, the Y doping decreased the creep rate of alumina by about 2 orders of magnitude (from ~$10^{-6}s^{-1}$ to ~$10^{-8}s^{-1}$). The Y-induced improvement became less pronounced with increasing temperature; hence at 1350°C, the creep rate in the Y-doped alumina was about 1 order of magnitude lower ($10^{-5}s^{-1}$ compared to $10^{-6}s^{-1}$) than the undoped alumina. French *et al.* attributed the beneficial effect of yttrium to the grain boundary segregation of yttrium ions, and the resulting effect on the rate of ion transport along grain boundaries. However, it is not clear whether yttrium decreases the creep rate by directly interfering with grain boundary diffusion processes, or by inhibiting other processes such as grain boundary sliding.

A possible approach to differentiate these mechanisms is to investigate the effect of Y-doping on sintering kinetics, because sintering is a purely diffusion-controlled phenomenon at high temperature. Several studies[4-6] utilizing the linear shrinkage technique have qualitatively shown that Y doping retards the overall densification rate of alumina. However, these studies were not able to identify unambiguously the dominant densification mechanism.

In the present study, we have focused on the effect of 1000 ppm Y on the final stage sintering kinetics of ultra-pure alumina. The models for final stage sintering [7-9] will be applied to assess the densification mechanism, and the change in diffusivity due to the Y doping. It is hoped that such quantitative information will yield insight into the role of Y in the improvement of creep resistance. In addition, the effect of 1000 ppm La-doping was also studied to investigate the effect of ion size on sintering kinetics of alumina, and hence to assess the potential of La as a dopant for enhancing creep resistance. Lanthanum was

selected because the La ion has the same valence as Al and Y, but a much larger radius (ionic radii are 0.51, 0.893 and 1.061 for Al^{3+}, Y^{3+} and La^{3+}, respectively)[10].

II. Experimental Procedure

Three types of alumina samples (pure Al_2O_3, Y-doped Al_2O_3 and La-doped Al_2O_3) were prepared using an ultra-high-purity-alumina powder (Sumitomo AKP-53), for which the manufacturer claims 99.995% purity and a mean particle size of 0.2 μm. Yttrium (Y/Al = 1000×10^{-6}) or lanthanum (La/Al = 1000×10^{-6}) doping was achieved by the addition of aliquots of a high-purity $Y(NO_3)_3$ or $La(NO_3)_3$ solution in deionized water (with 18 MΩcm electrical resistivity) to a batch of alumina powder. In order to promote uniform mixing of the dopant ions, all powders were dispersed in high-purity methanol. The slurries were simultaneously mixed using a magnetic stirrer and dried under an infrared lamp. The dried powders were subsequently crushed to remove soft agglomerates resulting from the drying procedure. Next, the powders were cold-pressed at 27 MPa in a high-purity alumina punch and die set to form cylindrical pellets (about 5 mm thick and 14 mm in diameter). All processing was performed using pre-cleaned Teflon ware in a contamination-free environment (a class 100 laminar flow hood). The pellets were subsequently isostatically pressed at 69 MPa to obtain a uniform green density of 50±0.7%. The undoped sample was processed using the same procedures as the doped materials.

The green pellets were embedded in a powder of identical composition and calcined at 1000°C for 8 hours to remove carbon contamination. Pressureless sintering was conducted at 1350°C in air using a $MoSi_2$-element resistance heated furnace. Again, each sample was packed within a powder of the same composition to minimize dopant volatilization and furnace contamination. Also, a different high-purity alumina crucible was used for each composition for both calcining and sintering to avoid cross contamination. Zero sintering time was taken to correspond to the point at which the equilibrium temperature setting was reached.

Sintered densities were measured to an accuracy of 0.001 $g \cdot cm^{-3}$ using the Archimedes method with deionized water as the immersion medium. Grain boundaries were revealed by thermally etching polished sections at 1150~1250°C in air for various times; in general, higher temperatures were used for the doped samples. Calibrated latex spheres were applied to all polished surfaces to ensure accurate grain size measurement. Grain sizes were determined from SEM micrographs using the linear intercept technique. The average grain size, G, was determined from the average intercept length, L, using the relationship G=1.5L. Approximately 400 intercepts were counted for each sample.

III. Results and Discussion

1. Effect of dopants on densification kinetics

Figure 1 shows the density as a function of sintering time at 1350°C for pure Al_2O_3, Y-doped Al_2O_3 and La-doped Al_2O_3. The curves through the experimental data were plotted in the form of a polynomial term log(t+1), where t was measured in minutes. It can be seen that both Y and La doping inhibited the overall densification rate, with Y showing the stronger overall effect. (It should be pointed out that this does not necessarily indicate that yttrium doping has more effectively inhibited the diffusion process for densification, because the grain size has not yet been taken into account). After sintering for short times (<100 minutes), the density is highest for the undoped sample, lowest for the Y-doped Al_2O_3 and intermediate for the La-doped Al_2O_3. After prolonged sintering (beyond 700 minutes), the density approaches a limiting value of approximately 99.2% for all three materials.

The microstructure was similar for all three materials over the density range 91.7 to 99.2%. Fig. 2 shows a typical micrograph taken from Y-doped Al_2O_3 sintered for 5 minutes, which resulted in a density of 91.7%. The morphology consists of equiaxed grains with near spherical pores situated at grain boundaries, conforming to the classical geometry described in final stage sintering models[8]. During final stage sintering, the

densification rate, dρ/dt, can be expressed in the following form[8,11, 12, 13]

$$\frac{d\rho}{dt} = \frac{C\gamma_s D N_g}{G^n} \qquad (1)$$

where ρ is the density, C is a constant, γ_s is the solid/gas surface energy, D represents either the lattice diffusion coefficient (D_L) or the grain boundary diffusivity $\delta_b D_b$ where δ_b is the grain boundary width, N_g is the number of pores per grain and G is the grain size. The grain size exponent, n, is 3 for lattice diffusion control and 4 for grain boundary diffusion control. Fig. 3 shows a fit of experimental data to Eq. (1), which is plotted in the form of the logarithm of the densification rate versus the logarithm of the grain size (assuming Ng is a constant). The densification rates (dρ/dt) were obtained by differentiating the fitted curves in Fig. 1.

It can be seen from Eq. (1) that the controlling densification mechanism can be identified by determining the slopes of the log(densification rate) vs. log(grain size) plots depicted in Fig. 3. In this manner, the grain-size exponent was found to be 3.8 for undoped alumina, 3.9 for Y-doped alumina and 4.1 for La-doped alumina. The fact that the grain-size exponents are close to 4.0 for all three materials strongly suggests that grain boundary diffusion was the predominant transport mechanism during densification process, consistent with previous studies of sintering kinetics for model final-stage microstructures of Al_2O_3[12, 13].

Further, it is evident from Eq. (1) that a reduction in densification rate may result either directly from a decrease of the grain boundary diffusivity, or indirectly from an increase in the grain size (G). To evaluate the direct effect of a dopant on the diffusion mechanism responsible for densification, densification rates were compared at constant grain size. This revealed that Y and La doping decreased the densification rate directly by a factor of 11 and 21, respectively. Since upon doping, the change in the surface energy (γ_s) can be expected to be much smaller than the change in diffusivity, the observed reduction in

the densification rates for the doped materials may be attributed to the reduced grain boundary diffusivity.

The decrease of densification rate due to Y-doping is consistent with recent measurement of diffusion coefficients by Le Gall *et al* [14] in both undoped Al_2O_3 and Al_2O_3 doped with 500 ppm Y_2O_3. These workers reported that in the case of the undoped Y_2O_3, values of both lattice and grain boundary diffusivities were lower for the oxygen ion than for the aluminum ion, thus indicating that the oxygen ions are the rate-controlling species in both cases. Le Gall *et al* also found that, in the temperature range from 1500°C to 1600°C, the oxygen grain boundary diffusion coefficient is about three orders of magnitude smaller in the Y-doped alumina than in the undoped alumina. Further, when the data was extrapolated linearly to 1300°C, it was found that Y_2O_3 doping decreased the oxygen grain boundary diffusion coefficient by a factor of 20.

It is difficult to account for the lower diffusion coefficients in the doped alumina in terms of defect chemistry, since Y and La ions are isovalent with Al^{+3} and hence can substitute for Al ions without creating point defects. The more likely explanation for the reduction in grain boundary diffusivity is segregation of dopant ions to grain boundaries to reduce the elastic strain energy arising from the difference in ionic radius between the dopants and Al^{+3}. Figure 4 shows a pair of X-ray spectra obtained from Y-doped Al_2O_3 using a dedicated STEM. Whereas only background noise was detected from the grain matrix, there were pronounced yttrium peaks from the grain boundary, suggesting that the yttrium ions strongly segregated to the grain boundaries. Segregation of yttrium and lanthanum ions has also been observed in polycrystalline Al_2O_3[4, 15-17] and in alumina scale formed on heat resisting alloys[18-21]. Most recently, high resolution SIMS mapping was used to reveal grain boundary enhancement of dopant concentrations for Y and La doped alumina[22]. It is postulated that the large yttrium cations at grain boundaries block the diffusion of ions along grain boundaries, leading to the reduced grain boundary diffusivity. It is interesting to note that the factor of 11 decrease in densification rate due to Y-doping

compares reasonably well with the factor of about 10 decrease in creep rate[3]. This result implies that the beneficial effect of yttrium in the creep experiment may arise mainly from a lowering of the grain boundary diffusivity. La should, therefore, also have a beneficial influence on the creep resistance of Al_2O_3 and the recent work has indeed indicated this to be the case[27].

Although we believe that the reduced densification and improvement in creep results from the lowering of the grain boundary diffusivity, it should be recognized that Lartigue and coworkers have proposed an alternate explanation (for reduced creep) based on their observation that Mg doping and Mg and Y codoping in alumina resulted in a large proportion (~30%) of special grain boundaries (near coincidence boundaries), compared with undoped alumina [28,29,30]. These investigators postulated that because the special boundaries are less able to accomodate intergranular dislocations, the grain boundary sliding process was limited. Work is in progress to characterize the nature and concentration of boundary types in our undoped, Y-doped and La-doped samples, in order to assess this mechanism[31].

2. *Effect of dopants on grain growth*

Fig. 5 shows the dependence of the average grain size on the sintering time at 1350°C for the undoped, Y-doped and La-doped Al_2O_3. The curves through the data points were obtained from a polynomial fit of grain size vs. log(t+1). Clearly, both Y and La doping retard grain growth during sintering, with La doping showing the stronger effect. All the grain structures observed in this study were found to be uniform, and free of abnormal grain growth. Fig. 6 shows representative microstructures of the three materials after 720 minutes at 1350°C.

Previous studies[11, 12] on pure alumina showed that grain growth during the final stage of sintering is governed by surface-diffusion-controlled pore drag, for which the

grain growth rate can be expressed by

$$\frac{dG}{dt} = \frac{CN_g D_s}{G^3(1-\rho)^{4/3}} \qquad (3)$$

where C is a constant and D_s the surface diffusion coefficient. As can be seen from Fig. 7, the present data for the undoped alumina is in excellent agreement with the above model. Note that the grain growth rates, dG/dt, were determined by differentiation of the fitted curve in Fig. 5.

In contrast, the grain size data for the doped materials did not fit the pore-drag models. Instead, it was observed (see Fig. 8) that the grain growth kinetics followed a cubic kinetic relationship:

$$G^3 - G_0^3 = Kt \qquad (4)$$

where G is the grain size after time t, G_0 the initial grain size and K a temperature-dependent grain growth constant. The growth rate constants for Y-doped and La-doped samples were determined to be 4.2×10^{-3} and 2.0×10^{-3} $\mu m^3 s^{-1}$, respectively.

In addition to pore drag, another possible grain growth limiting mechanism is particle pinning. It should be noted that the doping level in the present work is well beyond the solubility limit (e.g. the solubility of yttrium in alumina is <10 ppm[23]). Both SIMS[22] and TEM[24] examinations of Y-doped samples revealed that precipitates were present both within the interior of grains and along grain boundaries. These observations are consistent with earlier results in Y and Mg co-doped Al_2O_3[17], and in Y-doped Al_2O_3[25, 26]. However, given the small volume fraction of precipitates present (<0.5%), it is thought that precipitate pinning is not likely to be the dominant mechanism. A more plausible explanation is that grain growth is controlled by the dragging influence of the solute ions along the pore-free

sections of the boundaries (i.e. by the boundary mobility M_b). In keeping with this possibility are the observed cubic kinetics and grain boundary segregation. To unambiguously identify the controlled mechanism, further work such as grain growth in the fully dense materials should be carried out.

3. Effect of the dopants on Microstructure Development

Fig. 9 shows the microstructure of the undoped and Y-doped Al_2O_3 sintered for 160 minutes. It can be seen that the majority of pores are located within the interior of the grains in the undoped sample (Fig. 9 (a)), but are situated at the grain boundaries and triple grain junctions in the Y-doped material (Fig. 9 (b)). These observations indicate that in pure Al_2O_3 pore-boundary separation has taken place within 160 minutes at 1350°C, whereas in the doped Al_2O_3, the pores remained attached to the grain boundaries.

A figure of merit to evaluate the resistance to pore-boundary separation is given by[11]

$$\left(\frac{1}{G^2}\right)_\rho \frac{D_s}{M_b} \qquad (5)$$

It is postulated that Y and La doping increased this figure of merit by increasing $(1/G^2)_\rho$ and decreasing M_b (grain boundary mobility), resulting in the improved resistance to pore-boundary separation.

Fig. 10 shows grain size/density trajectories for undoped Al_2O_3, Al_2O_3+Y and Al_2O_3+La. The grain size/density trajectory is a function of the relative ratio of densification rate to grain growth rate. The flattening of the G-ρ trajectories observed in the Y and La-doped materials reflects the fact that the doping enhances the densification rate relative to the grain growth rate. Interestingly, the G-ρ curve for the two doped materials are quite similar. This is because the densification rate:grain growth rate ratio is similar for these two materials.

IV. Conclusions

In undoped alumina and alumina doped with either 1000 ppm Y or 1000 ppm La, the densification kinetics were consistent with grain-boundary diffusion as the controlling mechanism during densification. At a given grain size, doping with Y and La decreased the densification rate directly by a factor of about 11 and 21, respectively. It is believed that this results from a suppression of grain boundary diffusion, due to the segregation of the misfitting Y and La ions to the alumina grain boundaries. In the case of undoped alumina, grain growth was indicated to be governed by surface-diffusion controlled-pore drag. The study showed that doping with Y and La inhibited grain growth during sintering. However, it was not possible to unambiguously identify the inhibiting mechanism. Overall, the effect of Y and La was to enhance the densification rate relative to the grain growth rate, thereby displacing the grain size-density trajectory to higher density for a given grain size.

Acknowledgments

The authors wish to thank Dr. J. Bruley for performing STEM experiments. This work was supported by AFOSR under grant # F49620-94-1-0284.

References

(1) S. Lartigue, C. Carry and L. Priester, "Grain Boundaries in High Temperature Deformation of Yttria and Magnesia Co-Doped Alumina", *Coll. Phys.* **C1**, 51 [1] 985-90 (1990).

(2) P. Gruffel and C. Carry, "Strain Rate Plateau in Creep of Yttria Doped Fine Grained Alumina", pp305-311 in Proc. of the 11th RISO International Symposium on Metallurgy and Materials Science: *Structural Ceramics-Microstructure and Properties*. Ed. by J. J. Bentzen, J. B. Bilde-Sorensen, N. Christiansen, A. Horsewell and B. Ralph, Riso National Lab. Roskilde, Denmark, 1990.

(3) J. D. French, J. Zhao, M. P. Harmer, H. M. Chan and G. A. Miller, "Creep of Duplex Microstructures",*J. Am. Ceram. Soc.*, **77** [11] 2857-65 (1994).

(4) P. Nanni, C. T. H. Stoddart and E. D. Hondros, "Grain Boundary Segregation and Sintering in Alumina", *Materials Chemistry*, **1** 297-320 (1976).

(5) D. Delaunay, A. M. Huntz and P. Lacombe, "The Influence of Yttrium on the Sintering of Al_2O_3", *J. Less-Common Metals*, **70** 115-117 (1980).

(6) E. Sato and C. Carry, "Sintering and Yttrium Grain Boundary Segregation in Sub-micron Grain Size Alumina", *J. De Physique IV*, **3** [11]1335-40 (1993).

(7) C. Herring, "Effect of Change of Scale on Sintering Phenomena", *J. Appl. Phy.*, **21** 301-03 (1950).

(8) R. L. Coble, "Sintering Crystalline Solids. I. Intermediate and Final Stage Diffusion Models", *J. Appl. Phys.*, **32** 787-92 (1962).

(9) R. J. Brook, "Controlled Grain Growth", pp 331-64 in Treatise on Materials Science and Technology, Vol. 9, *Fabrication Processes*, Ed. by F.F.Y. Wang, Academic Press, New York (1976).

(10) *CRC Handbook of Chemistry and Physics*, 71st Edition, Ed. by D. R. Lide, CRC Press Inc., p. 12-1(1991).

(11) J. Zhao and M. P. Harmer, "Effect of Pore Distribution on Microstructure Development: III, Model Experiments", *J. Am. Ceram. Soc.*, **74** [4] 830-43 (1992).

(12) J. Zhao and M. P. Harmer, "Sintering Kinetics for a Model Final-Stage Microstructure Al_2O_3", *Phil. Mag. Lett.*, **63** [1] 7-14 (1991).

(13) A. M. Thompson and M. P. Harmer, "Influence of Atmosphere on the Final-Stage Sintering Kinetics of Ultra-High-Purity Alumina",*J. Am. Ceram. Soc.*, **76** [9] 2248-56 (1993).

(14) M. Le Gall, A. M. Huntz, B. Lesage, C. Monty and J. Bernardini, "Self-Diffusion in α-Al_2O_3 and Growth Rate of Alumina Scales Formed by Oxidation: Effect of Y_2O_3 Doping", *J. Mater. Sci.*, **30** [1] 201-211 (1995).

(15) B. Bender, D. B. Williams and M. R. Notis, "Investigation of Grain-Boundary Segregation

in Ceramic Oxides by Analytical Scanning Transmission Electron Microscopy", *J. Am. Ceram. Soc.*, **63** [9] 542-46 (1980).

(16) C-W. Li and W. D. Kingery, "Solute Segregation at Grain Boundaries in Polycrystalline Al_2O_3", pp 368-378 in Advances in Ceramics Vol. 10, *Structure and Properties of MgO and Al_2O_3 Ceramics*, Ed. by W. D. Kingery, American Ceramic Society, Columbus, OH (1984).

(17) P. Gruffel and C. Carry, "Effect of Grain Size on Yttrium Grain Boundary Segregation in Fine Grained Alumina", submitted to *J. Eur. Ceram. Soc.*, (1994).

(18) K. Przybylski, A. J. Garratt-Reed, B. A. Pint, E. P. Katz and G. J. Yurek, "Segregation of Y to Grain Boundaries in the Al_2O_3 Scale Formed on an ODS Alloy", *J. Electrochem. Soc.*, **134** 3207-08 (1987).

(19) B. A. Pint, J. R. Martin and L. W. Hobbs, "^{18}O/SIMS Characterization of the Growth Mechanism of Doped and Undoped α-Al_2O_3", *Oxidation of Metals*, 39 [3-3] 167-195 (1993).

(20) H. M. Tawancy and N. M. Abbas, "An Analytical Electron Microscopy Study of the Role of La and Y during High-Temperature Oxidation of Selected Ni-Base Alloys", *Scripta Metall.*, **29** 689-694 (1993).

(21) E. Schumann, J. C. Yang, M. Rühle and M. J. Graham, "High Resolution SIMS and Analytical TEM Evaluation of Alumina Scales on β-NiAl Containing Zr or Y", submitted to *Oxidation of Metals*, (1994).

(22) A. M. Thompson, K. K. Soni, H. M. Chan, M. P. Harmer, D. B. Williams, J. M. Chabala and R. Levi-Setti, "Rare Earth Dopant Distributions in Creep-Resistant Al_2O_3", submitted to *J. Am. Ceram. Soc.* (1995).

(23) J. D. Cawley and J. W. Halloran, "Dopant Distribution in Nominally Yttrium-Doped Sapphire", *J. Am. Ceram. Soc.*, **69** [8] C195-C196 (1986).

(24) J. Fang, H. M. Chan and M. P. Harmer, unpublished results (1994).

(25) M. K. Loudjani, J. Roy and A. M. Huntz, "Study by Extended X-Ray Absorption Fine-Structure Technique and Microscopy of the Chemical State of Yttrium in α-Polycrystalline Alumina", *J. Am. Ceram. Soc.*, **68** [11] 559-562 (1985).

(26) R. C. McCune, W. T. Donlon and R. C. Ku, "Yttrium Segregation and Yag Precipitation at Surfaces of Yttrium-Doped-Al_2O_3", *J. Am. Ceram. Soc.*, **69** [8] C196-C199 (1986).

(27) A. M. Thompson, H. M. Chan and M. P. Harmer, unpublished work (1995).

(28) S. Lartigue and L Priester, "Influence of Doping Elements on the Grain Boundary Characteristics in Alumina", *Coll. Phys.* **C5** [49] 451-456 (1988).

(29) H. Grimmer, R. Bonnet, S. Lartigue and L. Priester, "Theoretiical and Experimental descriptions of Grain Boundaries in Rhombohedral Alpha-Al_2O_3", Phil. Mag., A6:493 (1990).

(30) S. Lartigue, C. Carry and L. Priester, "Grain Boundary in high Temperature deformation of Yttria and Magnesia Co-doped Alumina", J. Phys., C1, 51:985 (1990).

(31) J. Bruley, M.P.Harmer, H.M.Chan and M.Ruhle, work in progress (1996).

Figure Captions

Fig. 1. Density as a function of sintering time at 1350°C for undoped, Y-doped and La-doped Al_2O_3.

Fig. 2. Fracture surface of Y-doped Al_2O_3 sintered at 1350°C for 5 minutes.

Fig. 3. Densification rate vs. grain size for undoped, Y-doped and La-doped Al_2O_3.

Fig. 4. EDS spectra from grain matrix and grain boundary in Y-doped Al_2O_3 showing strong segregation of yttrium to grain boundary.

Fig. 5. Grain size as a function of sintering time at 1350°C for undoped, Y-doped and La-doped Al_2O_3.

Fig. 6. Microstructure of (a) undoped, (b) Y-doped and (c) La-doped Al_2O_3 sintered for 720 minutes at 1350°C.

Fig. 7. Grain growth rate plotted according to the model for surface diffusion-controlled pore drag for undoped Al_2O_3.

Fig. 8. Grain growth kinetics during sintering for Y-doped and La-doped Al_2O_3.

Fig. 9. Microstructure of (a) undoped and (b) Y-doped Al_2O_3 sintered for 160 minutes at 1350°C.

Fig. 10. Grain size-density trajectory for undoped, Y-doped and La-doped Al_2O_3 sintered at 1350°C.

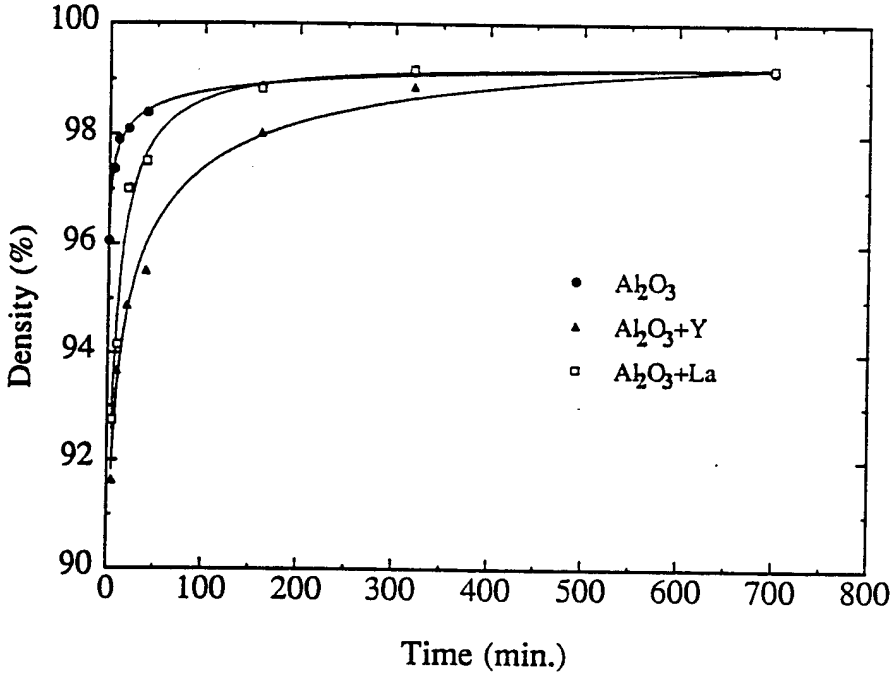
100
98
96
94
92
90
Density (%)
0
100
200
300
400
500
600
700
800
Time (min.)
Al2O3
Al2O3+Y
Al2O3+La


500 nm

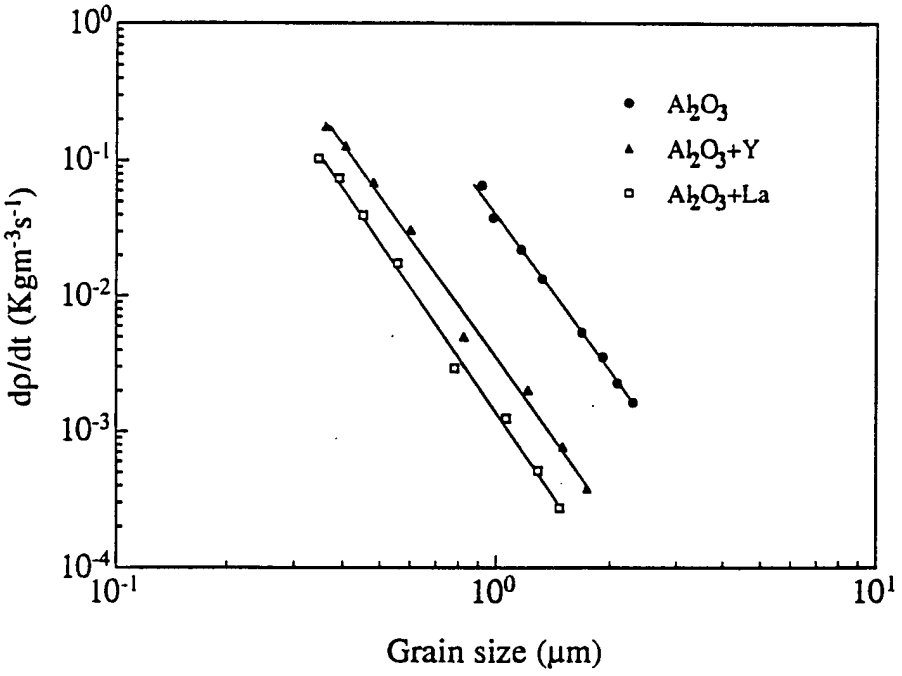
10^0
10^{-1}
10^{-2}
10^{-3}
10^{-4}
10^{-1}
10^0
10^1
dρ/dt (Kgm^{-3}s^{-1})
Grain size (μm)
Al_2O_3
Al_2O_3+Y
Al_2O_3+La

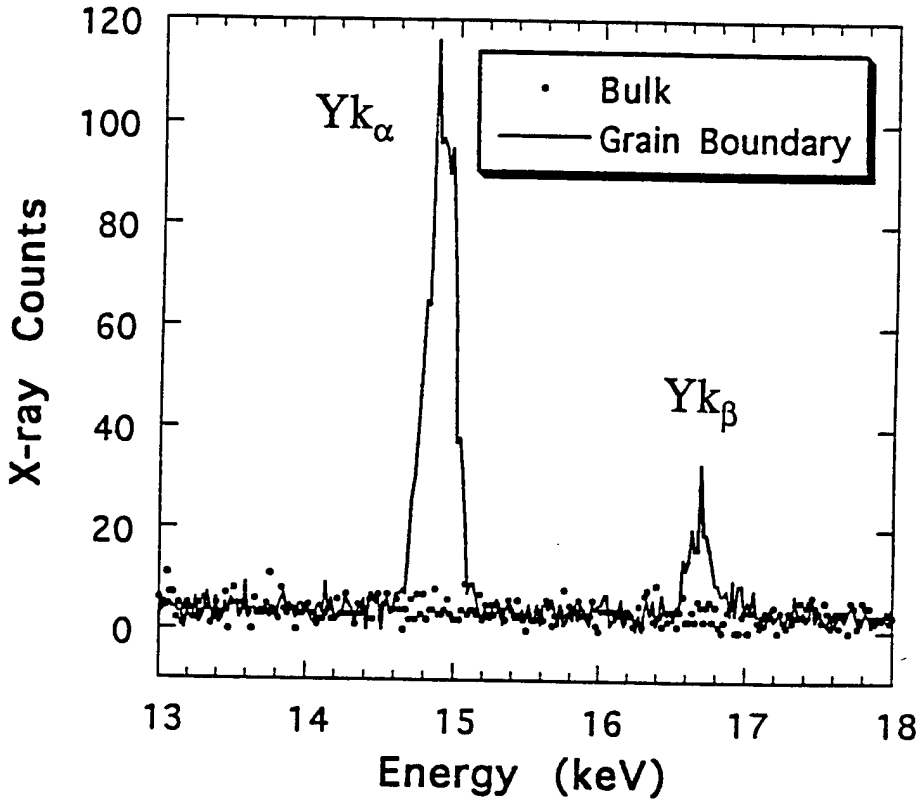
120
100
80
60
40
20
0
X-ray Counts
Yk$_\alpha$
Yk$_\beta$
Bulk
Grain Boundary
13
14
15
16
17
18
Energy (keV)

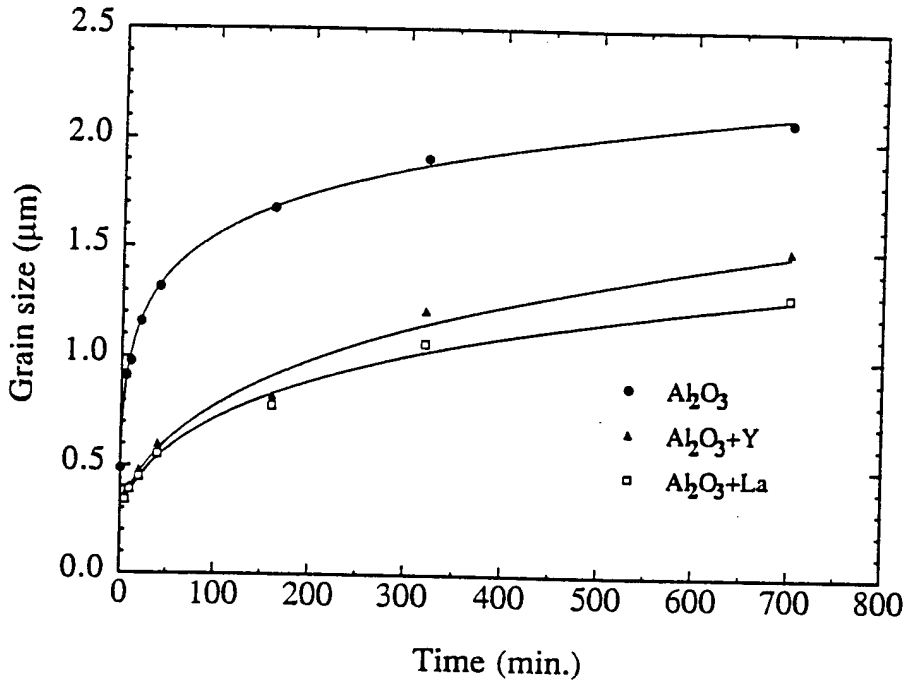
2.5
2.0
1.5
1.0
0.5
0.0
Grain size (μm)
0
100
200
300
400
500
600
700
800
Time (min.)
Al_2O_3
Al_2O_3+Y
Al_2O_3+La

A
B
C

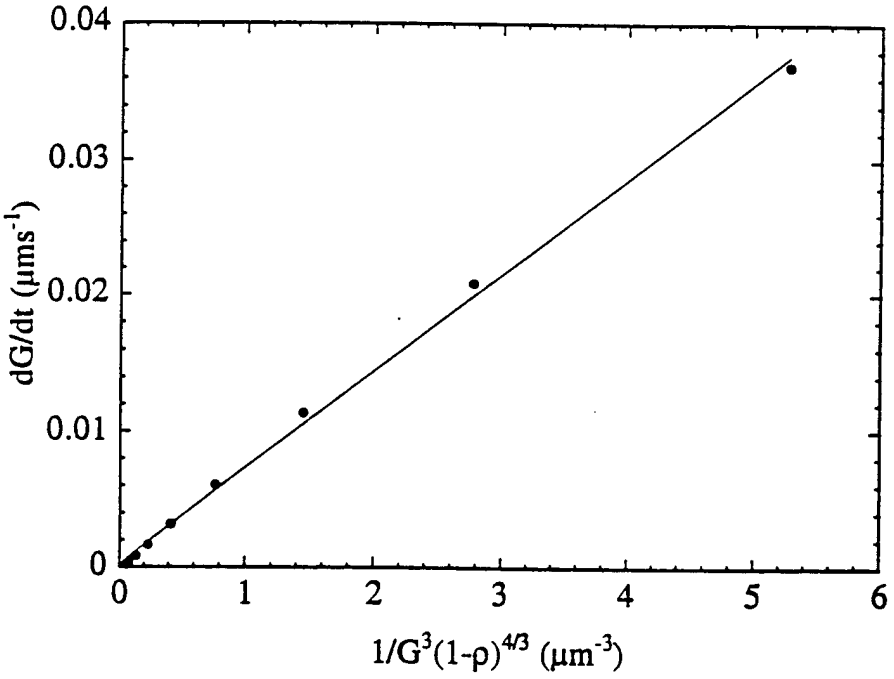
0.04
0.03
0.02
0.01
0
dG/dt (μms-1)
0
1
2
3
4
5
6
1/G3(1-ρ)4/3 (μm-3)

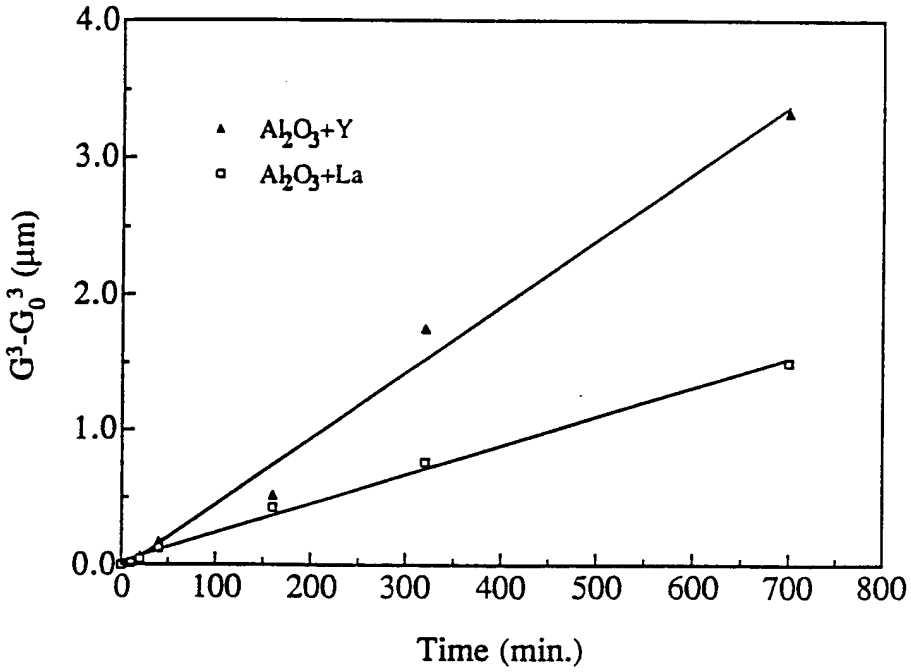
4.0
3.0
2.0
1.0
0.0
0
100
200
300
400
500
600
700
800
$G^3-G_0^3$ (μm)
Time (min.)
Al_2O_3+Y
Al_2O_3+La

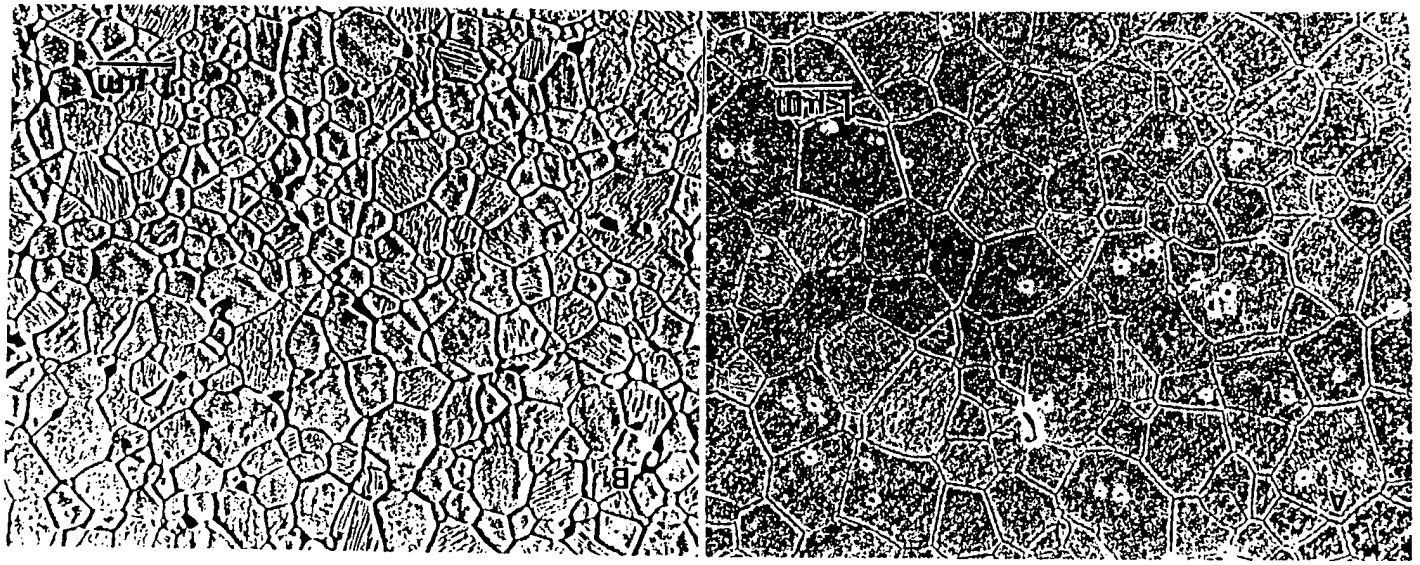
B
C

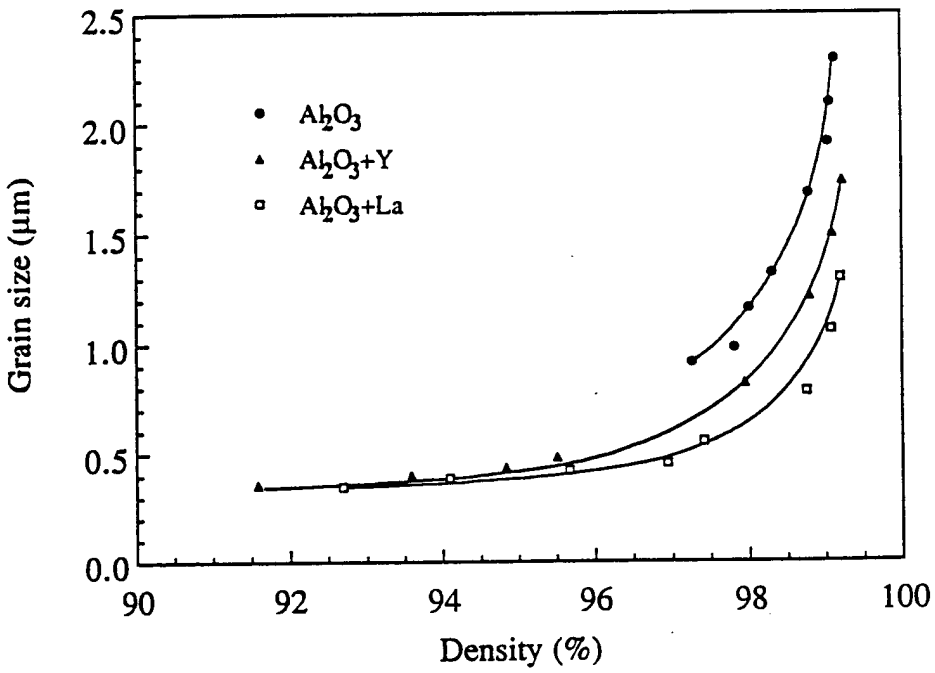
2.5
2.0
1.5
1.0
0.5
0.0
Grain size (μm)
Al_2O_3
Al_2O_3+Y
Al_2O_3+La
90
92
94
96
98
100
Density (%)

Section 1.6

Creep Resistance of Alumina from Nd, Sc, and Zr Doping

by

Y. Li, M. P. Harmer, H. M. Chan, J. M. Rickman, J. Chabala, and R. Levi-Setti

To be Published in Journal of the American Ceramic Society

Creep Resistance of Alumina from Nd, Sc, and Zr Doping

Yan Z. Li*[1] Martin P. Harmer*[1], Helen M. Chan*[1], Jeffrey M. Rickman*[1], J. Chabala[2] and R. Levi-Setti[2]

[1]Department of Materials Science and Engineering and Materials Research Center, Lehigh University, Bethlehem, PA 18015

[2]University of Chicago

Abstract

The tensile creep behavior of hot-pressed alumina samples doped with 100 ppm zirconium and codoped with either 100, 350, 1000 ppm neodymium, or 1000 ppm scandium have been studied in the temperature range of 1200-1350°C and the stress range of 20-100 MPa. An extensive steady-state creep regime was observed and a stress exponent of about 2 was found for all the compositions. The inverse grain size exponent was found to be close to 3 for Zr-doped and Sc/Zr codoped alumina, and about 2 for the Nd/Zr codoped materials containing 100 ppm and 350 ppm Nd. When the creep data was corrected to account for the different grain sizes of the specimens, it was found that Zr-doped alumina and Sc/Zr codoped alumina exhibited comparable creep rates that were lowered by one order of magnitude in comparison to undoped alumina. In the case of the Nd/Zr codoped alumina, the observed creep rates that decreased by two to three orders of magnitude. SIMS analysis showed direct evidence of the segregation of Nd^{3+}, Zr^{4+}, and Sc^{3+} to grain boundaries for all the ceramics. It is suggested that the segregation of the oversized dopants to the alumina grain boundaries reduces the grain boundary diffusivity and thus the creep rate. Further improvement in creep resistance may possibly be achieved through the simultaneous

inhibition of both the lattice diffusion and the grain boundary diffusion process by the addition of appropriate dopants.

(Key words: creep, alumina, neodymium, zirconium, scandium, segregation).

1. Introduction

Recently it has been shown that yttrium [12345] or lanthanum [5] additions can significantly improve the creep resistance of polycrystalline alumina. For example, the results of French et al. [1] and Cho et al. [5] demonstrated that the addition of 1000 ppm (atomic ratio) yttrium or 500 ppm lanthanum gave rise to a two orders of magnitude reduction in the tensile creep rate of alumina. Lartigue et al. [2] and Robertson et al. [3] showed a reduction (by factors of 5 and 15) in the creep rate of magnesia-doped alumina with the addition of 500 ppm and 360 ppm yttrium, respectively. Finally, Wakai et al. [6] reported a decrease in the creep rate by a factor of 15 with the addition of 1000 ppm Zr to Al_2O_3. The enhancement in creep resistance resulting from yttrium and lanthanum additions is believed to be a result of segregation of the oversized solute ions to the grain boundaries [1,7-12]. The role of the segregants at the grain boundaries could be to inhibit grain boundary diffusion [7-9], or to retard the interface reaction believed to be controlling the rate of ion transport along the grain boundaries [1,10,8??]. In the study by Wakai et al., the creep rate reduction due to Zr addition was attributed to the zirconium oxide particles formed at the grain boundaries and the attendant decrease in the interface reaction rate and, thus, the creep rate [6].

The steady-state creep rate predicted by diffusional mechanisms is commonly expressed in the form,

$$\dot{\varepsilon} = A\,(d)^{-p}\,(\sigma)^{n}\,\exp(-Q/RT) \qquad (1)$$

where A is a constant determined by the slowest diffusion species along the fastest diffusion path for a simple ionic compound such as alumina, d the grain size, σ the applied stress, p the inverse grain size exponent, n the stress exponent, Q the apparent activation energy for creep, R the gas constant, and T the absolute temperature. For lattice diffusion controlled creep (Nabarro-Herring) [9,10] p=2 and n=1, while p=3 and n=1 for grain boundary diffusion controlled creep (Coble) [11]. If the grain boundaries do not behave as perfect sources and sinks of vacancies, the interface reaction process may be rate-limiting [13, 12], then p=1 and n=2. Details of creep characteristics and other mechanisms can be found in a number of review articles [13, 14].

Sintering studies carried out on the same materials as characterized by the creep investigations have shown that the addition of yttrium [15-17??] and lanthanum [20] to alumina reduced both the densification rate and the grain growth rate. Fang et al. [20] determined that sintering was controlled by grain-boundary diffusion and found that the densification rate was reduced by a factor of 10 and 20 for 1000 ppm yttrium and 1000 ppm lanthanum doped alumina, respectively. Grain boundary diffusion experiments by Le Gall et al. [9] recently revealed a three orders of magnitude reduction with a doping level of 500 ppm yttrium. These findings suggest that the segregation of the dopant Y or La to the grain boundaries slows down the grain boundary diffusion process, and thus leads to the decrease of the creep rate and the densification rate.

In this paper, we report the results of creep studies of Zr-doped, Nd/Zr codoped, and Sc/Zr codoped alumina. The purpose of this work is to explore possibilities for further improvement in the creep resistance of alumina and to elucidate the creep mechanism(s) of doped alumina ceramics.

2. Experimental Procedure

2.1 Specimen Preparation

Ultra pure α-Al_2O_3 powders (AKP-53, 99.995%, mean particle size of 0.35 μm, Sumitomo Chemical America, New York, NY), neodymium nitrate ($Nd(NO_3)_3 \cdot 6H_2O$, 99.99%), scandium nitrate ($Sc(NO_3)_3 \cdot 4H_2O$, 99.99%), and aluminum nitrate ($Al(NO_3)_3 \cdot 9H_2O$, 99.999%) (Alfa AESAR, Ward Hill, MA) were used as the starting powders. Alumina slurries of roughly equal mass of alumina powders and DDI (deionized + distilled) water were prepared. Doping levels of 100 ppm, 350 ppm, 1000 ppm Nd (Nd/Al ratio), and 1000 ppm Sc were achieved by adding the appropriate amount of neodymium or scandium nitrate aqueous solution to the alumina slurries. A few drops of aluminate nitrate aqueous solution (equivalent of 250 ppm doping level of Al ions) were added to all the slurries as a defloculant. The slurries were then ball-milled with ZrO_2 grinding media (Tosoh U.S.A. Inc., Bridgewater, NJ) for 20 hours to achieve uniform mixing. It should be mentioned here that the ball-milling process introduced into the alumina. Chemical analysis by the ICP-OES (inductively coupled plasma-optical emission spectroscopy) technique revealed that the measured doping levels differed from nominal levels (see Table 1). To evaporate the liquid, the slurries were placed in a Teflon evaporating dish under an infrared heat lamp, and magnetically stirred during evaporation to minimize differential settling. The dried cakes were then placed in a polyethylene bag and crushed with a rolling pin. The powders were then calcined at 850°C for 10 hours to remove possible organic contaminants in high purity alumina crucibles (99.8%, Vesuvius McDanel Ceramic Company, Beaver Falls, PA) and then re-crushed. A new set of labware was used for each composition to avoid cross contamination. Typical powder batch sizes were 200-250 grams each. All powder preparation was carried out in a class 100 clean environment using acid-washed containers. The acid wash was conducted in the following sequence: trichloroethylene, acetone, ethanol, DI water rinses, hydrochloric/nitric acids (3:1), hydrofluoric acid/DI water (1:5), and finally DI water rinses.

The hot pressing (Vacuum Industries, Inc., Somerville, MA) was carried out under

vacuum, in a graphite resistance furnace in 7.62-cm (3-in.) inner diameter graphite dies at NIST (National Institute of Standards and Technology, Gaithersburg, MD). 0.28-mm (0.015-in.) graphite foil liners and BN powder were used to facilitate specimen removal after hot pressing. For all compositions the heating rate was 1000°C/h, and the soaking time was 30 min with an applied pressure of 45 MPa. The Zr-doped and Sc/Zr codoped Al_2O_3 were hot-pressed at 1320°C, the Nd/Zr codoped Al_2O_3 containing 100 ppm Nd was hot-pressed at 1400°C, whereas the 350 ppm and 1000 ppm Nd samples were hot-pressed at 1475°C. After soaking, the materials were furnace cooled to room temperature, still under 45 MPa applied pressure.

The hot-pressed billets were machined by a commercial shop (Bomas Machine Specialties, Inc., Somerville, MA) into dogbone tensile specimens of the 2 -inch specimen design developed at NIST by French and Wiederhorn [16]. SiC flags were attached to the specimen with carbon cement to establish the gauge length (the flags remain attached frictional forces at high temperatures). A laser extensometer (LaserMike, Inc., Dayton, OH) was used to measure the gauge length (precision of ±1 μm) as a function of time under load. Stress was applied to the specimen at constant load using either a lever-arm or hydraulic testing machine (Applied Test Systems, Inc., Butler, PA).

2.2 Characterization

2.2.1 Microstructure

Microstructural characterization was performed using scanning electron microscopy (SEM, JOEL 6300F). The grain structures were revealed by taking polished specimens (1 μm diamond finish) and thermally etching in a box furnace at 1300-1400°C for 30-60 minutes. The grain size was measured from SEM photos using the linear intercept technique, with at least 600 intercepts counted for each measurement. The grain size and density values for all the specimens studied are

summarized in Table 2. Figure 1 shows the typical as-fired microstructures for all the aluminas. These microstructures are seen to be fairy uniform, consisting of roughly equiaxed grains.

A few tensile specimens for each material were acid washed and then annealed at 1450°C and 1500°C for 10 hours except for Sc/Zr codoped alumina where 5 hours annealing was used, in doubly wrapped (acid washed) alumina containers to obtain larger grain sizes. The grain sizes of the annealed specimens are also shown in Table 2.

Secondary Ion Mass Spectroscopy (SIMS) maps of Zr, Nd, Sc, and Si were taken from the polished surfaces of all the doped materials, at the Fermi Institute, University of Chicago. Energy Dispersive Spectroscopy (EDS) analysis of the second phase particles in the microstructures were also conducted on the JEOL 6300F SEM system.

2.2.2 Creep

Tensile tests were performed in air under a constant load in the temperature range of 1200-1350°C and a stress range of 20-100 Mpa. Since all the experimental data except for the creep rupture tests were collected under a total strain of 2-3%, the tests could be considered to be under constant stress. The maximum strains at rupture were as follows: a.) 10-12% for Zr-doped, Nd 100/Zr and Sc/Zr codoped samples, b.) 4% for Nd 350/Zr and c.) 1.5% for Nd 1000/Zr. Three types of creep tests were performed: (i) standard creep rupture tests in which the specimen was loaded at a constant load and temperature until failure, (ii) temperature step tests in which the stress was kept constant but the temperature was altered periodically, and (iii) stress step tests in which temperature was held constant while the stress was altered periodically. In this approach, the strain rate was measured at one temperature (the second type of test) or one stress (the third type of test) over a strain range, and then the temperature or the stress stepped to another interval, and the process repeated. The overall creep behavior of each type of the doped ceramics was obtained from the first type of test. For most specimens, the creep rate under each set of conditions was

measured two or three times on a given specimen to ensure that the strain rate was not dependent on strain history. It was found that the strain rates under the same conditions were typically within about 10%, and the average value was taken as the strain rate under that set of conditions. A typical sample strain history is shown in Fig. 2. No significant concurrent grain growth was observed in these materials, except for a 20% increase in grain size associated with the 0.48 μm Zr-doped alumina after being crept 12% at rupture. The grain size changes for all other compositions were found to be less than 5% after being crept.

2.2.3 Sintering Behavior

A limited sintering study was also carried out for Zr-doped, Nd 1000/Zr and Sc/Zr samples. The starting powders were identical to those prepared for the creep study. The powders were cold-pressed at 55 MPa in acid-washed, high-purity alumina die sets to form cylindrical pellets (about 3 mm thick and 13 mm in diameter). The pellets were subsequently isostatically pressed at 350 MPa to obtain a green density of about 50%. The green pellets were embedded in a powder of identical composition and calcined at 850°C for 10 hours. Each pellet was subsequently embedded in powders of the same composition and pressurelessly sintered at 1400°C in air. About 10 specimens were sintered for each material. Each specimen was sintered for a given period of time from 1 to 500 min. The densities of the sintered specimens were then measured using the Archimedes method with DI water as the immersion medium. The grain size was measured the same way as for creep specimens, namely from the SEM photos of thermally-etched polished sections using the linear intercept technique.

3. Results

The results of the creep tests are presented in the following subsections: the test reproducibility, general creep behavior, creep rates, the stress effect, the grain size effect, sintering rates, evidence of segregation, and microstructural observations.

3.1 The test reproducibility

Fig. 3 shows the results from the tests of nine specimens (Nd/Zr codoped alumina containing 1000 ppm Nd). Three specimens were tested for three temperature steps (specimens #1, #2, and #5), one at two temperature steps (specimen #3), while the rest at just one temperature (1275°C). All the specimens but the #1 and #2 were annealed at 1250°C for 24 hours in the creep testing machine with a stress <5 MPa before the creep test was carried out. This annealing eliminated the primary stage of creep (see section 3.2).

As seen from Fig. 3, the two specimens that didn't receive the initial annealing had the highest strain rates (fine dotted lines), most likely the creep rate in the stage of primary creep. The averaged strain rate from the rest seven specimens which received the initial annealing is shown as the solid line in the figure. The standard deviation was about 35% of the averaged strain rate, which was pretty good bearing in mind that the accuracy of the measurement was dependent on a number of factors such as SiC flag slippage, misalignment, concurrent grain growth, the room temperature fluctuation, air flow, etc [17,18].

3.2 General creep behavior

Most of the doped materials exhibited an initial primary stage of creep, though the strain range and the difference between the primary and the steady state creep rates were not the same for each composition. It was found that an initial annealing treatment at 1250°C for 24 hours in the creep testing machine with an applied stress <5 MPa significantly shortened or completely suppressed the primary stage of creep. Without this annealing, primary creep up to 0.5% strain was observed for most of the doped aluminas. The reason for this phenomenon is not clear. Possible explanations include dopant redistribution, local stress relaxation and subtle changes in the microstructure. In order to facilitate the accurate measurement of the steady-state creep rate, all the

specimens were pre-annealed, including those for the creep rupture tests.

The strain-time curves from creep rupture tests are shown in Fig. 4. It can be seen from the figure that Zr-doped and Sc/Zr codoped alumina exhibit reasonably well-defined steady-state and tertiary creep regimes. Nd/Zr codoped aluminas seemed to exhibit all the conventional three stages of creep with a very small strain rate difference, less than 10%, which was within the experimental reproducibility for multiple measurements under the same set of conditions. For the Nd/Zr codoped aluminas, the existence of primary and tertiary creep was not certain because the very small strain rate difference, less than 10%, was not statistically significant (???). For this reason, the entire creep regime for the Nd/Zr-codoped alumina was considered to be steady-state for the purpose of creep rate measurements.

3.3 Creep rates

The as measured creep rates from temperature step tests under a constant stress of 50 MPa are shown in Fig. 5. It should be noted here that, due to differences in grain size, the effect of the dopant on the creep rates is not entirely clear from this figure. However, rough comparisons can be made for those materials with similar grain size. It can be seen that for Nd 100/Zr the creep rate was one order of magnitude lower relative to that of the Zr-doped and Sc/Zr codoped aluminas. The creep rates for Nd/Zr codoped aluminas with 350 and 1000 ppm Nd was decreased by two to three orders of magnitude in comparison with that of pure alumina.

The apparent activation energy for pure alumina was previously determined to be 450 kJ/mol [1]. 100 ppm Zr addition to alumina increased the activation energy to 690 kJ/mol. Additional doping from Nd and Sc further increased the activation energy to 780, 990, 1060, and 720 kJ/mol for Nd 100/Zr, Nd 350/Zr, Nd 1000/Zr and Sc/Zr, respectively. Clearly, the activation energy increases with increasing level of the Nd dopant. This is consistent with the obstruction of grain boundary transport processes by the oversize dopant ions segregating to the grain boundaries (see section 3.7). Higher activation energies caused by dopants were also reported by Cho et al. [5] in

Y and La doped alumina, where the activation energy was 745 and 760 kJ/mol for 1000 ppm Y and 500 ppm La doped aluminas, by Sato and Carry [19] in Y and Mg codoped alumina, and by Wakai et al. [6] in Zr doped alumina. [The relative higher activation energies of Nd/Zr codoped alumina as compared with that of Y and La doped aluminas can be attributed to the contribution from Zr ions.????????]

3.4 Stress

The effect of stress on the steady state creep rate was investigated in the stress range of 20-100 MPa and at a constant temperature of 1275°C. The results for all the compositions are shown in Fig. 6. The stress exponent was measured to be close to 2 for all the materials, consistent with the results of French et al. [1] and Robertson et al. [3]. This value reflects a possible role of interface-reaction in the creep process [13,17].

3.5 Grain size

The effect of grain size on the creep rate was investigated for all the compositions except for the Nd 1000/Zr alumina; this is because of the large starting grain size (5.2 μm) of the as hot-pressed material for this composition. [It was found that the microstructural inhomogeneities became more severe with increasing doping levels of Nd (see Fig. 1)???]. The strain rates at temperature steps in the range of 1200-1350°C (under a constant stress of 50 MPa) were obtained for each specimen. Three specimens with different grain sizes were tested for each composition. Figure 7 shows the dependence of the strain rates on grain size at 1275°C. As seen in the figure, the inverse grain size exponent was measured to be over 3 for Zr-doped and Sc/Zr codoped materials, and close to 2 for the Nd/Zr codoped materials. The dependence of the strain rates on the grain size was the same under all the temperatures.

3.6 Sintering rates

The sintering results for the Zr-doped, Nd 1000/Zr and Sc/Zr specimens at 1400°C are shown in Fig. 8. As can be seen from the figure, Nd and Zr codoping decreased the densification rate dramatically, in comparison with that of the Zr-doped material, whereas Sc codoping slightly increased the densification rate. The density of all the materials seemed to approach about 98% after sintering at 1400°C for an extended period of time (8 hours). In addition, it was found that, relative to the sample doped with Zr alone, Nd/Zr codoping also slowed down the grain growth during the sintering process, while Sc/Zr codoping increased the grain growth slightly.

The above observations are consistent with the creep results in terms of the magnitude of the influence of the codopant (Nd or Sc) relative to the Zr-doped alumina. This will be discussed in more detail in Section 4.1.

3.7 Evidence of segregation

SIMS maps showing the distribution of dopant ions are given in Fig. 9. For the Nd/Zr and Sc/Zr codoped specimens, the Nd and Zr maps (Fig. 9b & c, d & e, f & g), Sc and Zr maps (Fig. 9h and i) were taken from the same area of the specimen. Clearly, Zr^{4+}, Nd^{3+}, and Sc^{3+} segregated to the alumina grain boundaries. Given that simultaneous segregation to the boundaries by different ions takes place, this suggest a possible additive effect on the grain boundary transport process. [Comparing the brightness of the maps, it is clear that the segregation of Nd is stronger than that of Zr and Sc ions.?????]

[Si maps were also taken from some of these materials. Fig. 9j shows a Si map from the Nd/Zr codoped material. The Si ions in the materials were partially from the initial powders and partially from the course of powder processing. Chemical analysis found about 100 ppm Si in the initial powders. The effect of Si on the creep rate is not clear. However, it is believed to be

minimal as compared with the effects of the other dopants.]

The segregated Nd, Zr, and Sc ions at the grain boundaries occupied an unusually thick layer, with a thickness of about 0.12 μm. Other single segregants occupy a rather thin layer at the boundaries [20]. One possible reason could be the formation of a complex compound of aluminum-neodymium-zirconium oxides or aluminum-scandium-zirconium oxides, as indicated in the EDS analysis (see the following section).

3.8 Microstructural observations

The as-fired microstructures of the Zr-doped (Fig. 1a), Nd 100/Zr and Sc/Zr codoped (Fig. 1e) aluminas were very uniform. The grains were mostly equiaxed, though some grains showed irregular shapes. The range of the grain size was rather broad, 0.1-1.5 μm for Zr-doped, 0.1-3.0 μm for Nd 100/Zr doped and 0.1-2.0 μm for Sc/Zr doped aluminas. In addition, high-resolution SEM did not reveal the presence of any second phase particles in any of the above materials.

In general, it was observed that with increasing Nd doping there was an increase in the degree of microstructural inhomogeneity and the propensity for abnormal grain growth. The range of the grain sizes for the Nd/Zr codoped materials with 350 ppm and 1000 ppm Nd was very broad, 0.2-5.0 μm for Nd 350/Zr and 0.2-10 μm for Nd 1000/Zr. Furthermore, second phase particles were clearly visible for these two compositions (Fig. 10). In the 350 ppm Nd material, the second phase particles were isolated and spread in the microstructure rather uniformly and isolated. By contrast, for Nd 1000/Zr, the second phase particles were nonuniformly distributed in the microstructure. While most of the precipitates were isolated, many of them seemed to stay closer and appeared as loose clusters. This microstructural examination clearly suggests that the solubility limit of Zr in alumina is > 110 ppm, Nd in the range of 40 ppm and 270 ppm, and Sc greater than 1000 ppm.

Higher level of Nd dopants promoted both the normal and abnormal grain growth in Nd/Zr codoped aluminas. Under the same hot-pressing conditions, Nd/Zr codoped alumina with 1000

ppm Nd had an average grain size of 5.2 μm, while that of Nd/Zr codoped alumina with 350 ppm Nd had a grain size of 1.5 μm only (Tables 1 and 2). Sc doping also seemed to promote grain growth in Sc/Zr codoped alumina. The grain size was 0.66 μm and 0.48 μm for Sc/Zr codoped and Zr-doped only aluminas, respectively, under the same hot-pressing conditions.

EDS (energy dispersive spectroscopy) analysis was performed on the second phase particles (Fig. 11). Because of the relative low sensitivity of the EDS techniques, no dopant or impurities were detected in the matrix or at the grain boundaries (Fig. 11a). Some of the second phase particles showed the presence of Nd only (although a much low level of Zr might also exist beyond the detectability of the EDS). Conversely, many precipitates were found to contain both Nd and Zr (Fig. 11c), indicating a possible complex compound of aluminum, neodymium and zirconium oxides.

[The fracture surfaces of the specimens after rupture tests were examined using SEM (Fig. 12). It seemed that cavities developed mainly at the grain boundaries and the triple joints. This observation may indicate the role of grain boundary diffusion and grain boundary sliding in the creep process. The fracture was dominantly intergranular for all the materials. As the Nd doping level increased, transgranular fracture at the inhomogeneities (most likely Nd and/or Zr and Al compounds) were seen more often.

In addition, the fracture toughness of these materials were measured from the indentation technique [21]. The toughness was 3.54±0.30, 3.20±0.17, 3.65±0.34, and 3.41±0.38 MPa·m$^{?¿}$ for Zr-doped, Nd/Zr codoped with 100 and 350 ppm Nd, and Sc/Zr codoped aluminas. The toughness of Nd/Zr codoped material with 1000 ppm Nd could not be determined from this technique, where no well defined cracks were generated from the indentation, a badly deformed and microcracked region was formed under the indentation instead. The toughness of the Nd/Zr codoped alumina with 100 ppm Nd seemed to have a lower value. This may indicate weaker grain boundaries of this material because the fracture was dominated by intergranular mode. However,

toughness change due to the dopants could not be determined with certainty because of the large scatter of experimental data.???????]

4. Discussion

4.1 Controlling Mechanisms

The creep of single phase polycrystalline alumina over a broad range of stress, temperature, and grain size is dominated by grain boundary related diffusion processes [19, 22, 23], as commonly expressed in Eq. (1). As discussed earlier, under such conditions theory predicts a stress exponent n = 1 and an inverse grain size exponent p = 3. In practice, however, many creep experiments have shown a stress exponent of close to 2 and an inverse grain size exponent greater than 1 [19]. Figure 6 shows a stress exponent of about 2, while Fig. 7 shows the inverse grain size exponents close to 3 and 2 for the doped aluminas. The values of the stress exponent notwithstanding, our belief is that the improvement in creep resistance results from the lowering of grain boundary diffusivity due to the segregation of the oversized dopant ions to the boundaries. The reasons for this belief are listed below.

First, consider the values obtained for the inverse grain size. The exponent p = 3 suggests that the creep is controlled by grain boundary diffusion. Although p=2 suggests a lattice diffusion mechanism, we will later argue that the grain boundary diffusivity has been suppressed to an extent that lattice diffusion is now rate controlling. Second, sintering studies of yttrium and lanthanum [20] doped alumina have concluded that sintering process was grain boundary diffusion controlled, and found a reduction of densification rate by a factor of 10 and 20 for 1000 ppm yttrium and lanthanum addition to alumina, respectively. The densification rate of Nd/Zr codoped alumina decreased significantly as compared with that of Zr-doped alumina, while that of the Sc/Zr codoped alumina increased slightly (Fig.8), indicating the reduction and no significant change of grain

boundary diffusivity by Nd and Sc addition to alumina, respectively, consistent with the results of the creep study (Figs. 5 and 13). Third, direct measurement of the coefficient of oxygen grain boundary diffusion by Le Gall et al. [9] recently revealed a three orders of magnitude reduction with a doping level of 500 ppm yttrium, while the oxygen lattice diffusivity increased slightly. These findings are all consistent with the premise that the segregation of the rare earth dopant ion to the grain boundaries slows down the grain boundary diffusion process, and thus leads to a decrease of the creep rate and the densification rate.

However, the measured value of n=2 can't be explained by the conventional diffusive creep mechanisms, which are based on vacancy flow under stress either through the crystalline lattice or along the grain boundaries. Recently, Inomata [24] has provided a different explanation by re-examining the basic equations describing diffusional creep. By assuming the elastic strain energy is the driving force for the stress-directed diffusion creep, he arrived at conclusions consistent with Eq. (1) with n=2 and p=3 and 2 for grain boundary and lattice diffusion controlled creep, respectively. This theory seems to be in excellent agreement with the experiments in the present study, which indicate that the creep of Zr-doped and Sc/Zr codoped aluminas is grain boundary diffusion controlled, and that of Nd/Zr codoped aluminas is lattice diffusion controlled.

4.2 Normalized creep rates

In order to directly compare the strain rates associated with different dopants, the strain rates shown in Fig. 5 were adjusted to reflect a grain size of 0.72μm, the grain size of the Nd 100/Zr sample. The strain rates of Zr-doped and Sc/Zr codoped aluminas were corrected assuming p = 3 (grain boundary diffusion controlled creep) while that of the other Nd/Zr codoped aluminas were corrected assuming p = 2 (lattice diffusion controlled creep). The corrected strain rates are shown in Fig. 13. From the work of French et al. [1] and Cho et al. [5], the inverse grain size exponent for undoped alumina was close to 3. The corrected strain rates of undoped alumina according to the grain boundary diffusion controlled creep were also included in Fig. 13.

Figure 13 shows that 100 ppm Zr addition to alumina reduced the creep rate by a factor of 10. The addition of 100 ppm Nd further reduced the creep rate by another factor of 20. The total reduction of the creep rate due to 100 ppm Zr and 100 ppm Nd addition to alumina was two and a half orders of magnitude. Higher doping levels of Nd did not further reduce the creep rate. Instead, the creep rate reduction due to the addition of Nd saturated at a level of only 100 ppm, though the apparent activation energy was increased with increasing level of Nd doping. One possible explanation for this is that the degree of suppression of grain boundary diffusivity achieved by 100 ppm Nd and Zr codoping is sufficiently great that lattice diffusion becomes the rate-controlling mechanism, as evidenced from the measured value of p=2. On the other hand, the addition of 1000 ppm Sc to 100 ppm Zr-doped alumina did not significantly change the creep rate and the creep mechanism may remain the same, as indicated by the measured value of p~3.

The creep rates of 1000 ppm Y-doped and 500 ppm La-doped alumina are also shown in Fig. 13 for comparison. These points were adjusted to reflect a grain size of 0.72 μm given their original grain sizes of 3.1 μm and 1.9 μm, respectively [5], assuming a lattice diffusion mechanism. It can be seen that the creep rates of the Nd/Zr codoped alumina are very close to that of Y and La doped alumina after normalizing to the same grain size.

4.3 The effect of grain boundary diffusivity and lattice diffusivity on the creep rate

As discussed above, the creep of doped alumina in the range of stress, temperature, and grain size studied in the present work is most likely controlled by the grain boundary diffusion or lattice diffusion. To explore the possibility of further lowering the creep rate, we need to take a closer look at the dependence of creep rate on grain size and diffusivity (?????). For the purpose of direct comparison with the experimental results in this work, the temperature is assumed to be 1275°C and the stress 50 MPa.

Because many of the values of the Inomata theory are unknown, the conventional grain boundary and lattice diffusion creep models with n=1 will be used in the analysis.

The strain rate with the presence of ambipolar diffusion is [29]:

$$\dot{\varepsilon} = 28\frac{D_{comlex}Gb}{kT}\left[\frac{b}{d}\right]^2\left[\frac{\sigma}{G}\right] \qquad (2)$$

where $D_{complex}$ is a complex diffusion coefficient defined as:

$$D_{complex} = \frac{(1/2)[D_l^+ + 1.2(\delta^+ D_{gb}^+ / d)}{1+(3/2)\dfrac{[D_l^+ + 1.2(\delta^+ D_{gb}^+)]}{[D_l^- + 1.2(\delta^- D_{gb}^-)]}} \qquad (3)$$

In Eq. (3), D is diffusivity, the subscripts l and gb represent lattice and grain boundary, δ is the effective grain boundary width and + and - represent the cation (Al^{3+}) and anion (O^{2-}), respectively.

Figure 14 shows the effect of grain boundary and lattice diffusivities on the creep rate of undoped alumina based on ambipolar diffusion (Eq. (2)). The diffusivity data of undoped alumina were taken from references [29, 25]. It is seen from this figure that Al^{3+} ions along the grain

boundary diffusion (D_{gb}^+) controls the creep in undoped fine-grained alumina with a grain size of

up to about 10 μm. Creep by the lattice diffusion of Al^{3+} ions (D_l^+) predominates at larger grain sizes. When the Al^{3+} grain boundary diffusivity is reduced while the other diffusivities are kept unchanged, the creep rate for grain sizes on the order of 1 μm is reduced at the beginning and then becomes saturated when the D_{gb}^+ is reduced by about two orders of magnitude (dadot line (????) in Fig. 14). Further reduction in D_{gb}^+, say by another two orders of magnitude, does not lead to any significant reduction on the creep rate (dashed line). This is because lattice diffusion of Al^{3+} (D_l^+) is now rate-controlling even at the very small grain sizes.

When the lattice diffusivity of Al^{3+} is also reduced along with D_{gb}^+, the creep rate for fine-grained alumina is still controlled by the grain boundary diffusion of Al^{3+} ions, while that for larger grain sizes by the lattice diffusion of Al^{3+}. For example, a reduction of D_{gb}^+ by four orders of magnitude and at the same time a reduction of D_l^+ by two orders of magnitude, the creep rate for fine-grained alumina drops almost also four orders of magnitude (the solid line in Fig. 14).

The experimental data in this work shown in Fig. 7 are re-plotted in Fig. 14. The experimental results of the creep rate reduction of one order of magnitude by Zr-doped and Sc/Zr codoped aluminas seems to agree with that caused by the reduction of roughly one order of magnitude in the grain boundary diffusivity of aluminum ions. Similarly, the over two orders of magnitude reduction in creep rate by Nd/Zr codoped alumina agrees very well with that caused by the reduction of two orders of magnitude or more in the grain boundary diffusivity of aluminum ions. The agreement between the experimental results and that of the analysis is impressive. However, caution has to be taken to draw this conclusion. In the numerical analysis, the behavior of the creep rate depends on the lattice and grain boundary diffusivities of both the aluminum and oxygen ions. Unfortunately, no conclusive diffusivity data is available to date.

If the observed creep rate reduction by the dopants is indeed caused by the reduction of grain boundary diffusivity of aluminum ions due to the segregated ions at the grain boundaries, and the diffusivity data used in the numerical analysis are reliable, we can speculate on possible routes that will lead to further improvement in the creep resistance of alumina. From the numerical analysis, the creep rate reduction can be no more than two orders of magnitude by reducing D_{gb}^{+} while D_{l}^{+} is unchanged. Therefore, the over two orders of magnitude reduction in the creep rate by the addition of Nd/Zr (containing 100, 350, and 1000 ppm Nd), 1000 ppm Y, and 500 ppm La could well be the maximum achievable result. Indeed, 100 ppm addition of Nd and Zr is enough in achieving such a reduction. Further improvement in creep resistance can only come from the reduction of the lattice diffusivity of aluminum ions while the reduced grain boundary diffusivity is maintained. This implies that further improvement in the creep resistance of alumina is possible by introducing dopants which act as aluminum lattice diffusion inhibitors to the Nd/Zr codoped systems.

4.4 Effect of Nd or additive effect of Nd and Zr in lowering the creep rate

Although SIMS maps of Sc and Zr of the Sc/Zr codoped material clearly demonstrated that both ions segregated to the grain boundaries, the creep resistance did not further improve as compared with that of alumina doped only with Zr (see Fig. 13). The ionic sizes of Sc^{3+} and Zr^{4+} are very similar, 0.73Å. One possible explanation for this result is that for dopants of similar size, there is no additive effect in lowering the creep rate. The creep resistance is determined by the segregation of the dominant type of ion which results in the highest reduction in creep rate. The fact that the Sc/Zr codoped alumina and the Zr doped alumina had comparable apparent activation energies (720 kJ/mol and 690 kJ/mol, respectively) provides indirect evidence to support this argument.

By contrast with the Sc/Zr codoped case, In the Nd/Zr codoped alumina the Nd ions do have a significant contribution towards improving the overall creep resistance. Fig. 13 demonstrates that all the Nd/Zr codoped materials had a significantly lower creep rate than that of Zr only doped alumina. Because of the relative larger ionic size of Nd^{3+} (.995Å) as compared to that of Zr^{4+} (.73Å), and the stronger segregation of Nd to grain boundaries (see Fig. 9) (?????), Nd ions are expected to be more effective in obstructing the grain boundary mass transport process than Zr ions. Because of the relatively close ionic size of Y (.89Å), Nd (.995Å), and La (1.06Å), the comparable creep rates suggest that the creep rate is dictated by the segregation of Nd, Y, and La ions to alumina grain boundaries. However, from the present study alone, it is not possible to rule out a contribution from the Zr^{4+} ions. The creep rate of alumina singly doped with Nd is currently under investigation.

5. Summary

The tensile creep behavior of hot-pressed fine-grained alumina ceramics, doped with 100 ppm Zr and co-doped with 100, 350, 1000 ppm Nd, 1000 ppm Sc has been studied in the temperature range of 1200-1350°C and the stress range of 20-100 MPa. An extensive steady-state creep regime was observed for each material. A stress exponent of about 2 was found for all the compositions. The inverse grain size exponent was found to be close to 3 for Zr-doped and Sc/Zr codoped alumina, and about 2 for the Nd/Zr codoped materials containing 100 ppm and 350 ppm Nd. It was found that the creep rate of Zr-doped alumina and Sc/Zr codoped alumina was lowered by one order of magnitude, and that of the Nd/Zr codoped aluminas was lowered by two to three orders of magnitude in comparison to pure alumina. The improvement in the creep resistance of alumina by these dopant ions was a solid solution effect and direct evidence of segregation by Nd, Sc, and Zr ions was obtained by SIMS analysis. It is suggested that the segregation of the

oversized dopant ions to the alumina grain boundaries reduce the grain boundary diffusivity and thus the creep rate.

The comparable creep rates of Nd/Zr-codoped and Y and La doped alumina are consistent with the numerical analysis of the diffusional creep of alumina that roughly two orders of magnitude reduction in creep rate is the maximum one can achieve based on the concept of inhibiting grain boundary diffusion process alone. Further improvement in creep resistance is possible through simultaneous inhibition of both the grain boundary and lattice diffusion.

Acknowledgments

The authors would like to thank R. Krause and Dr. E. R. Fuller, Jr. at NIST for help with hot-pressing the 3-inch billets, and Dr. W. Luecke at NIST for providing the engineering graph of the 2-inch tensile specimen design and a preprint of his paper on "Sources of Strain Measurement Error in Flag-Based Extensometry". The authors would also like to thank J. Cho for providing the original creep data of pure and 1000 ppm Y and 500 ppm La doped aluminas and Drs. J.D. French and A.M. Thompson for helpful discussions. This work was supported by AFOSR under grant # F49620-94-1-0284.

Figure Captions

Fig. 1 Typical as-fired microstructures of the Zr-doped (a), Nd/Zr codoped containg 100 ppm Nd (b), 350 ppm Nd (c), 1000 ppm Nd (d), and Sc/Zr codoped alumina containing 1000 ppm Sc.

Fig. 2 A typical temperature step and stress step test: The stress was fixed at 50 MPa when temperature stepped to different values and the temperature was fixed at 1275°C when the stress stepped. The tested material was 100 ppm Zr-doped alumina with a grain size of 1.64 μm.

Fig. 3 Strain rates of Nd/Zr codoped alumina containing 1000 ppm Nd. All data fell in ±35% of the averaged data points. Specimens #1 and #2 were excluded from the average (see text for reasons).

Fig. 4 The strain-time relationships from the creep rupture tests.

Fig. 5 The as-measured strain rates at an applied stress of 50 MPa for un-annealed specimens.

Fig. 6 The effect of stress on the creep rates at 1275°C for all the compositions.

Fig. 7 The effect of grain size on the creep rates at 1275°C and 50 MPa.

Fig.8 Density as a function of sintering time at 1400°C.

Fig. 9 SIMS map of Zr in 100 ppm Zr-doped alumina (a), maps of Nd and Zr in Nd/Zr codoped

alumina containing 100 ppm Nd (b) and (c), 350 ppm Nd (d) and (e), 1000 ppm Nd (f) and (g), maps of Sc and Zr in Sc/Zr codoped alumina (h) and (i), and a typical map of Si (j) (in Zr-doped alumina).

Fig. 10 Nd-rich and both Nd- and Zr-rich second phase particles observed only in the Nd/Zr codoped alumina containing 350 ppm (a) and 1000 ppm Nd (b).

Fig. 11 EDS analysis of the second phase particles: (a) in the matrix, (b) on an Nd-rich particle, and (c) on a both Nd and Zr rich particle.

Fig. 12 Fracture surfaces of the crept specimens: Zr-doped (a), Nd/Zr codoped containing 100 ppm Nd (b), 350 ppm Nd (c), 1000 ppm Nd (d), and Sc/Zr codoped alumina (e).

Fig. 13 Creep rates corrected to a grain size of 0.72 μm according to the grain boundary diffusion controlled creep for pure alumina, Zr-doped alumina, Sc/Zr codoped alumina, and lattice diffusion controlled creep for Nd/Zr codoped compositions.

Fig. 14 Strain rates as a function of grain size for pure alumina showing the effect of reducing the grain boundary diffusivity and lattice diffusivity on the creep rate. Also shown are the experimental data in the present work (solid data points).

[1]. J.D. French, J. Zhao, M.P. Harmer, H.M. Chan, and G.A. Miller, "Creep of Duplex Microstructures," J. Am. Ceram. Soc. 77 [11], 2857-65 (1994).

[2]. S. Lartigue, C. Carry, and L. Priester, "Grain Boundaries in High Temperature Deformation of Yttria and Magnesia Co-Doped Alumina," J. Phys. (Paris), C1-51, 985-90 (1990).

[3]. A.G. Robertson, D.S. Wilkinson, and C.H. Cáceres, "Creep and Creep Fracture in Hot-Pressed Alumina," J. Am. Ceram. Soc. 74[5], 915-21 (1991).

[4]. P. Gruffel and C. Carry, "Strain-Rate Plateau in Creep of Yttria-Doped Fine Grained Alumina," pp.305-11 in Proceedings of the 11th RISϕ International Symposium on Metallurgy and Materials Science: Structural Ceramics-Microstructure and Properties. Ed. by J.J. Bentzen, J.B. Bilde-Sorensen, N. Christiansen, A. Horsewell, and B. Ralph. Risϕ National Lab. Roskilde, Denmark, 1990.

[5]. J. Cho, M.P. Harmer, H.M. Chan, J.M. Rickman, and A.M. Thompson, "The Effect of Y and La on Tensile Creep Behavior of Aluminum Oxide," submitted to J. Am. Ceram. Soc. (1996).

[6]. F. Wakai, T. Iga, and T. Nagano, "Effect of Dispersion of ZrO_2 Particles on Creep of Fine-Grained Al_2O_3," J. Ceramic Soc. Jpn. 96[12], 1206-09 (1988).

[7]. P. Gruffel and C. Carry, "Effect of Grain Size on Yttrium Grain Boundary Segregation in Fine Grained Alumina," J. Eur. Ceram. Soc. 11, 189-99 (1993).

[8]. E. Arzt, M.F. Ashby, and R.A. Verrall, "Interface Controlled Diffusional Creep," Acta Metall. 31[12], 1977-89 (1983).

[9]. F.R.N. Nabarro, "Deformation of crystals by the motion of single ions, in: Report of a Conference on the Strength of Solids," p. 231, Phys. Soc., London (1948).

[10]. C. Herring, "Diffusional viscosity of a polycrystalline solid," J. Appl. Phys. 21:437 (1950).

[11]. R.L. Coble, "A model for boundary diffusion controlled creep in polycrystalline materials," J. Appl. Phys. 34:1679 (1963).

[12]. G.W. Greenwood, "The possible effects on diffusional creep of some limitation of grain boundaries as vacancy sources and sinks," Scripta Metall. 4[3], 171-3 (1970).

[13]. A.G. Evans and T.G. Langdon, "Structural ceramics," Prog. Mater. Sci. 21:171 (1976).

[14]. W.R. Cannon and T.G. Langdon, "Review: Creep of Ceramics," Part I: "Mechanical Characteristics," J. Mater. Sci. 18, 1-50 (1983); Part II: "An Examination of Flow Mechanisms," J. Mater. Sci. 23, 1-20 (1988).

[15]. J. Fang, A.M. Thompson, H.M. Chan, and J. Cho, "Effect of Y and La on the Sintering Behavior of Ultra-High-Purity Al2O3," in press, J. Am. Ceram. Soc. (1997).

[16]. J.D. French and S.M. Wiederhorn, "Tensile Specimens from Ceramic Components," J. Am. Ceram. Soc. 79[2], 550-52 (1996).

[17]. H.T. Lin, P.F. Becher, and M.K. Ferber, "Improvement of Tensile Creep Displacement

Measurements," J. Am. Cerm. Soc. 77[10], 2767-70 (1994).

[18]. W.E. Luecke and J.D. French, "Sources of Strain Measurement Error in Flag-Based Extensometry," J. Am. Ceram. Soc. 79[6], 1617 (1996).

[19]. E. Sato and C. Carry, "Yttria Doping and Sintering of Submicrometer-Grained α-Alumina," J. Am. Ceram. Soc. 79[8], 2156-60 (1996).

[20]. Dr. J. Chabala, private communications.

[21]. G.R. Anstis, P. Chantikul, B.R. Lawn, D.B. Marshall, "A Critical Review of Indentation Techniques for Measuring Fracture Toughness: I. Direct Crack Measurements," J. AM. Ceram. Soc. 64, 533-38 (1981).

[22]. A.H. Chokshi and T.G. Langdon, "Diffusion Creep in Ceramics: a Comparison with Metals," Defect and Diffusion Forum 66-69, 1205-26 (1989).

[23]. R.M. Cannon, W.H. Rhodes, and A.H. Heuer, "Plastic Deformation of Fine-Grained Alumina(Al_2O_3): I, Interface-Controlled Diffusional Creep," J. Am. Ceram. Soc. 63[1-2], 46-53 (1980).

[24]. Y. Inomata, "," in Fundamental Structural Ceramics, S. Somiya and R.C. Bradt, eds, Terra, Tokyo, 1987, p. 49.

[25]. T.G. Langdon, "," Ceram. Intl. 6, 11 (1980).

Fig. 9 SIMS map of Zr in 100 ppm Zr-doped alumina (a), maps of Nd and Zr in Nd/Zr codoped alumina containing 100 ppm Nd (b) and (c), 350 ppm Nd (d) and (e), 1000 ppm Nd (f) and (g), maps of Sc and Zr in Sc/Zr codoped alumina (h) and (i), and a typical map of Si (j) (in Zr-doped alumina).

Fig. 10 Nd-rich and both Nd- and Zr-rich second phase particles observed only in the Nd/Zr codoped alumina containing 350 ppm (a) and 1000 ppm Nd (b).

Fig. 11 EDS analysis of the second phase particles: (a) in the matrix, (b) on an Nd-rich particle, and (c) on a both Nd and Zr rich particle.

Fig. 12 Fracture surfaces of the crept specimens: Zr-doped (a), Nd/Zr codoped containing 100 ppm Nd (b), 350 ppm Nd (c), 1000 ppm Nd (d), and Sc/Zr codoped alumina (e).

Fig. 13 Creep rates corrected to a grain size of 0.72 μm according to the grain boundary diffusion controlled creep for pure alumina, Zr-doped alumina, Sc/Zr codoped alumina, and lattice diffusion controlled creep for Nd/Zr codoped compositions.

Fig. 14 Strain rates as a function of grain size for pure alumina showing the effect of reducing the grain boundary diffusivity and lattice diffusivity on the creep rate. Also shown are the experimental data in the present work (solid data points).

Table 1. Nominal and Measured Doping Levels by ICP-OES

	Zr-doped	Nd/Zr codoped			Sc/Zr codoped
Nominal	100 ppm Zr	100 ppm Nd	350 ppm Nd	1000 ppm Nd	1000 ppm Sc
Measured	110 ppm Zr	40 ppm Nd 70 ppm Zr	270 ppm Nd 220 ppm Zr	735 ppm Nd 190 ppm Zr	610 ppm Sc 200 ppm Zr

Table 2. Densities of as Hot-Pressed Materials and Grain Sizes

	Zr-doped	Nd/Zr codoped			Sc/Zr codoped
Nominal Comp.	100 ppm Nd	100 ppm Nd	350 ppm Nd	1000 ppm Nd	1000 ppm Sc
Density	97.0%	98.0%	100%	100%	95.0% (?)
Grain size (μm) (as hot-pressed)	0. 48	0.72	1.50	5.2	0.66
Grain size (μm) (Annealed at 1450°C)	1.45[a]	1.31[a]	2.30[a]	-	1.66[b]
Grain size (μm) (Annealed at 1500°C)	1.64[a]	1.97[a]	3.90[a]	-	1.93[b]

Notes:

a. Annealed for 10 hours at the specified temperature.
b. Annealed for 5 hours at the specified temperature.

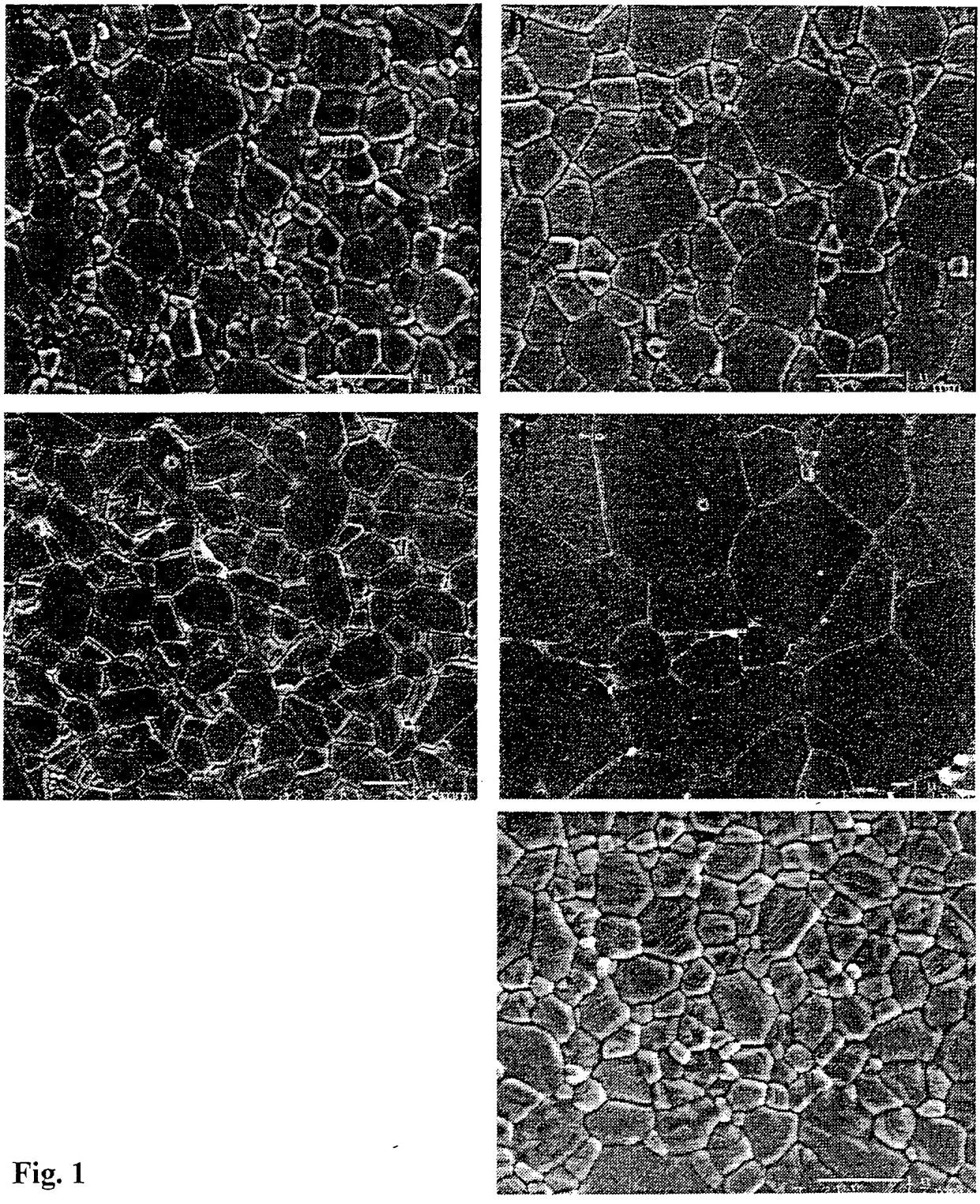

Fig. 1

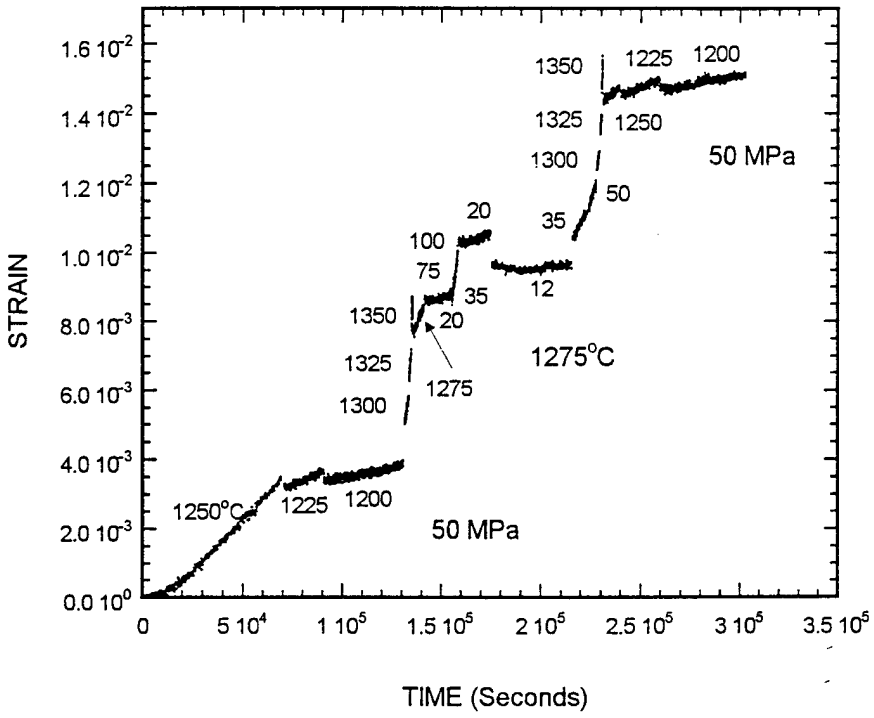
STRAIN
1.6 10-2
1.4 10-2
1.2 10-2
1.0 10-2
8.0 10-3
6.0 10-3
4.0 10-3
2.0 10-3
0.0 10^0
0
5 10^4
1 10^5
1.5 10^5
2 10^5
2.5 10^5
3 10^5
3.5 10^5
TIME (Seconds)
1250°C
1225
1200
50 MPa
1350
1325
1300
1275
20
100
75
35
1275°C
1350
1325
1300
1225
1200
1250
50 MPa
20
35
50
12

Fig. 2

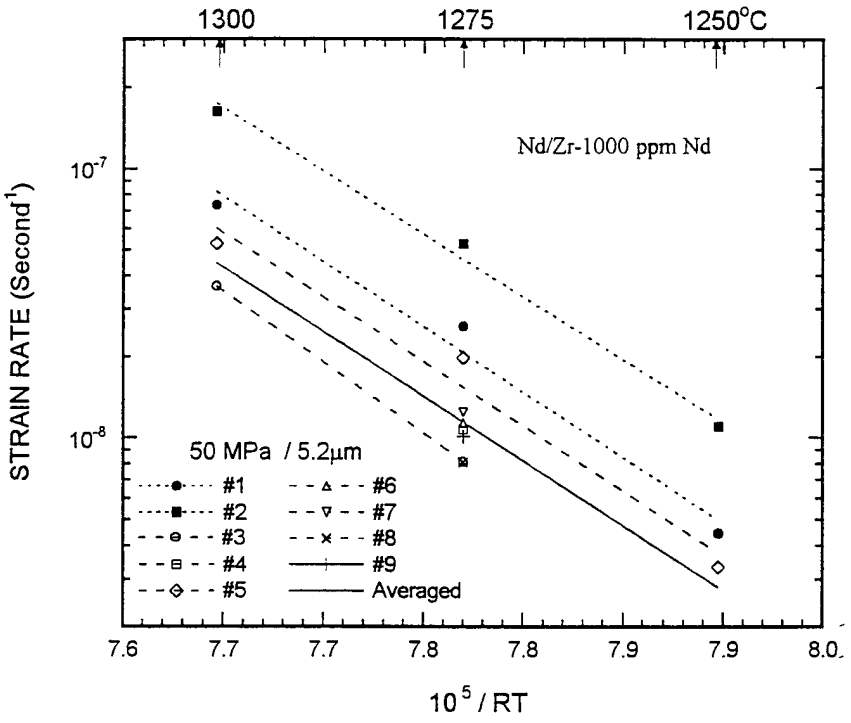
1300
1275
1250°C
Nd/Zr-1000 ppm Nd
10^{-7}
10^{-8}
STRAIN RATE (Second^{-1})
50 MPa / 5.2μm
#1
#2
#3
#4
#5
#6
#7
#8
#9
Averaged
7.6
7.7
7.7
7.8
7.8
7.9
7.9
8.0
10^5 / RT

Fig. 3

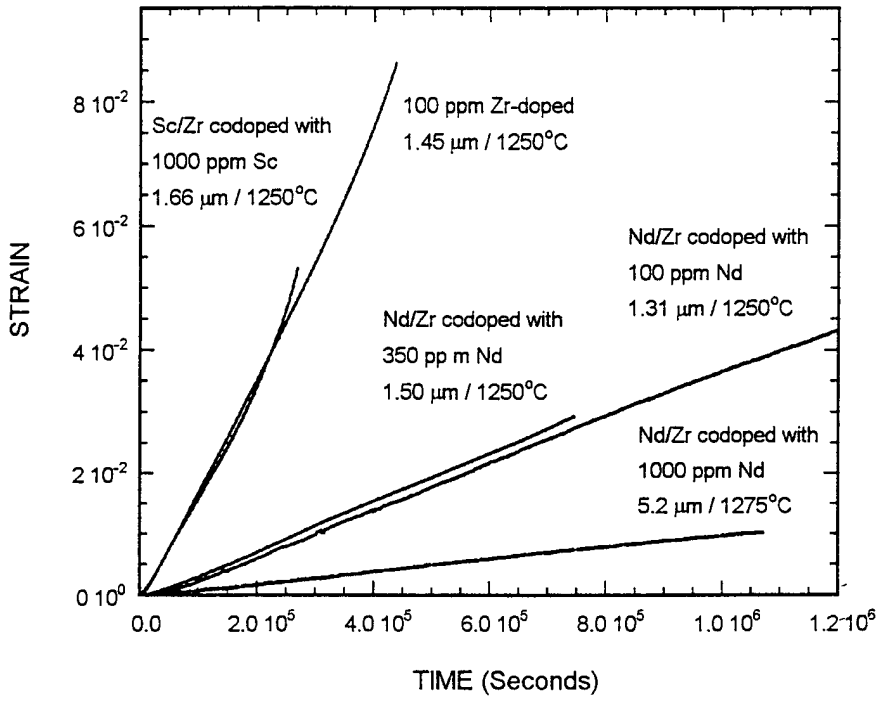
8 10-2
6 10-2
4 10-2
2 10-2
0 10^0
STRAIN
0.0
2.0 10^5
4.0 10^5
6.0 10^5
8.0 10^5
1.0 10^6
1.2 10^6
TIME (Seconds)
Sc/Zr codoped with
1000 ppm Sc
1.66 μm / 1250°C
100 ppm Zr-doped
1.45 μm / 1250°C
Nd/Zr codoped with
100 ppm Nd
1.31 μm / 1250°C
Nd/Zr codoped with
350 pp m Nd
1.50 μm / 1250°C
Nd/Zr codoped with
1000 ppm Nd
5.2 μm / 1275°C

Fig. 4

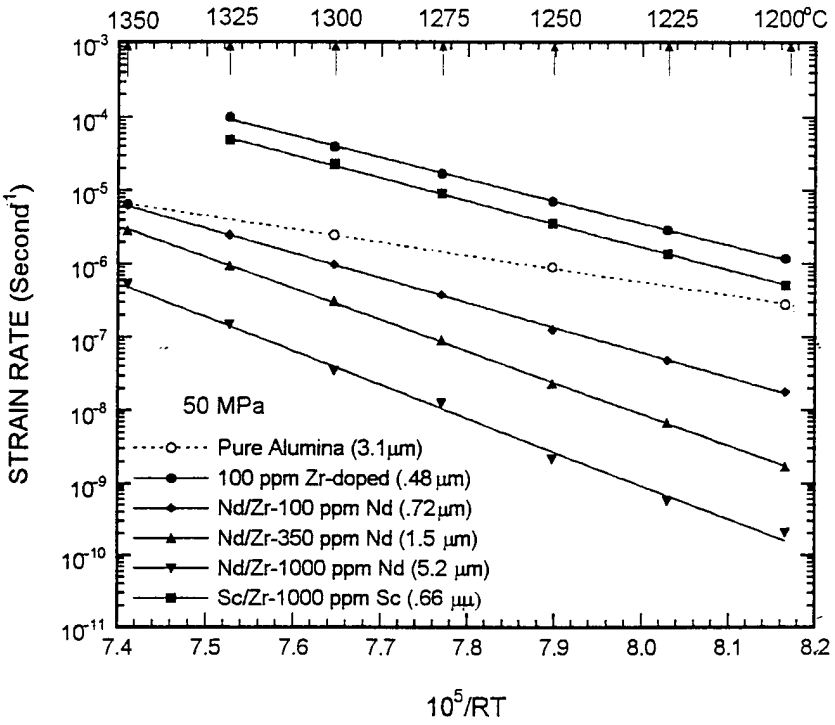
1350
1325
1300
1275
1250
1225
1200°C
STRAIN RATE (Second-1)
10-3
10-4
10-5
10-6
10-7
10-8
10-9
10-10
10-11
50 MPa
Pure Alumina (3.1μm)
100 ppm Zr-doped (.48 μm)
Nd/Zr-100 ppm Nd (.72μm)
Nd/Zr-350 ppm Nd (1.5 μm)
Nd/Zr-1000 ppm Nd (5.2 μm)
Sc/Zr-1000 ppm Sc (.66 μμ)
7.4
7.5
7.6
7.7
7.8
7.9
8.0
8.1
8.2
10^5/RT

Fig. 5

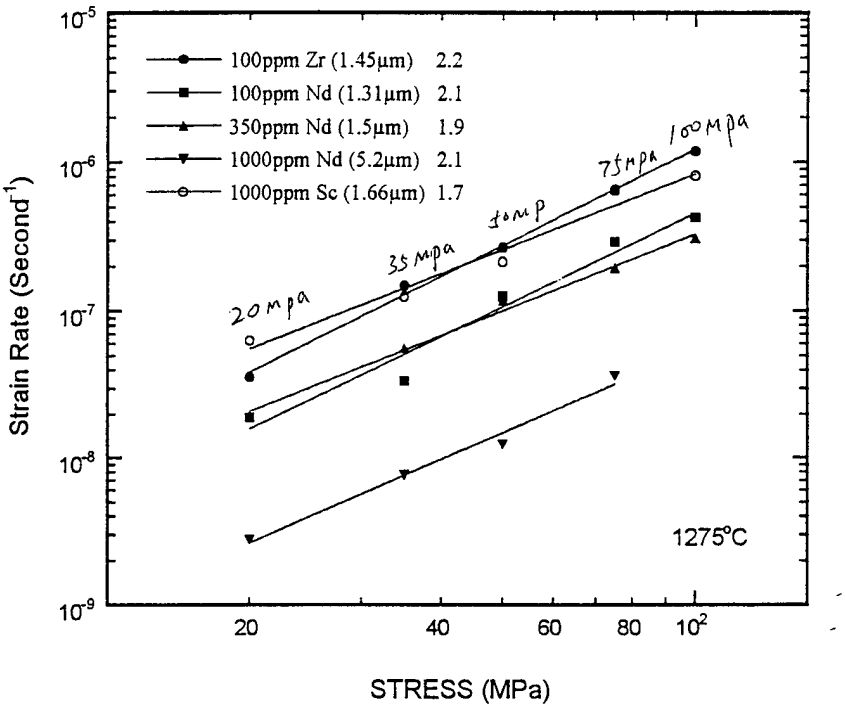
100ppm Zr (1.45μm) 2.2
100ppm Nd (1.31μm) 2.1
350ppm Nd (1.5μm) 1.9
1000ppm Nd (5.2μm) 2.1
1000ppm Sc (1.66μm) 1.7
20 mpa
35 mpa
50 mp
75 mpa
100 mpa
1275°C
Strain Rate (Second-1)
STRESS (MPa)

Fig. 6

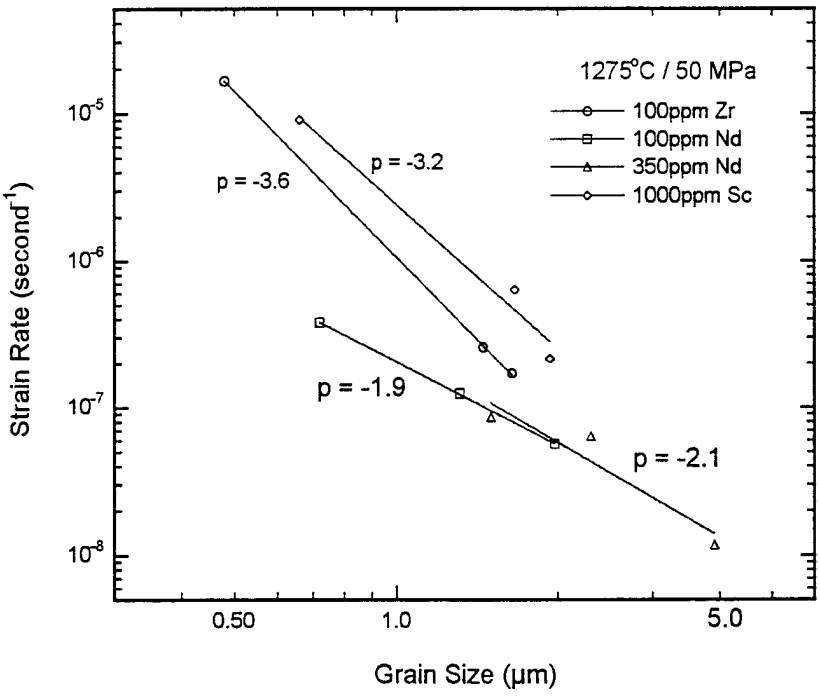
1275°C / 50 MPa
100ppm Zr
100ppm Nd
350ppm Nd
1000ppm Sc
p = -3.6
p = -3.2
p = -1.9
p = -2.1
Strain Rate (second-1)
10-5
10-6
10-7
10-8
0.50
1.0
5.0
Grain Size (μm)

Fig. 7

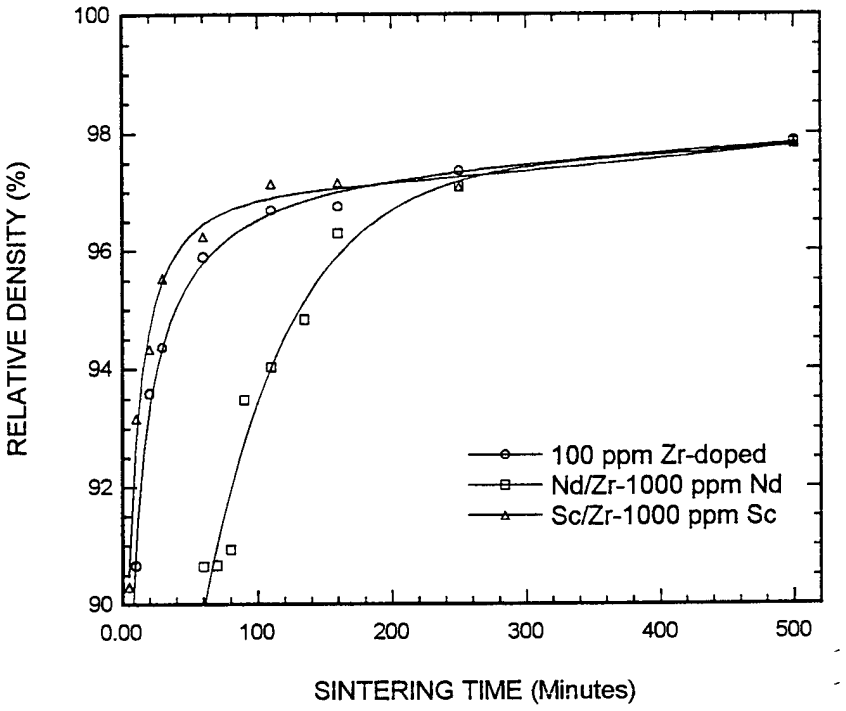
100
98
96
94
92
90
0.00
100
200
300
400
500
RELATIVE DENSITY (%)
SINTERING TIME (Minutes)
100 ppm Zr-doped
Nd/Zr-1000 ppm Nd
Sc/Zr-1000 ppm Sc

Fig. 8

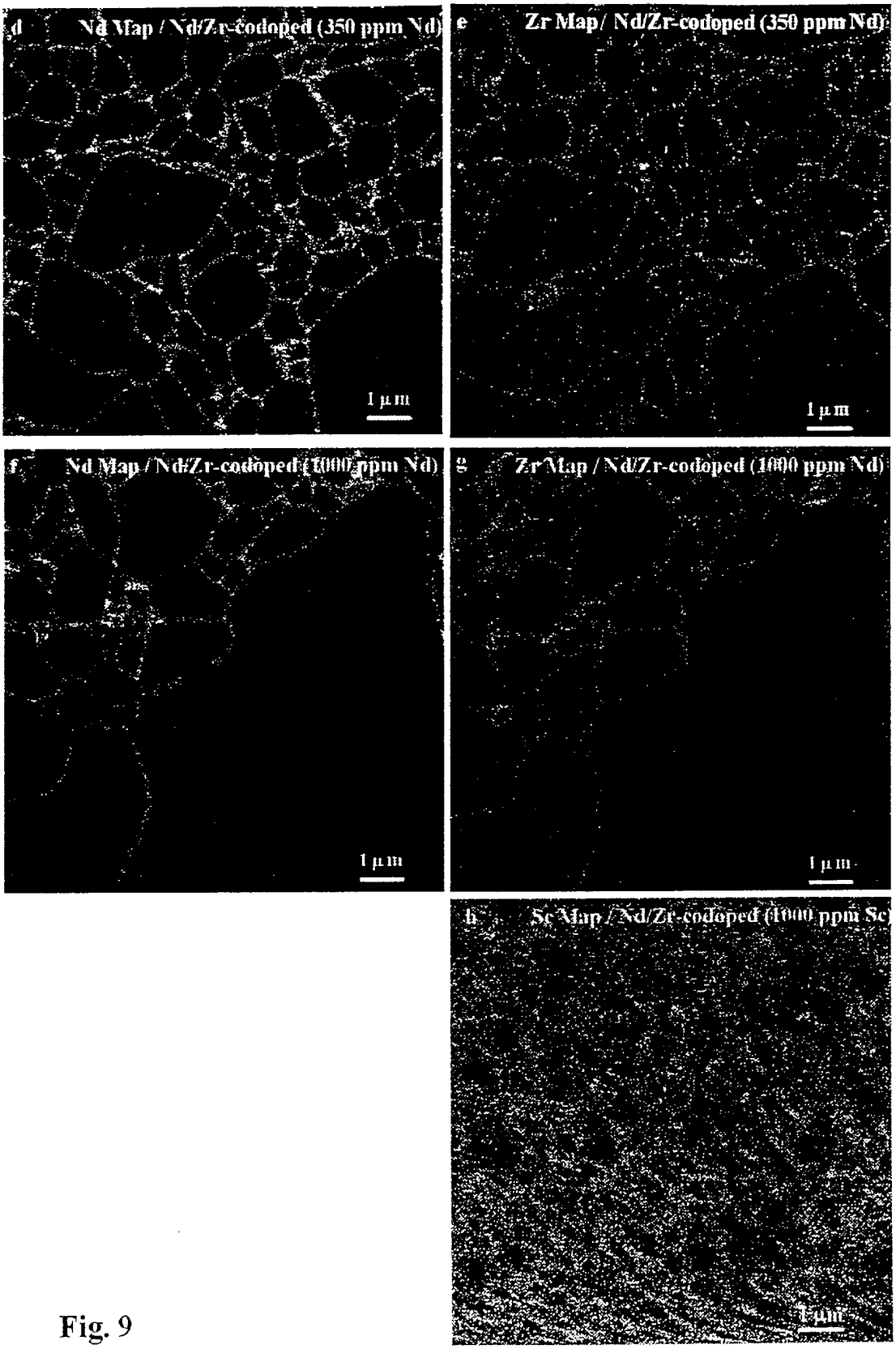
d Nd Map / Nd/Zr-codoped (350 ppm Nd)
1 μm
e Zr Map / Nd/Zr-codoped (350 ppm Nd)
1 μm
f Nd Map / Nd/Zr-codoped (1000 ppm Nd)
1 μm
g Zr Map / Nd/Zr-codoped (1000 ppm Nd)
1 μm
h Sc Map / Nd/Zr-codoped (1000 ppm Sc)
1 μm

Fig. 9

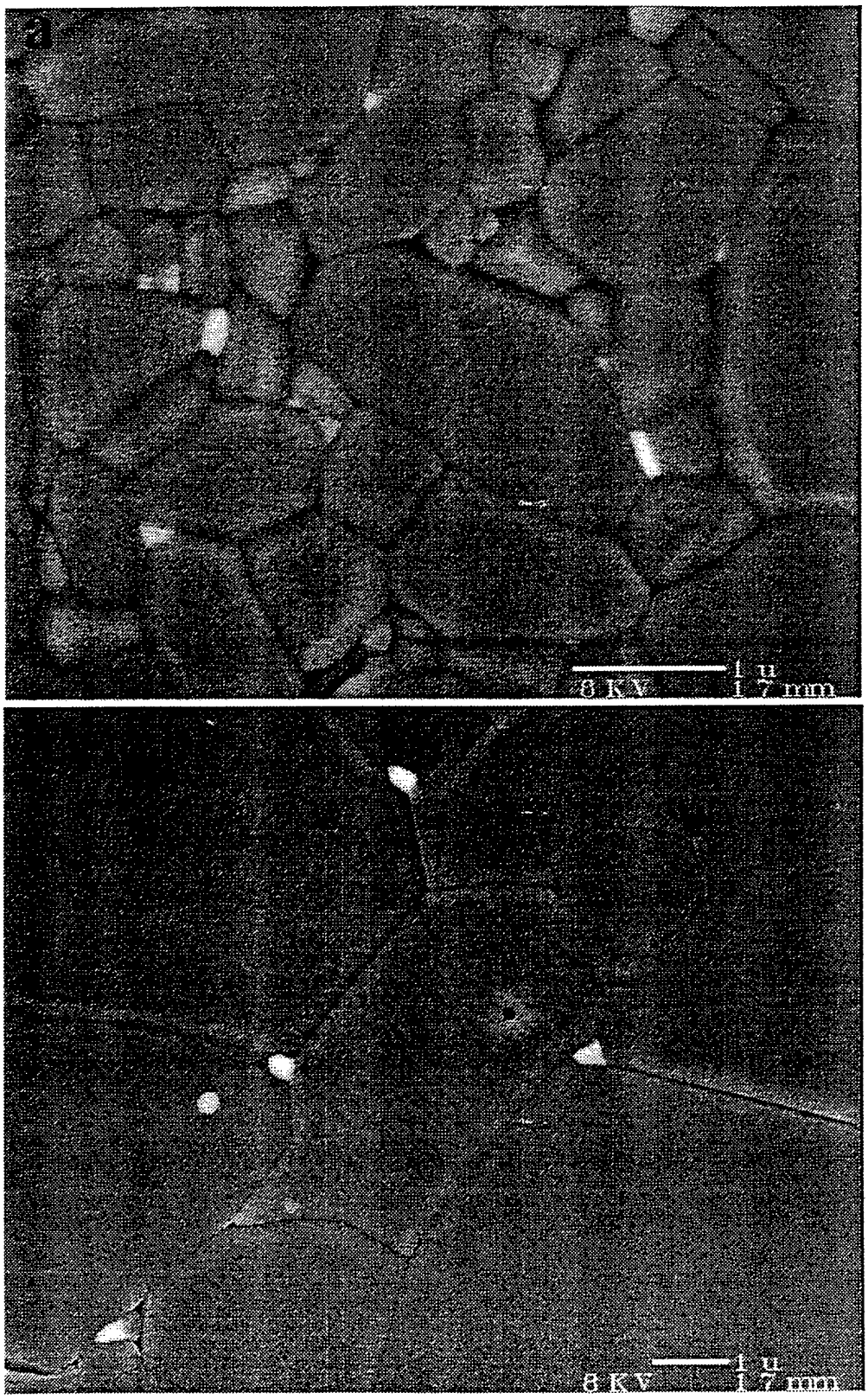

Fig. 10

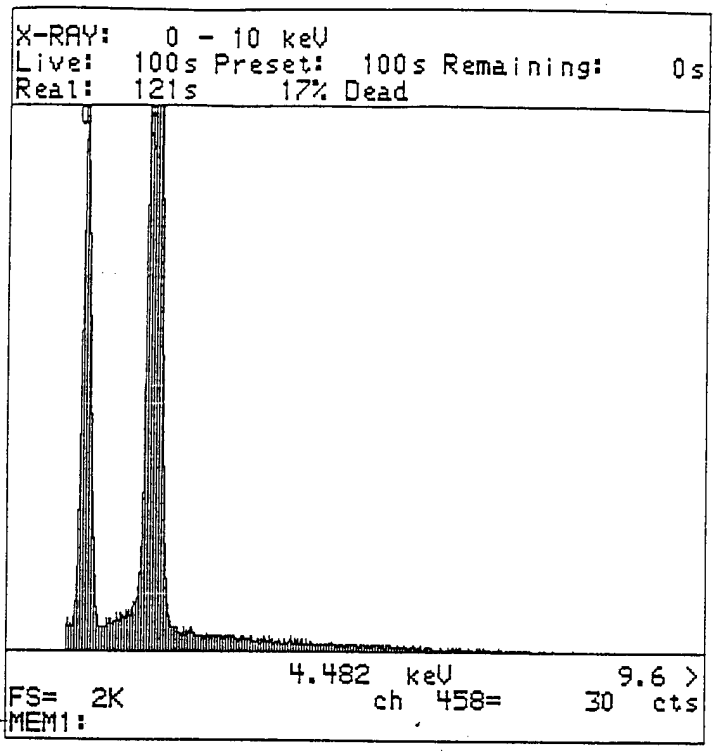
X-RAY: 0 - 10 keV
Live: 100s Preset: 100s Remaining: 0s
Real: 121s 17% Dead
4.482 keV 9.6 >
FS= 2K ch 458= 30 cts
MEM1:

(a)

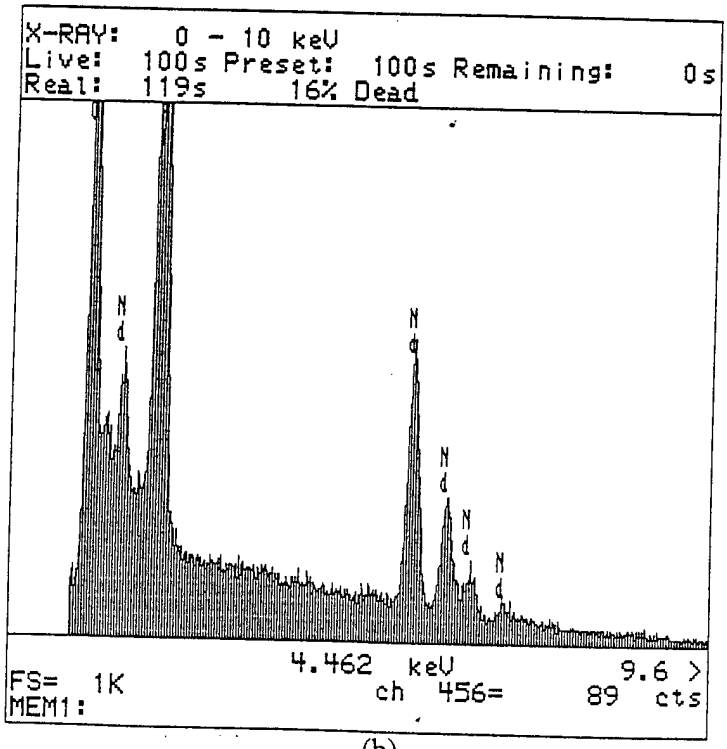
X-RAY: 0 - 10 keV
Live: 100s Preset: 100s Remaining: 0s
Real: 119s 16% Dead
Nd
Nd
Nd
Nd
Nd
4.462 keV 9.6 >
FS= 1K ch 456= 89 cts
MEM1:

(b)

Fig. 11

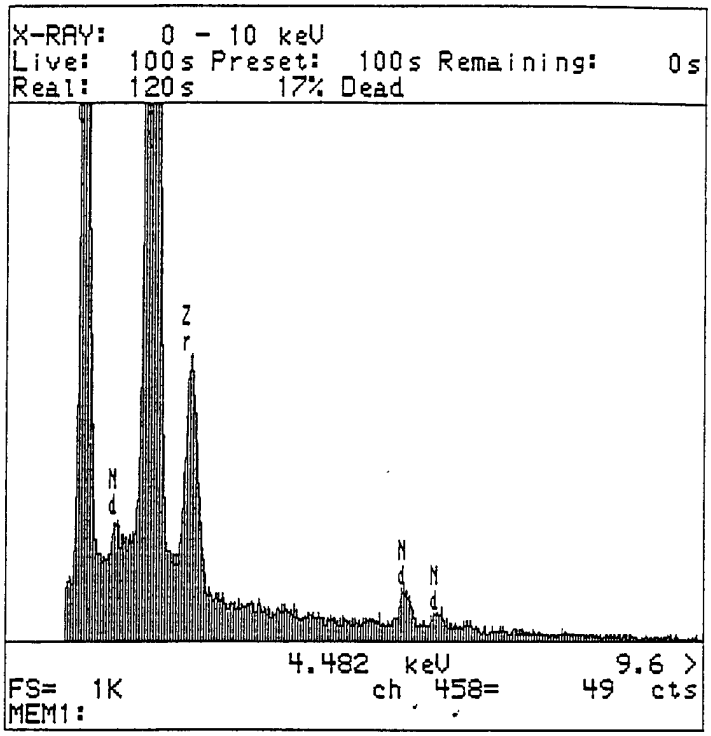
X-RAY: 0 - 10 keV
Live: 100s Preset: 100s Remaining: 0s
Real: 120s 17% Dead
Z
r
N
d
N
d
N
d
4.482 keV
9.6 >
FS= 1K
ch 458= 49 cts
MEM1:

(c)

Fig. 11

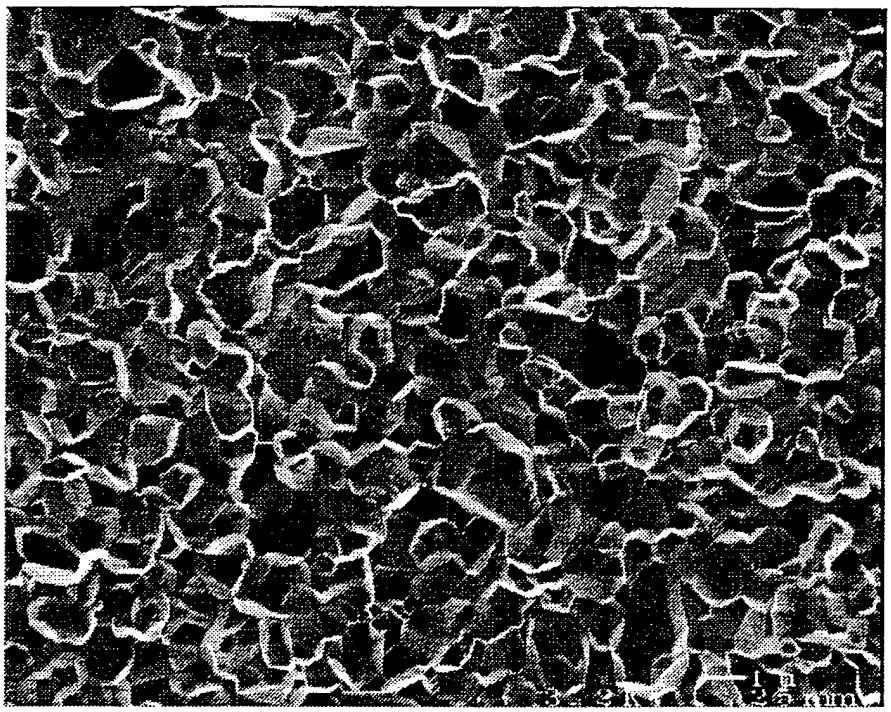

Fig. 12

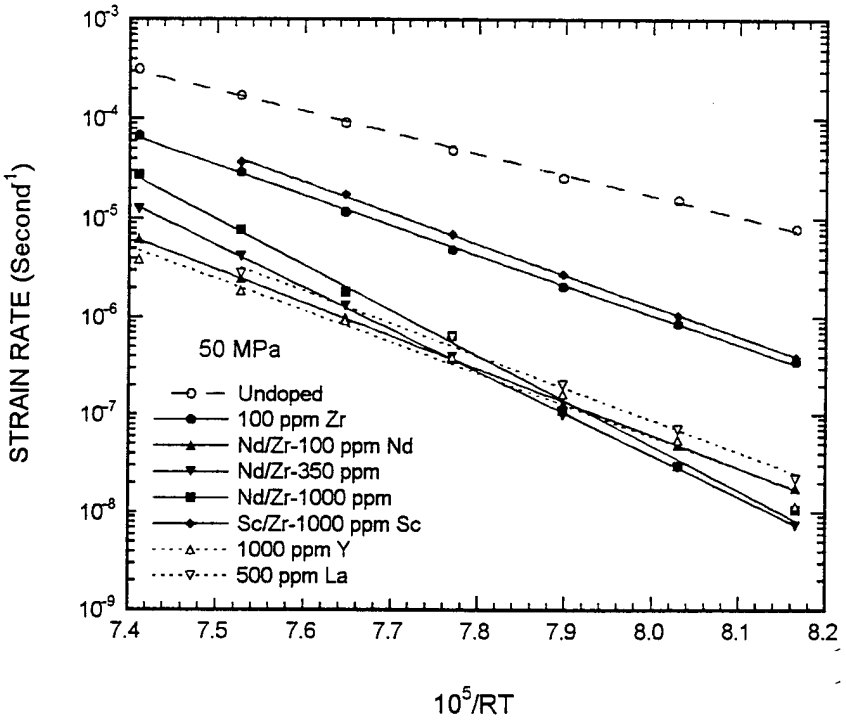
STRAIN RATE (Second^{-1})
10^{-3}
10^{-4}
10^{-5}
10^{-6}
10^{-7}
10^{-8}
10^{-9}
7.4
7.5
7.6
7.7
7.8
7.9
8.0
8.1
8.2
10^5/RT
50 MPa
Undoped
100 ppm Zr
Nd/Zr-100 ppm Nd
Nd/Zr-350 ppm
Nd/Zr-1000 ppm
Sc/Zr-1000 ppm Sc
1000 ppm Y
500 ppm La

Fig. 13

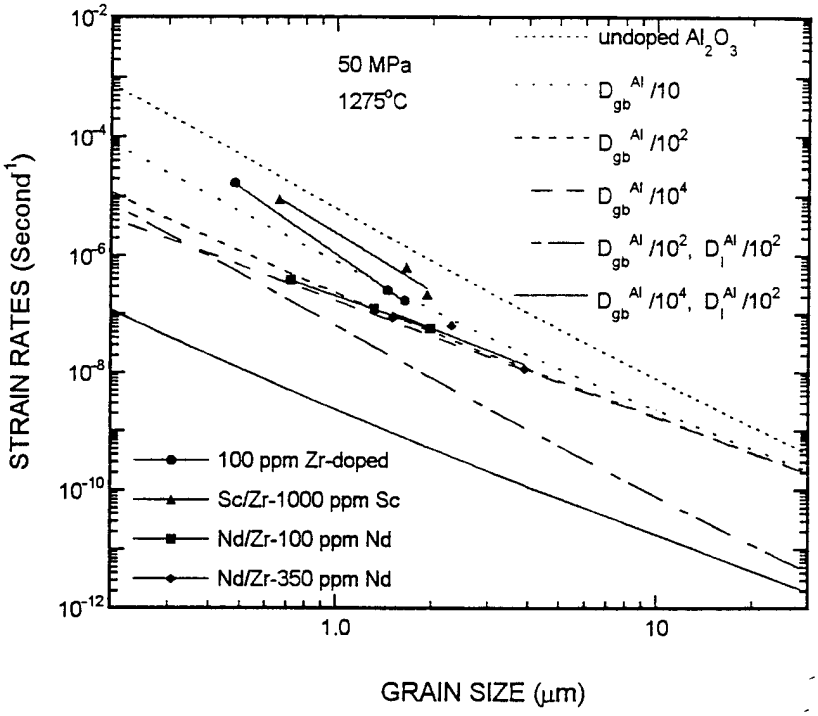
50 MPa
1275°C
undoped Al_2O_3
$D_{gb}^{Al}/10$
$D_{gb}^{Al}/10^2$
$D_{gb}^{Al}/10^4$
$D_{gb}^{Al}/10^2$, $D_l^{Al}/10^2$
$D_{gb}^{Al}/10^4$, $D_l^{Al}/10^2$
100 ppm Zr-doped
Sc/Zr-1000 ppm Sc
Nd/Zr-100 ppm Nd
Nd/Zr-350 ppm Nd
STRAIN RATES (Second^{-1})
10^{-2}
10^{-4}
10^{-6}
10^{-8}
10^{-10}
10^{-12}
1.0
10
GRAIN SIZE (μm)

Fig. 14

Section 1.7

Application of Nano-scale EELS Spectrum Lines to Grain Boundaries

by

J. Bruley, J. Cho, M. P. Harmer, and H. M. Chan

Published in *Microscopy and Microanalysis,* Vol. 3, Suppl. 2, Proceedings of Microscopy and Microanalysis '97, pp941-42, (Cleveland, OH, August, 1997), Springer, New York, NY, 1997.

APPLICATION OF NANO-SCALE EELS SPECTRUM LINES TO GRAIN BOUNDARIES

J. Bruley*, J. Cho**, M.P. Harmer**, H.M. Chan**,

*IBM, East Fishkill, NY 12533
** Dept of Materials Science, Lehigh University, Bethlehem Pa 18015

Polycrystals containing small quantities of impurity can exhibit dramatically different properties from that of the pure material. One example of this is the tenfold increase in the creep resistance of Y or La doped alumina relative to ultra-pure alumina.[1] Such changes are correlated to grain boundary segregation, however the segregant's potency to influence properties remains unexplained. Determining the driving force to segregation only partially addresses this issue. A full understanding must take account of the chemical bonding and structural changes occurring at the boundary after segregation. The purpose of this study is to observe the electronic structure associated with the segregating species using EELS spectrum-line profiling. This is accomplished by monitoring the segregation profile along with the characteristic near edge absorption fine structures which reflect changes in the localized density of unoccupied states along that profile. In these experiments a finely focused beam was sequentially stepped across the boundary of interest and a spectrum recorded at each step. The resultant spectrum-line profile is a two-dimensional data set, with the spectral intensity is a function of energy-loss and beam position. The spatial resolution of the data presented here is limited to 1 nm by interface roughness and curvature as well as instrumental probe size. The pixel size for the profiles was half the spatial resolution and there are typically about 30 pixels per profile. Detector artifacts, channel-to-channel gain variations and poor signal-to-background ratio render the interface bonding effects invisible in the raw data. To discern such effects spectral processing is necessary. Each spectrum in the profile is corrected for dark-current, gain variation and sharpened by deconvolution of the spectrometer point-spread function. Each spectrum is normalized in the pre-edge background region and a smooth power-law or polynomial background is removed. The compositional variation is monitored using a 2nd spatial difference filter applied to the data. The 2nd spatial difference intensity, $d^2I(x,E)$, is defined as,

$$d^2I(x,E) = 2.I(x,E) - I(x-dx,E) - I(x+dx,E),$$

where $I(x,E)$ and $I(x!\ dx,E)$ represent the spectra at position x and at positions displaced from x by and amount dx along the line scan. For small displacements, $d^2I(x,E)$ becomes a partial derivative and is analogous to the more commonly encountered 2nd energy difference transform. To optimize sensitivity dx is chosen to be about the half-width of the spatial resolution. Common to all difference approaches, the signal to background ratio is increased by accentuating high frequency components but at the expense of signal-to-noise. The elemental profile is determined by integrating the signal over an energy-window of width ΔE. Intensity changes due to thickness variations such as grain boundary grooving are minimized by the background normalization. Background fitting errors and plural scattering artifacts are kept small by integrating over relatively small windows ($\Delta E<10$ eV). In the example studied here, the ELNES of both the Y L and La M edges are dominated by highly localised atomic states and so are not affected by bonding across the boundary. Thus narrow windows centered on the white-lines give reliable segregation profiles, fig 1. Quantification by EELS and EDX confirms that less than a monolayer of segregant is present on the boundary plane such that no second phase exists.
Principal component regression was applied to the ELNES of the Al and O data (fig 2). This procedure reduces the data to a product between a matrix of abstract Eigen-vectors representing the significant variance and a matrix containing the vector loading. Without further transformation the Eigen-vectors (or principal components) are, by themselves, difficult to interpret. However, the loading of the vectors along the profile delineates the spatial extent of any bonding changes (fig 3). Variations in the Al $L_{2,3}$ edge are observed but none in the O K edge suggesting that bonding changes to the Al are responsible for the changes to the creep. Since creep is controlled by diffusion the defect population and ionic mobility are critical. The

implication of these measurements is that the number of cationic defects is affected by a change in the Al binding energy. An additional effect may be associated with a modified defect mobility which will be influenced by the structure. Oversized cations will likely act as an additional diffusion barrier. The correlation between segregation and bonding affects supports this notion (fig 4).[2]

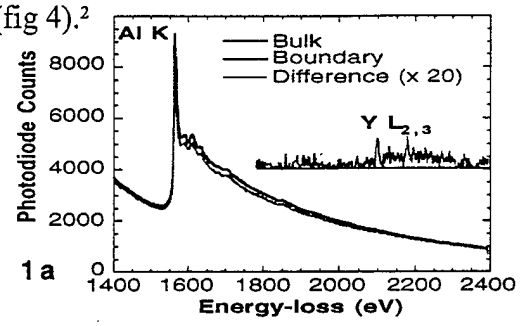

1a

1b

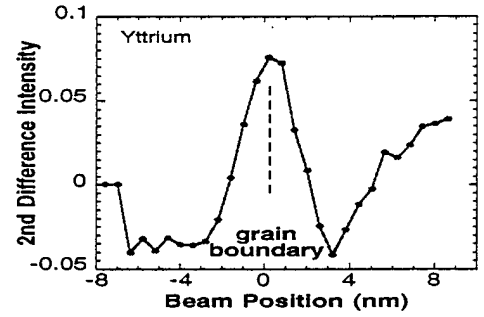

2

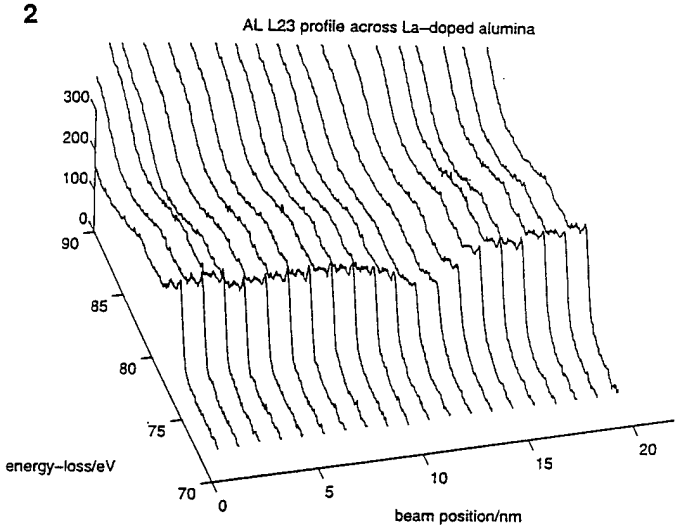

3

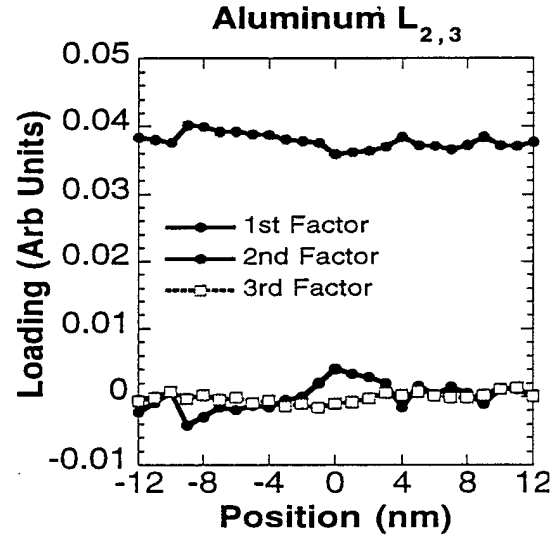

4

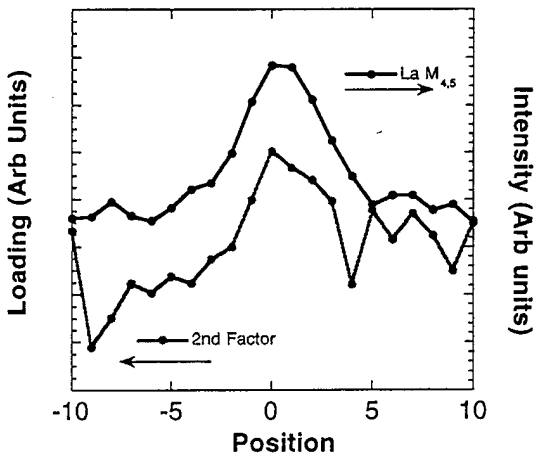

Fig 1 a) Spectrum illustating Y L edge b) 2nd spatial difference profile of Y L edge
Fig 2. Raw Al $L_{2,3}$ data after removal of smooth power-law background
Fig 3 Loadings of Al of 3 significant Eigen-vectors determined by principal component regression
Fig 4. Comparison between composition and bonding for La doped Al_2O_3

[1] J. Cho, et al, J Am. Cer. Soc. (1997) Accepted for publication
[2] Funding was provided by AFSOR under contract F49620-94-1-0284

Section 1.8

Grain Boundary Chemistry and Creep Resistance of Alumina

by

Y. Z. Li, M. P. Harmer, H. M. Chan, and J. M. Rickman

To be Published in Ceramic Microstructure '96

GRAIN BOUNDARY CHEMISTRY AND CREEP RESISTANCE OF ALUMINA

Yan Z. Li, Martin P. Harmer, Helen M. Chan, and Jeffrey M. Rickman

Department of Materials Science and Materials Research Center,
Lehigh University, Bethlehem, PA 18015

INTRODUCTION

Recently, it has been reported that a dramatic improvement in creep resistance of alumina ceramics is obtained by the addition of yttrium (Y)/lanthanum (La) ions [1,2]. The original discovery of the beneficial effect of Y_2O_3 doping was made by French et al. [1] in an investigation of the creep behavior of equi-volume duplex structures, Al_2O_3 : c-ZrO_2(Y) and Al_2O_3 : YAG systems. These investigators found that the creep rate of the duplex structures was significantly lower than their single phase constituents, and that the result could not be accounted for by simple composite theory. They suspected that the reduced creep rate of the duplex structures was a result of Y segregation to the grain boundaries, where the larger ionic size of the segregants obstructed the grain boundary mass transport process, the dominant creep mechanism for fine grained alumina. To test this concept, French et al. [1] added 1000 ppm Y (Y/Al atomic ratio) to pure Al_2O_3, and demonstrated that the creep rate was further reduced relative to that of the duplex structures. The tensile creep rate of the 1000 ppm Y-doped alumina was reduced two orders of magnitude as compared with undoped alumina. Subsequent work showed that the addition of 500 ppm La to alumina resulted in about the same amount of reduction in the creep rate as with Y addition [2]. Co-doping alumina with Mg and Y has also been reported by other investigators [3-5] to reduce the creep rate, but the effect was not as dramatic. Wakai et al. [6] reported that 1000 ppm Zr addition to alumina enhanced the creep resistance by a factor of about 15.

The steady-state creep rate predicted by diffusional mechanisms is commonly expressed in the form,

$$\dot{\varepsilon} = A\,(d)^{-p}\,(\sigma)^{n}\,\exp(-Q/RT)$$

where A is a constant, d is the grain size, σ is the applied stress, p is the inverse grain size exponent, n is the stress exponent, Q is the apparent activation energy for creep, R is the gas constant, and T is the absolute temperature. For lattice diffusion controlled (Nabarro-Herring) creep [7,8] p=2 and n=1, while p=3 and n=1 for grain boundary diffusion controlled (Coble) creep [9]. If the grain boundaries do not behave as perfect sources and sinks of vacancies, the interface reaction process may be rate-limiting [10,11], then p=1 and n=2. Details of creep characteristics and other mechanisms can be found in a number of review articles [12,13].

In the previous studies of Y [1], La [2], and Zr [6] doped alumina, the doping level exceeded the solubility limits of these elements in alumina, and thus resulted in dopant-rich second phase precipitates at the grain boundaries. As a result, the role (if any) of these second phase particles on the creep behavior of these materials is not clear. To avoid this complication, in the present study, alumina was doped with Zr and Nd ions at levels below their solubility limits in alumina. The effect of the dopants on the creep behavior of alumina may thus be attributed solely to solid solution/segregation effects. In this paper, we report the preliminary results of this investigation. The reason that Nd and Zr ions were chosen for this study was their ionic size. The size of Zr^{+4} (0.73Å) and Nd^{3+} (0.995Å), together with that of Y^{3+} (0.89 Å) and La^{3+} (1.06Å) makes up a range of ionic size, larger than that of Al^{3+} (0.53Å). The effect of the ionic size of the dopants on the creep resistance is currently under investigation.

EXPERIMENTAL PROCEDURE

Ultra pure α-Al_2O_3 powders (AKP-53, 99.995%, a mean particle size of 0.35 μm, Sumitomo Chemical America, New York, NY) and neodymium nitrate ($Nd(NO_3)_3 \cdot 6H_2O$, 99.99%, Alfa AESAR, Ward Hill, MA) were used as the starting powders. Alumina slurries of roughly equal mass of alumina powders and DDI (deionized + distilled) water were first made. Approximately 100 ppm Zr doping was achieved by ball-milling the alumina slurry with ZrO_2 grinding media (Tosoh U.S.A. Inc., Bridgewater, NJ) for 20 hours. Nd doping at 100 ppm level was achieved by adding the appropriate amount of neodymium nitrate aqueous solution to the alumina slurry. Nd-doped slurry was also ball-milled with ZrO_2 grinding media for 20 hours to achieve uniform mixing. Chemical analysis by ICP-OES (inductively coupled plasma-optical emission spectroscopy) technique revealed that the Zr-doped material had a doping level of 110 ppm Zr, and the Nd/Zr- codoped material contained a 40 ppm Nd and 70 ppm Zr dopant. After drying and crushing, the powders were then calcined at 850°C for 10 hours in high purity alumina crucibles (99.8%, Vesuvius McDanel Ceramic Company, Beaver Falls, PA). A new set of labware was used for each composition to avoid cross contamination. All powder preparation was carried out in a class 100 clean environment using acid-washed containers. Typical powder batch sizes were 200-250 grams each.

The processed powders were hot-pressed under vacuum in graphite dies at NIST (National Institute of Standards and Technology, Gaithersburg, MD) for 30 min with an applied pressure of 45 MPa. The Zr-doped Al_2O_3 was hot-pressed at 1320°C and the Nd/Zr-codoped Al_2O_3 at 1400°C. The grain size was measured by the linear intercept technique (1.5 × average intercept) with at least 600 intercepts counted for each measurement. The above hot-pressing conditions resulted in an average grain size of 0.48 and 0.72 μm, and a density of 97.1% and 98.0%, for the Zr-doped and Nd/Zr-codoped Al_2O_3, respectively.

The hot-pressed billets were machined commercially (Bomas Machine Specialties, Inc., Somerville, MA) into tensile specimens of the 2-inch specimen design developed at NIST by French and Wiederhorn [14]. SiC flags were attached to the specimen with carbon cement to establish the gauge length (the flags remain attached by friction at high temperatures). A laser extensometer (LaserMike, Inc., Dayton, OH) was used to measure the gauge length as a function of time under load with a precision of ±1 μm. Stress was applied to the specimen at constant load using either a lever-arm or hydraulic testing machine (Applied Test Systems, Inc., Butler, PA). Since all the experimental data were collected under a total strain < 3%, the tests could be considered to be constant stress. The maximum strain at rupture was about 10-12% for both materials. The temperature and stress range tested were respectively 1200-1350°C and 20-100 MPa. For each specimen, incremental temperature changes at constant stress, or incremental stress changes at constant temperature during the steady state creep were used to extract the maximum number of data points. For most specimens, the creep rate under each set of conditions was measured two or three times on a given specimen to ensure that the

strain rate was not strain-history dependent. Typically, the strain rates under the same conditions were within about 10%, and the average value was taken as the strain rate under that set of conditions. No significant concurrent grain growth during creep testing was observed in these materials. A maximum of 20% grain growth was observed for the Zr-doped alumina after being crept 12% at rupture.

RESULTS AND DISCUSSIONS

The as-fired microstructures of Zr- and Nd/Zr-codoped alumina are shown in Fig. 1. The microstructures of both materials were very uniform. The grains were mostly equiaxed, though some grains showed irregular shapes. The range of the grain size for both materials was rather broad, 0.1-1.5 μm for Zr-doped alumina with an average size of 0.48 μm, and 0.1-3.0 μm for Nd/Zr-codoped alumina with an average of 0.72 μm. The large ratio of the largest grain size to the smallest grain size may be an indication of microscopic inhomogeous distribution of the dopants.

The creep curves from tensile creep rupture tests at a fixed temperature and under a

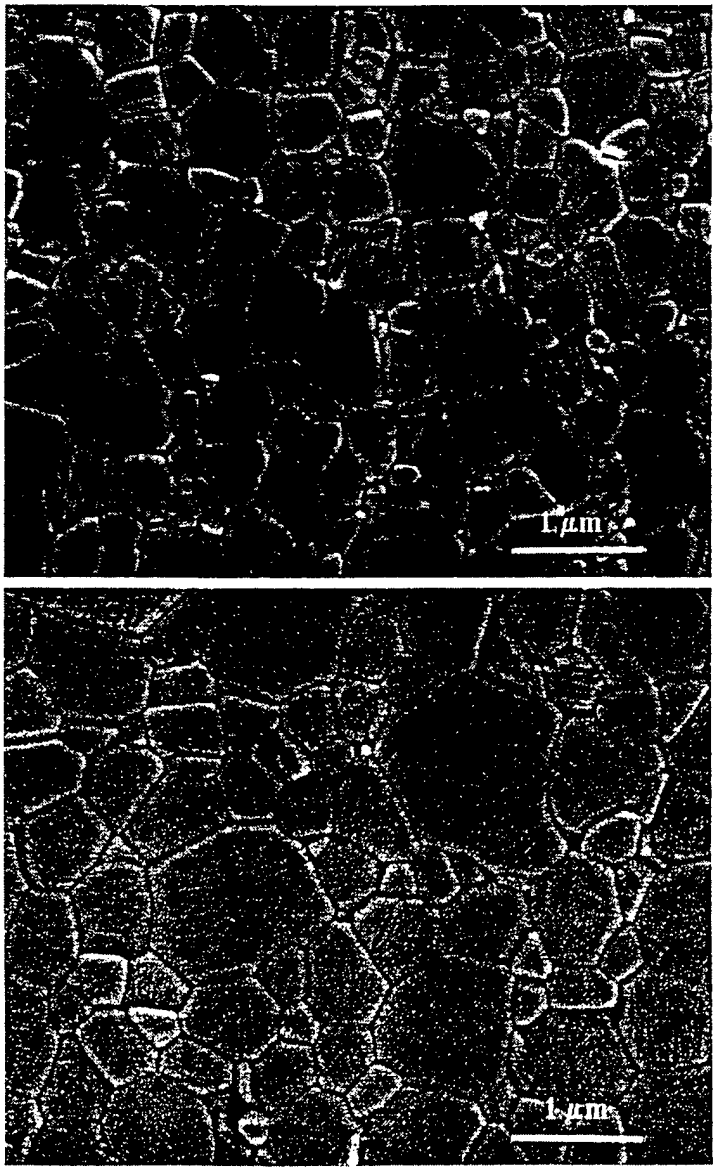

Fig. 1 Typical as-fired microstructures of (a) Zr-doped and (b) Nd/Zr-codoped alumina

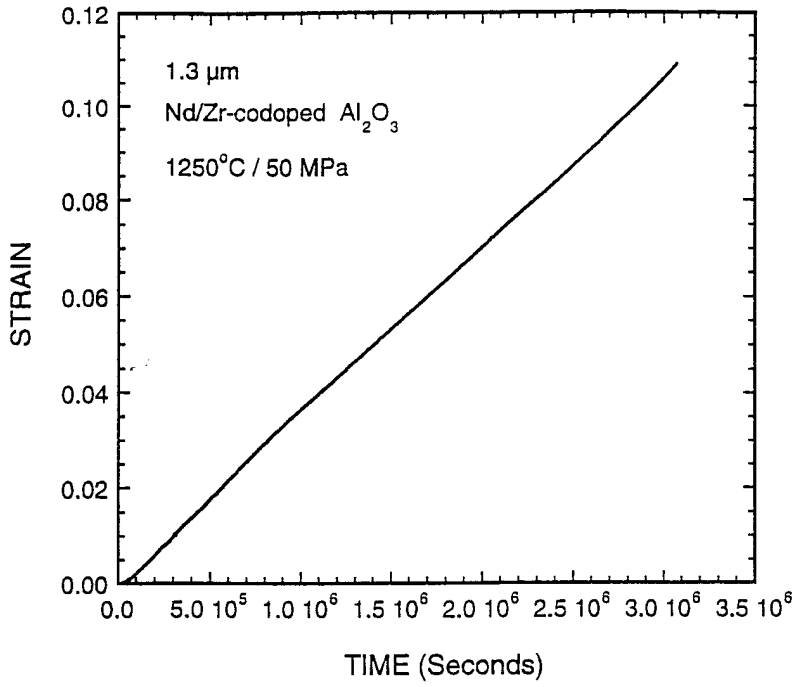

Fig. 2 A typical strain-rate relationship for a creep rupture test.

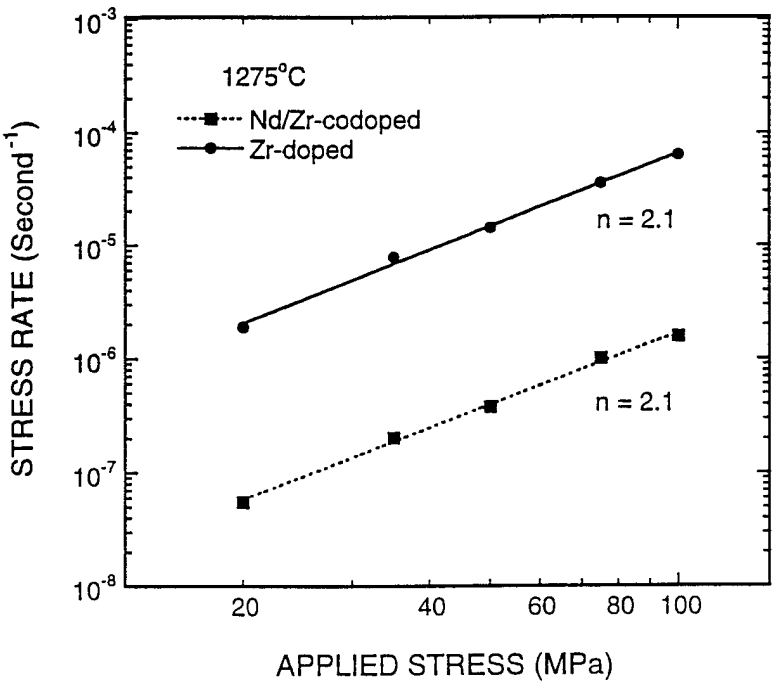

Fig. 3 The effect of applied stress on the creep rates at 1275°C.

constant load for both Zr- and Nd/Zr-codoped materials were very similar. Fig. 2 shows a typical strain-time curve for the Nd/Zr-codoped material. The specimen was annealed at 1200°C for 24 hours in the creep testing machine with a stress <5 MPa before the creep test was carried out. This annealing was found to significantly shorten the primary stage of creep, leaving an extensive steady state creep stage. The creep curve in Fig. 2 shows all the three

stages of creep. However, since the creep rate difference among the different creep stages was less than 10%, (which was within the experimental reproducibility for multiple measurements under the same set of conditions), the primary and tertiary creep can be neglected, and the entire creep can be considered to be steady state creep for the purpose of creep rate measurements.

The effect of stress on the steady state creep rate at 1275°C is shown in Fig. 3. The stress exponent was measured to be close to 2 for both materials, which is consistent with the results of French et al. [1] and Robertson et al. [4]. This value reflects a possible role of interface-reaction in the creep process [10,11].

The effect of temperature on the creep rate under an applied stress of 50 MPa is shown in Fig. 4. Due to the grain size differences of these materials, however, the effect of dopant

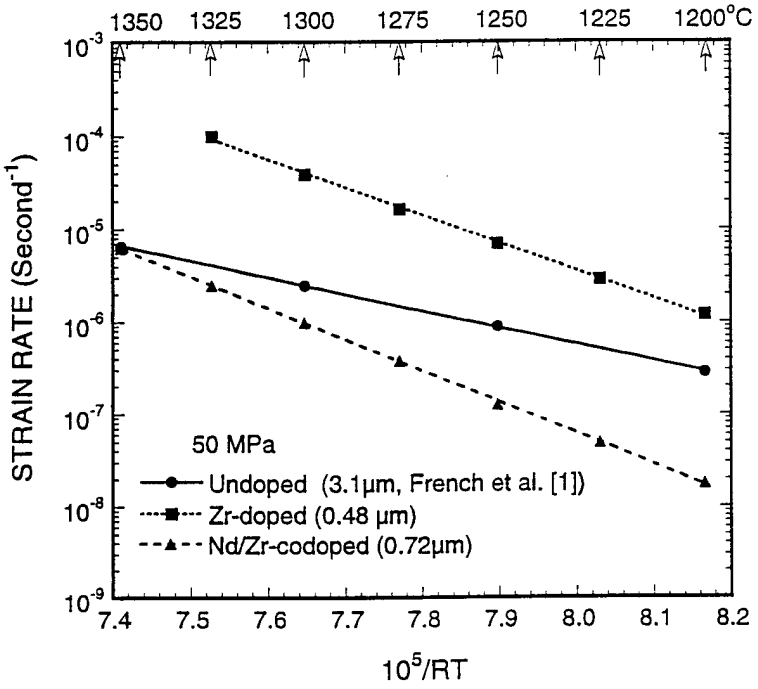

Fig. 4 The effect of temperature on the creep rate at an applied stress of 50 MPa.

on the creep rate is not clear. Sintering studies, carried out at Lehigh on samples processed from the same powder batches as the creep specimens, have shown that grain boundary diffusion was the dominant mechanism in the densification of Y-doped and La-doped alumina with similar dopants [15]. If, however, grain boundary diffusion is assumed to be the dominant creep mechanism [16-22], then one can assume an inverse grain size exponent of 3. The creep rates of the pure alumina and Nd/Zr-codoped alumina corrected to a grain size of 0.72 µm, (the grain size of Nd/Zr-codoped alumina), are shown in Fig. 5. As seen in this figure, 100 ppm Zr addition reduces the creep rate by a factor of about 15 as compared with undoped alumina. The addition of 40 ppm Nd further reduces the creep rate by another factor of about 20, which represents a combined effect of two and a half orders of magnitude as compared with the undoped alumina.

The activation energy was 470, 690, and 780 kJ/mol for undoped, Zr-doped, and Nd/Zr-codoped Al_2O_3, respectively. Clearly, the introduction of Nd/Zr- dopant ions resulted in an increase in the activation energy. This is consistent with the obstruction of grain boundary transport processes, by the oversize dopant ions segregated to the grain boundaries. Higher activation energies caused by dopants were also confirmed by Cho et al. [2] in Y and La doped alumina, by Sato and Carry [23] in Y and Mg codoped alumina, and by Wakai et al. [6] in Zr

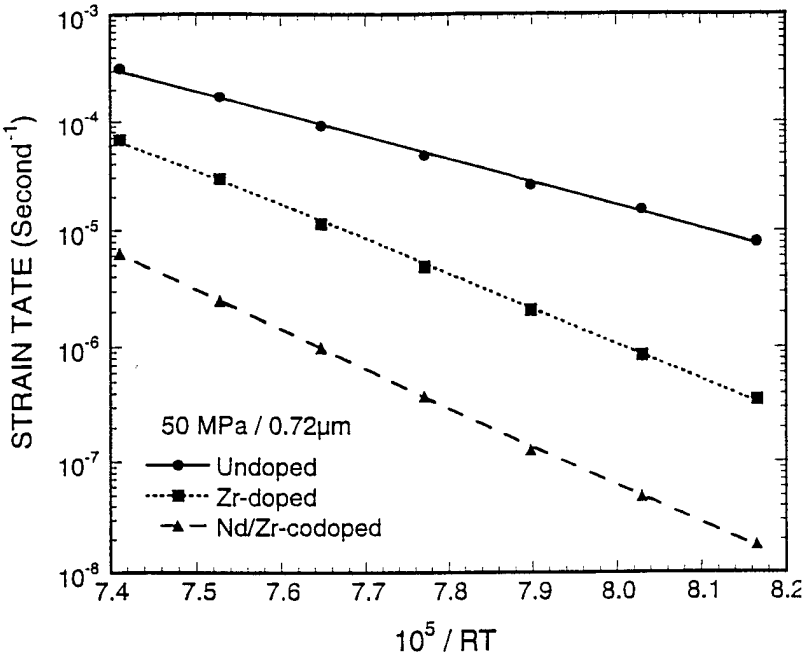

Fig. 5 The effect of temperature on the creep rate and corrected to a grain size of 0.72 μm according to the grain boundary diffusion controlled creep.

doped alumina.

From microstructural observation in the SEM, all the samples appeared to be single phase (Fig. 1); no second phase particles were observed in either material. This result clearly suggests that the solubility limit of Zr in alumina is >110 ppm, and that of Nd is >40 ppm. Moreover, the data demonstrate that the enhanced creep resistance is primarily a solid solution effect. This contrasts with the work of Wakai et al. [6], where the creep rate reduction by the Zr addition was attributed to the ZrO_2 particles at grain boundaries, reducing the interface-reaction rate and thus the creep rate. Interestingly however, the extent of creep rate reduction reported by Wakai et al. and observed in the present study agree closely (factor of 15).

To date, the codoping combination of Nd and Zr has produced the greatest benefit in terms of reduction of creep rate (two and half orders of magnitude versus two orders of magnitude for Y- and La-doped alumina). From the present results alone, it is not possible to conclude whether the Nd ions are having a greater effect than the Zr ions, or whether there is some beneficial interaction between the influences of the two dopant ions. The relative contribution of Nd ions alone to the creep rate is under current investigation.

As stated previously, our belief is that the improvement in creep results from the lowering of the grain boundary diffusivity due to the presence of oversize dopant ions. Lartigue and coworkers have proposed an alternative explanation based on their observation [24,25] that Mg doping and Mg and Y codoping in alumina resulted in a large proportion (~30%) of special grain boundaries (near coincidence boundaries), compared with undoped alumina. Lartigue et al. [26] further observed that Mg and Y codoping also lead to an increase in dislocation density both in the grains and in the grain boundaries. These investigators postulate that because the special grain boundaries are less able to accommodate intergranular dislocations, the grain boundary sliding process was limited. However, in the investigations of Y- and La-doped aluminas, neither grain boundary nor lattice dislocations were observed by the Lehigh researchers [1,2]. One possible explanation for the different observations is that the creep tests were conducted at different temperatures. The Y- and La-doped materials were tested in the range of 1200-1350°C by the Lehigh group, while the creep tests by the above investigators were carried out at or above 1450°C. At higher temperature, dislocations can be

created more easily and dislocation mobility is higher, hence the contribution of dislocation processes to creep may be greater. Given the absence of any detected dislocation activity to date, it is believed that the segregation argument provides the explanation which is the most consistent with the results. The relationship between the creep rate (grain boundary diffusivity) and the ionic size of the dopant is currently under our investigation both experimentally and by means of computer simulation.

SUMMARY

The tensile creep behavior of 100 ppm Zr-doped and Nd/Zr-codoped alumina ceramics was studied. The addition of 100ppm Zr alone resulted in a reduction of the creep rate by a factor of 10, whereas the presence of both Zr and Nd ions, reduced the creep rate by two and a half orders of magnitude. The activation energy was increased from the 470 kJ/mol for undoped alumina to 690 and 780 kJ/mol for 100 ppm Zr-doped and Nd/Zr-codoped alumina, respectively, consistent with impeded grain boundary transport process by the segregated dopant ions. Given that the dopant concentration of both the Nd and Zr ions was below the solubility limit, the present study suggests that the enhanced creep resistance is primarily a solid solution effect.

ACKNOWLEDGMENTS

The authors would like to thank R. Krause and E. R. Fuller, Jr. at NIST for help with hot-pressing the 3-inch billets, and W. Luecke at NIST for providing the engineering graph of the 2-inch tensile specimen design. This work was supported by AFOSR under grant # F49620-94-1-0284.

REFERENCES

[1]. J.D. French, J. Zhao, M.P. Harmer, H.M. Chan, and G.A. Miller, "Creep of Duplex Microstructures," J. Am. Ceram. Soc. 77:2857 (1994).

[2]. J. Cho, M.P. Harmer, H.M. Chan, J.M. Rickman, and A.M. Thompson, The effect of Y and La on tensile creep behavior of aluminum oxide, to be submitted to J. Am. Ceram. Soc. (1996).

[3]. S. Lartigue, C. Carry, and L. Priester, Grain boundaries in high temperature deformation of yttria and magnesia co-doped alumina, J. Phys. (Paris), C1-51:985 (1990).

[4]. A.G. Robertson, D.S. Wilkinson, and C.H. Cáceres, Creep and creep fracture in hot-pressed alumina, J. Am. Ceram. Soc. 74:915 (1991).

[5]. P. Gruffel and C. Carry, Strain-rate plateau in creep of yttria-doped fine grained alumina, pp.305-11 in Proceedings of the 11th RISϕ International Symposium on Metallurgy and Materials Science: Structural Ceramics-Microstructure and Properties. J.J. Bentzen, J.B. Bilde-Sorensen, N. Christiansen, A. Horsewell, and B. Ralph, ed. Risϕ National Lab. Roskilde, Denmark, 1990.

[6]. F. Wakai, T. Iga, and T. Nagano, Effect of dispersion of ZrO_2 particles on creep of fine-grained Al_2O_3, J. Ceramic Soc. Jpn. 96:1206 (1988).

[7]. F.R.N. Nabarro, Deformation of crystals by the motion of single ions, in: Report of a Conference on the Strength of Solids, p. 231, Phys. Soc., London (1948).

[8]. C. Herring, Diffusional viscosity of a polycrystalline solid, J. Appl. Phys. 21:437 (1950).

[9]. R.L. Coble, A model for boundary diffusion controlled creep in polycrystalline materials, J. Appl. Phys. 34:1679 (1963).

[10]. E. Arzt, M.F. Ashby, and R.A. Verrall, Interface controlled diffusional creep, Acta Metall. 31:1977 (1983).

[11]. G.W. Greenwood, The possible effects on diffusional creep of some limitation of grain boundaries as vacancy sources and sinks, Scripta Metall. 4:171 (1970).

[12]. A.G. Evans and T.G. Langdon, Structural ceramics, Prog. Mater. Sci. 21:171 (1976).

[13]. W.R. Cannon and T.G. Langdon, Review creep of ceramics, Part I, J. Mater. Sci., 18:1 (1983); Part II, J. Mater. Sci., 23:1 (1988).

[14]. J.D. French and S.M. Wiederhorn, Tensile specimens from ceramic components, J. Am. Ceram. Soc. 79:550 (1996).
[15]. J. Fang, A.M. Thompson, H.M. Chan, and M.P. Harmer, Effect of Y and La on the sintering behavior of ultra-high-purity Al2O3, in press, J. Am. Ceram. Soc. (1996)
[16]. P. Gruffel and C. Carry, Effect of grain size on yttrium grain boundary segregation in fine grained alumina, J. Eur. Ceram. Soc., 11:189 (1993).
[17]. B.A. Pint, Experimental observations in support of the dynamic-segregation theory to explain the reactive-element effect, Oxidation of Metals, 45:1 (1996).
[18]. M. Le Gall, A.M. Huntz, and B. Lesage, Self-diffusion in α-Al_2O_3 and growth rate of alumina scales formed by oxidation: effect of Y_2O_3 doping, J. Mater. Sci. 30:201 (1995).
[19]. S. Lartige-Korinek, C. Carry, F. Dupau, and L. Priester, Transmission electron microscopy analysis of grain boundary behavior in superplastic doped aluminas, Mater. Sci. Forum, 170-172:409 (1994).
[20]. A.M. Thompson, K.K. Soni, H.M. Chan, M.P. Harmer, D.B. Williams, J.M. Chabala, and R. Levi-Setti, Dopant distributions in rare earth-doped Al2O3, in press, J.Am. Ceram. Soc. (1996).
[21]. J. Bruley, J. Cho, H. Chan, M.P. Harmer, and J.M. Rickman, STEM analysis of grain boundaries of creep resistant Y and La doped alumina, to be submitted to J. Mater. Res. (1996).
[22]. T.G. Langdon, The significance of diffusion creep in simple and multicomponent ceramics, Defect and Diffusion Forum, 75:89 (1991).
[23]. E. Sato and C. Carry, Yttria doping and sintering of submicrometer-grained α-alumina, J. Am. Ceram. Soc. 79:2156 (1996).
[24]. S. Lartigue and L. Priester, Influence of doping elements on the grain boundary characteristics in alumina, J. Phys. C5,49:451 (1988).
[25]. H. Grimmer, R. Bonnet, S. Lartigue, and L. Priester, Theoretical and experimental descriptions of grain boundaries in rhombohedral alpha-Al_2O_3, Phil. Mag. A6:493 (1990).
[26]. S. Lartigue, C. Carry, and L. Priester, Grain boundary in high temperature deformation of yttria and magnesia co-doped alumina, J. Phys. C1, 51:985 (1990).

2. Publications and Presentations

2.1 Publications

1 A. M. Thompson, K. K. Soni, H. M. Chan, M. P. Harmer, D. B. Williams, J. M. Chabala, and R. Levi-Setti, "Dopant Distributions in Rare-Earth-Doped Alumina," J. Am. Ceram. Soc., **80**, 373-76(1997).

2 J. Cho, M. P. Harmer, H. M. Chan, J. M. Rickman and A. M. Thompson, "Effect of Yttrium and Lanthanum on the tensile Creep Behavior of Aluminum Oxide," J. Am. Ceram. Soc., **80**, 1013-17(1997).

3 J. Bruley, J. Cho, J. Fang, A. M. Thompson, H. M. Chan. M. P. Harmer, "STEM Analysis of Grain Boundaries of Creep Resistant Y and La Doped Alumina," Submitted to J. Am. Ceram. Soc.

4 J. Fang, A. M. Thompson, M. P. Harmer, and H. M. Chan, "Effect of Yttrium and Lanthanum on The Final-Stage Sintering Behavior of Ultra-High-Purity Al_2O_3," J. Am. Ceram. Soc., **80**, 2005-12(1997).

5 Y. Li, M. P. Harmer, H. M. Chan, J. M. Rickman, and J. Chabala, and R. Levi-Setti "Creep Resistance of Alumina from Nd, Sc, and Zr Doping," Submitted to J. Am. Ceram. Soc.

6 J. Bruley, J. Cho, M. P. Harmer, and H. M. Chan, "Application of Nano-scale EELS Spectrum Lines to Grain Boundaries," pp.941-42 in *Microscopy and Microanalysis,* Vol. 3, Suppl. 2, Proceedings of Microscopy and Microanalysis '97 (Cleveland, OH, August, 1997), Springer, New York, NY, 1997.

7 Y. Z. Li, M. P. Harmer, H. M. Chan, and J. M. Rickman, "Grain Boundary Chemistry and Creep Resistance of Alumina," Ceramic Microstructure, 96

2.2 Presentations

1 Y. Z. Li, M. P. Harmer, and H. M. Chan, "The Creep Behavior of Nd and Zr Doped Alumina," Presented at the 99th Annual Meeting of the American Ceramic Society, Cincinnati, May, 1997.

2 J. Cho, M. P. Harmer, H. M. Chan, J. M. Rickman, and A. M. Thompson, "Tensile Creep Behavior of Lanthanum and Yttrium-Doped Alumina," Presented at the 99th Annual Meeting of the American Ceramic Society, Cincinnati, May, 1997.

3 M. P. Harmer, "Grain Boundary Chemistry and Creep Resistance of Alumina," **Invited Presentation** on the International Conference on *Computer Modeling of High Temperature Structural Materials*, Sante-Fe, New Mexico, July 28 - August 2,1997.

4 M. P. Harmer, "Tailoring of Grain Boundary Chemistry in Alumina for Super Creep Resistance," **Invited Presentation** on Research Seminar of General Electric, June, 1997.

5 J. Cho, M. P. Harmer, H. M. Chan, J. M. Rickman, and A. M. Thompson, "Tensile Creep Behavior of Lanthanum- and Yttrium-Doped Alumina," Presented on the 8th Korean-American Scientists and Engineers Association Northeast Regional Conference (Rutgers University, New Brunswick, NJ), March 21-22, 1997.

6 J. Cho, J. M. Rickman, M. P. Harmer, and H. M. Chan, "Defect Interactions in Alumina by Atomistic Computer Simulation," Presented at the 99th Annual Meeting of the American Ceramic Society, Cincinnati, May, 1997.

3. Awards and Accomplishments

J. Cho received *The Gotshall Fellowship Award,* 1997.

4 Personnel

Faculty:

Professor Martin P. Harmer, Principle Investigator

Professor Helen M. Chan, Co-Prnciple Investigator

Professor Jeffrey M. Rickman, Co-Prnciple Investigator

Post-Doctoral Research Associates:

J. Bruley

Y. Z. Li

C. M. Wang

Graduate Students

J. Cho

A. Khan